COMPARISON OF AXIAL FLUX AND RADIAL FLUX BRUSHLESS DC MOTOR TOPOLOGIES FOR CONTROL MOMENT GYROSCOPE WHEEL APPLICATIONS

A THESIS SUBMITTED TO
THE GRADUATE SCHOOL OF NATURAL AND APPLIED SCIENCES
OF
MIDDLE EAST TECHNICAL UNIVERSITY

BY

KURTULUŞ YILMAZ

IN PARTIAL FULFILLMENT OF THE REQUIREMENTS
FOR
THE DEGREE OF MASTER OF SCIENCE
IN
ELECTRICAL AND ELECTRONICS ENGINEERING

APRIL 2009

Approval of the thesis

COMPARISON OF AXIAL FLUX AND RADIAL FLUX BRUSHLESS DC MOTOR TOPOLOGIES FOR CONTROL MOMENT GYROSCOPE WHEEL

submitted by **KURTULUŞ YILMAZ** in partial fulfillment of the requirements for the degree of **Master of Science in Electrical and Electronics Engineering, Middle East Technical University** by,

Prof. Dr. Canan Özgen
Dean, Graduate School of **Natural and Applied Sciences** _____

Prof. Dr. İsmet Erkmen
Head of Department, **Electrical and Electronics Engineering** _____

Prof. Dr. H. Bülent Ertan
Supervisor, **Electrical and Electronics Engineering, METU** _____

Examining Committee Members:

Prof. Dr. Muammer Ermiş
Electrical and Electronics Engineering, METU _____

Prof. Dr. H.Bülent Ertan
Electrical and Electronics Engineering, METU _____

Assist. Prof. Dr. M. Timur Aydemir
Electrical and Electronics Engineering, GAZİ University _____

Assist. Prof. Dr. Emre Tuna
Electrical and Electronics Engineering, METU _____

Ünsal Orlu, M.Sc.
Chief, TAI _____

Date: 30.05.2009

..

I hereby declare that all information in this document has been obtained and presented in accordance with academic rules and ethical conduct. I also declare that, as required by these rules and conduct, I have fully cited and referenced all material and results that are not original to this work.

Name, Last name: Kurtuluş Yılmaz

Signature :

ABSTRACT

COMPARISON OF AXIAL FLUX AND RADIAL FLUX BRUSHLESS DC MOTOR TOPOLOGIES FOR CONTROL MOMENT GYROSCOPE WHEEL APPLICATIONS

Yılmaz, Kurtuluş

M.S., Department of Electrical and Electronics Engineering

Supervisor: Prof. Dr. H. Bülent Ertan

April 2009, 196 Pages

In this thesis axial flux and radial flux brushless dc motors will be studied as a drive motor for the control of moment gyroscope wheel. Design equations for axial flux and radial flux brushless dc motor topologies will be reviewed. Based on these equations radial and axial flux motors with different number of poles will be designed that meet control moment gyroscope wheel application requirements. The results will be evaluated in terms of efficiency, torque/mass and torque/volume, and suitability for the control moment gyroscope application.

Keywords: CMG, Axial Flux Brushless Dc Motor, Radial Flux Brushless Dc Motor, Performance Comparison

ÖZ

EKSENEL VE RADYAL AKILI FIRÇASIZ DC MOTOR TOPOLOJİLERİNİN MOMENT KONTROL JİROSKOBU TEKERLEK UYGULAMARI İÇİN KARŞILAŞTIRILMASI

Yılmaz, Kurtuluş
Yüksek Lisans, Elektrik-Elektronik Mühendisliği Bölümü
Tez Yöneticisi: Prof. Dr. H. Bülent Ertan

Nisan 2009, 196 sayfa

Bu tez çalışmasında eksenel ve radyal akılı fırçasız dc motorlar moment kontrol jiroskobu tekerlek sürücü motoru olarak değerlendirilecektir. Eksenel akılı ve radyal akılı fırçasız dc motor yapıları tasarım denklemleri incelenecektir. Bu denklemlere bağlı olarak eksenel ve radyal akılı fırçasız dc motorlar farklı kutup sayılarında moment kontrol jıroskobu tekerelek sürücü gereksinimlerine uygun olarak tasarlanacaktır. Elde edilen sonuçlar verim, tork/ağırlık, tork/hacim ve moment kontrol jiroskobu uygulamasına uyum açısından değerlendirilecektir.

Anahtar Kelimeler: MKJ, Eksenel Akılı Fırçasız Dc Motor, Radyal Akılı Fırçasız Dc Motor, Performans Karşılaştırması

To my Family

ACKNOWLEDGEMENTS

I would like to express my gratitude to my supervisor Prof. Dr. H. Bülent Ertan for his invaluable guidance and suggestions.

I offer sincere thanks to Assist. Prof. Dr. M. Timur Aydemir, who encouraged me during my M.Sc. study.

I wish to thank my chief Mr. Ünsal Orlu, and Mr. Emre Yavuzoğlu for their kindness and support during my M. Sc. study.

I want to thank all my friends (Ahmet Cemal Durgun, Ozan Keysan, Emre Yurtoğlu, Volkan Sezgin, Çağlar Özyurt, Kutlay Aydın, Ali Gündoğdu, Elif Dirgin, İlker Şahin) for their support and great understanding during this study. Special thank to Hatice Güdücü for her support and understanding.

Finally I want to thank my family for their precious support during all stages of my life.

TABLE OF CONTENTS

LIST OF TABLES

TABLES

LIST OF FIGURES

FIGURES

CHAPTER 1

INTRODUCTION

1.1 Scope of the Thesis

In aerospace applications there are large amount of applications related to electromechanical systems such as deployment mechanisms, solar panel sun tracking or antenna tracking mechanisms, and actuators for satellite maneuvering etc. Since aero space applications are usually not in a mass production, so there is not to much published studies on aerospace application of electrical motors.

This study will focus on usage electrical motors on Control Moment Gyroscopes (CMG) which are used for satellite maneuvering. Proper motor selection and comparison of selected topologies are studied.

1.2 Outline of the Thesis

The thesis is composed of three main parts. Chapter 2 is including brief definition of LEO satellites, reason for maneuvering, actuators for maneuvering and description of actuation using electromechanical actuators. Definition and advantages of CMG usage is done. And problems related to motor in CMG is discussed. An overview of usage of electrical motors for different space applications is summarized. Selected motor type (brushless dc) possible topologies, equations are summarized.

Chapter 3 includes detailed definition of problems in CMG application. Requirements of CMG application is detailed in this part. Also in order to use in design process of motor materials used in electrical motor are studied (ferro magnets, permanent magnets). Some materials are selected in order to use in design process. Selected topologies for solving the problems are stated. For selected topologies, required equations for design process are stated.

Chapter 4 is assigned to calculation of dimensions, electrical parameters (resistance inductance etc,), current and voltages, losses efficiency for selected motor topologies.

Chapter 5 includes the comparison of calculated results in chapter 4 in terms of mass, efficiency, torque/mass torque/volume. Comparisons are extended for CMG application and advantages and disadvantages of different designs are stated. At the end of Chapter 6 possible future works are stated.

CHAPTER 2

SATELLITE ACTUATORS AND SUITABLE ELECTRICAL MOTORS

2.1 General Overview

Low Earth Orbit (LEO) satellites have to do attitude control for taking images from the earth or communication with the ground station (Figure 2-1). Orbit linear speed of LEO satellites is quite high. Period of their orbit is between 80-100 minutes.

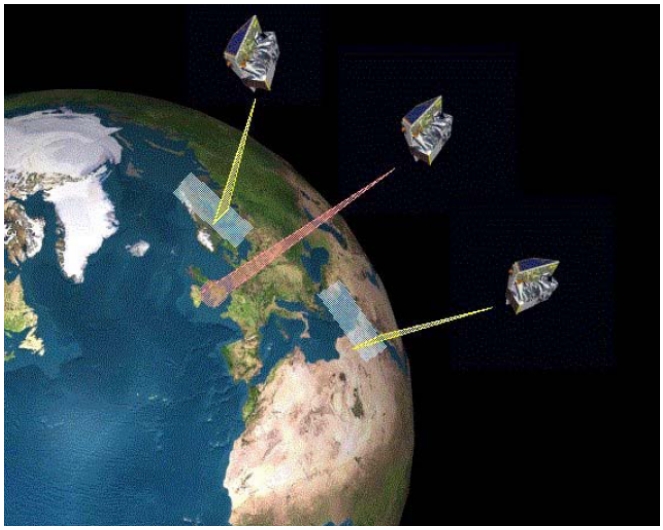

Figure 2-1: Satellite orbit illustration (taking image-communication)

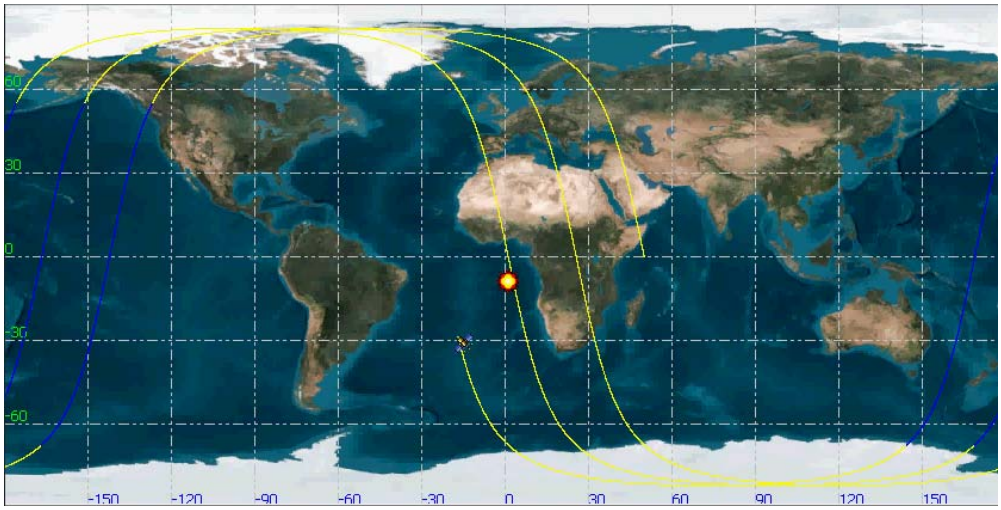

Figure 2-2: Footprint of satellite on the earth

Figure 2-2 shows the footprint of satellite during its orbit. Satellites are usually stabilized in nadir pointing position. In order to take images around the foot print or make communication with ground station, satellites should change attitude. The capability and the effectiveness of a satellite are determined by its maneuver capability. Satellites which can make fast maneuvers can take more images and download them to the ground station faster.

Satellites make maneuvers with the aid of actuators. Agility of satellite is determined by their actuators. Main actuators used in satellites are reaction wheels (Figure 2-3), momentum wheels and control moment gyroscopes. All three actuators are based on momentum exchange principle (conservation of angular momentum). In reaction wheels and momentum wheels a high inertial wheel is driven by an electrical motor. Necessary torque for maneuver is created by accelerating/decelerating the speed of motor.

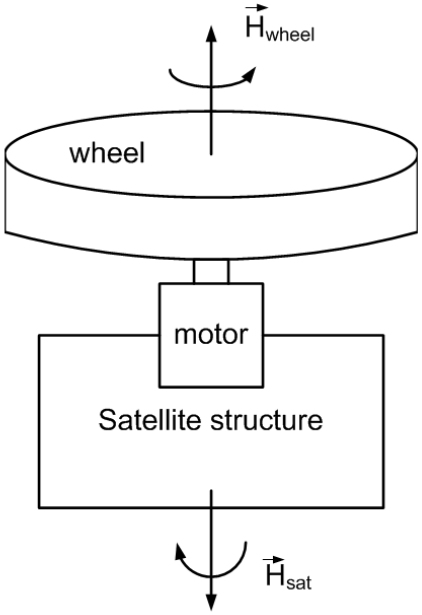

Figure 2-3: Reaction wheel

Necessary rotation is created by changing the angular momentum. Torque obtained from momentum wheels and the reaction wheels can be simplified to the Eq. (2.1) [1]and [2].

$$\begin{aligned} \vec{H} &= I \times w \\ \frac{d\vec{H}_{sat}}{dt} &= -\frac{d\vec{H}_{wheel}}{dt} \\ I_{sat}\frac{dw_{sat}}{dt} &= I_{wheel}\frac{dw_{wheel}}{dt} \\ T &= I\frac{dw}{dt} \end{aligned} \tag{2.1}$$

$\vec{H}$ is angular momentum vector

I is inetia

w is angular speed

I_{sat} is satellite inertia

I_{wheel} is wheel inertia

w_{sat} is satellite angular speed

w_{wheel} is wheel angular speed

T is created torque

Ignoring some friction forces, reaction wheels and momentum wheels generate torque on their wheel rotation axis. By using tree of reaction wheels 3-axis maneuvers can be done. Both actuators are widely used in LEO satellites. But both of them have some limitations. Main drawback of these actuators is the limit of wheels maximum speed. Torque can be produced only by changing the wheel speed and wheel maximum speed is limited. When wheel speed reaches its limits torque can not be created. Wheel speed should be slowly reduced in order to create torque again.

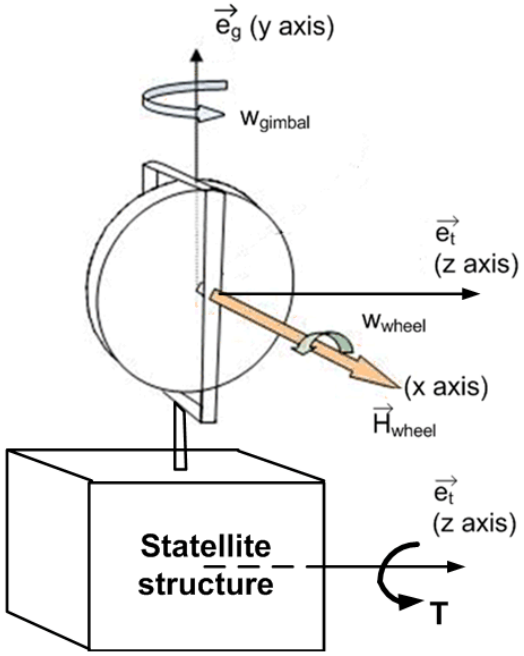

Figure 2-4: Control moment gyroscope reference axis [2]

Latest technology in actuators of LEO satellites is control moment gyroscopes (CMG). CMG working principle is as shown in Figure 2-4. A motor is used to

rotate a wheel around x-axis in order to reserve momentum by a high constant speed (i.e. 6000-10000RPM). In order to create torque angular momentum is changed in another axis (y axis) by using another motor with very low speed(i.e. 20 RPM). Torque is obtained in the third axis z-axis) which is perpendicular to both motion axis. Second motor is used to exchange momentum or create torque.

The torque obtained in CMG is described by the simplified Eq. (2.2) [1] - [3].

$$\begin{aligned} T\vec{e}_t &= w_{gimbal}\vec{e}_g \, x \vec{H}_{wheel} \\ T &= w_{gimbal} I_{wheel} w_{wheel} \end{aligned} \tag{2.2}$$

$\vec{e}_t$ is unit vector on torque axis (z axis)

$\vec{e}_g$ is unit vector on gimbal axis (y-axis)

w_{gimbal} is angular speed of gimbal motor

It can be seen from Eq. (2.2) that torque can be obtained continuously while both motor speed is non zero. Since acceleration is not required in CMG, torque saturation is not seen. Another advantage is since momentum is reserved in wheel and torque is created using gimbal speed more amount of torque can be obtained long time. CMG has a volume and mass advantage with respect to reaction/momentum wheels which is very important in aerospace applications. Figure 2-5 is a graphical comparison of reaction wheel and CMG volume on a satellite [1] [2].

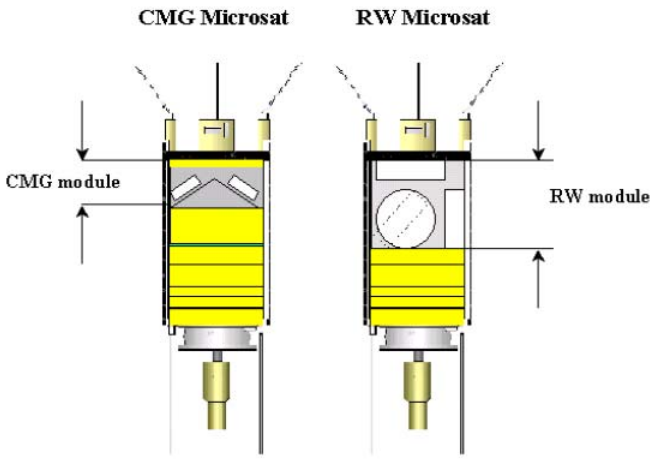

Figure 2-5: CMG versus Reaction wheel

2.2 Suitable Motor Selection for CMG Actuators

CMG systems contain two electrical motors. One is in order to rotate the wheel which is called wheel motor and second one is called gimbal motor which is used to rotate wheel system. Since speed is very low at gimbal motor power consumption in gimbal motor is small (2-4W). Power consumption is mainly due to wheel motor because its speed is very high and friction is high at wheel motor bearings (30-35W). Size and power consumption of CMG is determined by wheel system. This thesis will focus on the motor which will rotate the wheel. Wheel speed is constant and wheel should keep its speed during the mission life of satellite typically 5 years. Wheel should be capable of compensating the friction losses. Detailed constrains on wheel motor and resulting problems due to wheel motor is explained in Chapter 3.

For proper selection of motor type for the wheel motor following constraints should be considered.

- High speed
- High power to mass and volume ratio
- Reliability
- Low maintenance requirements
- Long life time

Motors used in aerospace technologies are A.C. induction motors, Brush D.C. motors, brushless D.C. motors and stepper motors. Among all type of motors brushless motors have greatest advantage for the requirements stated above [4].

D.C. motors have more specific power/mass ratio, because they are using permanent magnet materials. All electrical motors are based on two different magnetic fields. These two fields are based on armature and field fluxes. In D.C. machines one of the fluxes (usually field flux) is created by permanent magnets, which reduces the power consumption. If permanent magnets are not used in rotating part (rotor) current should be carried to moving part (rotor- exception squirrel cage rotors). Generally brushes or slip rings are used. For high speed applications these moving parts require maintenance. On the other hand brushless machines have permanent magnets on the rotating part and they do not require current for electromagnetic field creation. Also use of permanent magnets results in high air gap magnetic flux density which results higher efficiency.

Table 2-1: Applications of motor types for aerospace applications [4]

A.C. induction motors	D.C. brushless motors	Brushless D.C. motors	Stepper motors
1 Thrust Vector control applications 2 High torque and high rpm applications	1 Limited-life time applications 2 Low RPM applications 3 High torque applications	1 Thrust Vector control applications 2 Fuel valve control actuators 3 Solar array deployment 4 Control moment gyroscopes 5 High rpm applications 6 Light weight applications 7 Low thermal emission applications	1 Optic drives 2 Solar array deployment 3 gimbal positioning 4 Low torque applications 5 Open loop micro positioning 6 Timer switching

In aerospace applications life time is a main diving force while selecting the components. Typical life time of satellites in LEO orbit is around 5 years. Also weight and volume is very important because if satellite mass and volume is high, launch cost becomes high. Another problem is maintenance free design. In orbit there is no change to replace or maintenance. Application areas of different types of motors are summarized in Table 2-1. Brushless motors have most advantage for wheel motors of CMGs.

2.2 *General Overview of Brushless DC Motors*

2.2.1 Working Principles of Brushless DC Motors

Permanent magnet brushless motors are fed with three phase windings. Windings are located on the stator slots. Moving magnets on the rotor serves the excitation. Phase windings are activated with the exact synchronism with the rotor motion. Rotation is based on magnetic field rotation. Figure 2-6 and Figure 2-7 explains the phase excitation and rotor movement. In Figure 2-6 phase A is excited, stator flux is built by phase A excitation, rotor flux are build by permanent magnets. Two fluxes are tending to align, and then rotor rotates and settled in the position stated in Figure 2-7. Then phase B is excited and new stator magnetic flux settled in phase B magnetic axis and same physical sequence continue. By proper excitation of phases continuous motion is achieved.

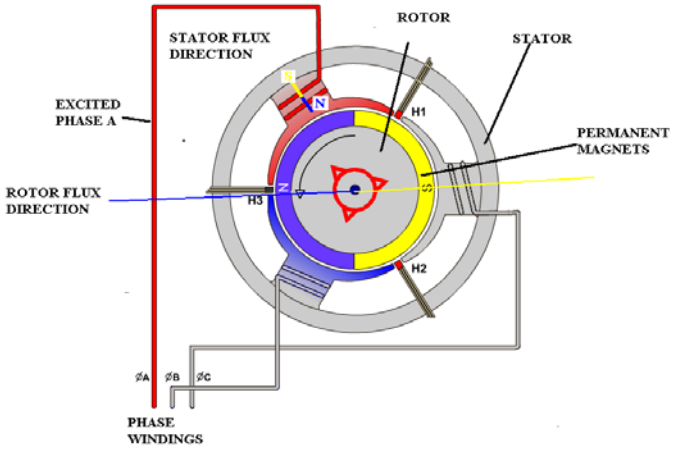

Figure 2-6: Brushless D.C. machine principle-1

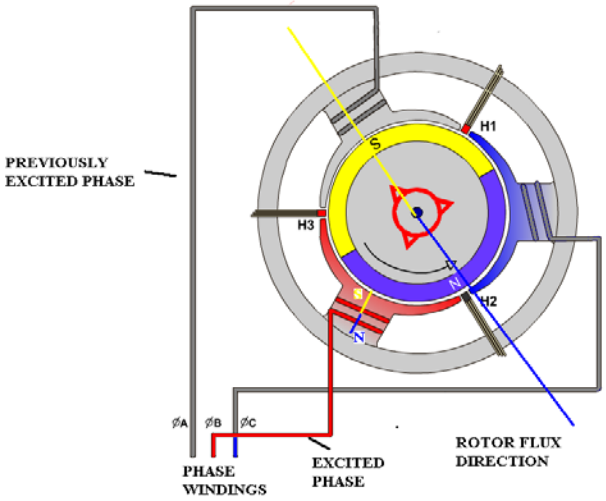

Figure 2-7: Brushless D.C. machine principle-2

2.2.2 Basic Equations of Brushless Motors

Brushless D.C. machines usually driven by balanced three phase waveforms. Equivalent circuit of each phase consists of a winding inductance, a resistance and induced back emf voltage due to the rotation of the rotor. Per phase equivalent circuit of machine is shown in Figure 2-8.

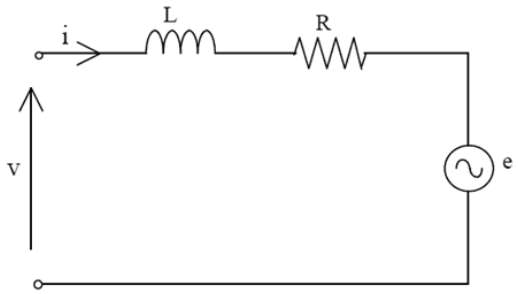

Figure 2-8: Phase equivalent circuit of Brushless D.C. machine

Using the equivalent circuit electrical equation can be obtained as in the Equation (2.3).

$$V = R \times i + L\frac{i}{dt} + e \tag{2.3}$$

V is applied phase voltage

I is phase current

L is phase inductance

e is back emf voltage

As stated before, Brushless D.C. motors are usually fed with there phase balanced voltage waveforms. Equations are written in matrix form in Eq. (2.4) [5].

$$\begin{bmatrix} V_a \\ V_b \\ V_c \end{bmatrix} = \begin{bmatrix} R & 0 & 0 \\ 0 & R & 0 \\ 0 & 0 & R \end{bmatrix} \begin{bmatrix} Ia \\ Ib \\ Ic \end{bmatrix} + \frac{d}{dt} \begin{bmatrix} L-M & 0 & 0 \\ 0 & L-M & 0 \\ 0 & 0 & L-M \end{bmatrix} \begin{bmatrix} Ia \\ Ib \\ Ic \end{bmatrix} + \begin{bmatrix} e_a \\ e_b \\ e_c \end{bmatrix} \tag{2.4}$$

V_a, V_b, V_c are applied phase voltages

I_a, I_b, I_c are phase currents

L is phase inductance

M is mutual inductance

R is phase resistance

Produced electromagnetic torque can be obtained by using the output power of electrical machine. Electrical output power of electrical machine is defined by production of three phase back emf voltages and phase currents. Form the mechanical point of view, power can be represented as output torque multiplied by the angular speed. Using these two definition electromagnetic torque is defined in Eq. (2.5).

$$T_e = (e_a I_a + e_b I_b + e_c I_c)/w \tag{2.5}$$

T_e is electromechanical torque

w is mechanical speed of motor

Mechanical relation between the speed and the torque are represented in Eq. (2.6).

$$\frac{dw}{dt} = (\frac{P}{2})\frac{T_e - T_{load}}{J}$$
$$w = \frac{d\theta}{dt} \tag{2.6}$$

T_{load} is load torque

J is rotoating inertia

θ is rotor mechanical position

P is number of pole

All the equations stated above are represented in stationary referenced frame. All electrical quantities (voltages and currents) are changing with the electrical frequency of the rotation. From the control point of view it is difficult the control variables changing with time. To make the control easy these equations can be represented in synchronously rotating frame with stator. If all quantities are represented in that frame all variables become constant values and these make the system easily controlled.

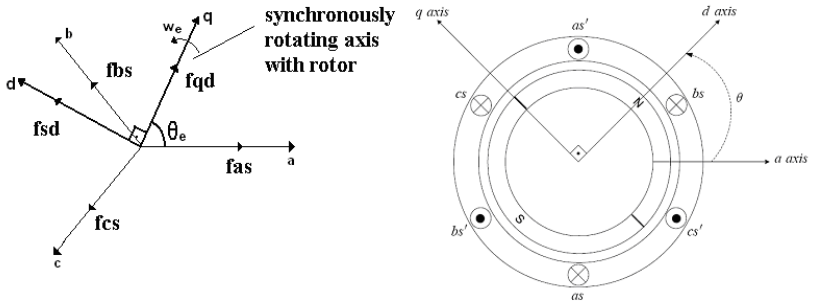

Figure 2-9: Stator and rotor reference frames

Figure 2-9 shows the stationary frame and the synchronously rotating frame. D-axis is the axis of permanent magnet flux and the q-axis is the perpendicular axis

to the d-axis. Voltage and current quantities can be transformed in to the d-q axis quantities using Clark-park transformation matrices. Equations for transformations are stated in Eq. (2.7) – Eq. (2.8).

$$\begin{bmatrix} i_{qs} \\ i_{ds} \end{bmatrix} = \frac{2}{3}\begin{bmatrix} \cos(\theta_e) & \cos(\theta_e - 2\pi/3) & \cos(\theta_e + 2\pi/3) \\ \sin(\theta_e) & \sin(\theta_e - 2\pi/3) & \sin(\theta_e + 2\pi/3) \end{bmatrix}\begin{bmatrix} i_a \\ i_b \\ i_c \end{bmatrix} \tag{2.7}$$

$$\begin{bmatrix} V_{qs} \\ V_{ds} \end{bmatrix} = \frac{2}{3}\begin{bmatrix} \cos(\theta_e) & \cos(\theta_e - 2\pi/3) & \cos(\theta_e + 2\pi/3) \\ \sin(\theta_e) & \sin(\theta_e - 2\pi/3) & \sin(\theta_e + 2\pi/3) \end{bmatrix}\begin{bmatrix} V_a \\ V_b \\ V_c \end{bmatrix} \tag{2.8}$$

Equivalent of Eq. (2.4) in d-q axis are represented in Equation (2.9).

$$\begin{aligned} V_{qs} &= Ri_{qs} + L\frac{i_{qs}}{dt} + e_q \\ V_{ds} &= Ri_{ds} + L\frac{i_{ds}}{dt} - e_d \\ e_q &= w_e\lambda_d = w_r(i_{sd}L_d + \lambda_m) \\ e_d &= w_e\lambda_q = w_r(i_{sq}L_q) \end{aligned} \tag{2.9}$$

L_d is d-axis inductance

L_q q-axis inductance

λ_d is d-axis flux linkage,

λ_q is q-axis flux linkage

λ_m is rotor flux linkage due to permanent magnets,

w_e is rotor electrical speed

θ_e is rotor electrical position

Electromagnetic torque representation in d-q axis is stated in Eq. (2.10).

$$T_e = \frac{3}{2}P\left[\lambda_m i_{qs} + (L_d - L_q)i_{qs}i_{ds}\right] \tag{2.10}$$

2.2.3 Types of Brushless Motors

Brushless DC motors can be classified by rotor structural design and rotor flux direction.

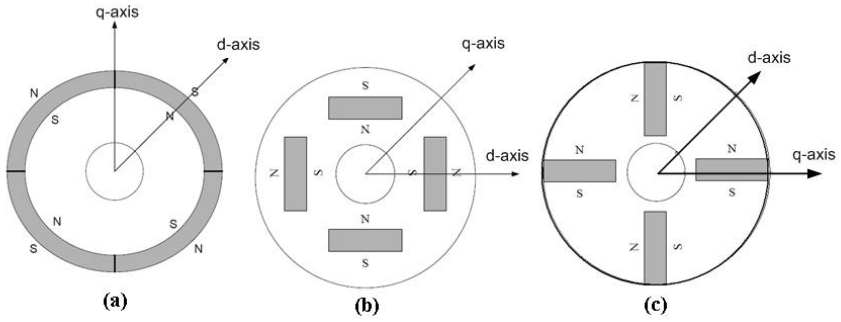

Figure 2-10: Rotor structures of BLDC motors, (a) surface mounted magnets, (b) interior mounted magnets, (c) buried magnets

Classifications based on rotor structures are shown in Figure 2-10. In surface mounted rotor motors magnets are mounted to the surface of rotor. This process is relatively easy and low cost process. Magnets are easily skewed in this type and skewing helps to reduce the torque oscillations (cogging torque) [6]. Also since magnets are on the surface of rotor, air gap can be large and effective and saliency effect is minimized. L_q and L_d inductances are equal and this makes the reluctance torque minimized (Eq. (2.10)). Main drawback of this type is that magnets can detach from the rotor at high speeds.

In interior mounted magnet of motors magnets are inserted inside the rotor rather then bounding the surface. This makes a robust design and motor can operate at high speeds. But due to difference in d and q axis inductances reluctance torque exists in this type of motors. Electrical properties of buried magnet motors are nearly same with the interior mounted magnet machines. In buried magnet

machines fluxes can go through the motor shaft, to prevent these flux non magnetic shafts should be used [8].

Brushless dc motor can also classified in terms of flux direction. Usually brushless dc motors are used in radial flux topology (Figure 2-11). These motors are used in servo applications. Motor axial length is longer and inertia of the rotor is kept small in order to have small response time to load changes.

Axial Flux motors differ from the other types of the motors not for the magnet construction shape but the flux direction and the shape of the motor. Flux goes through the radially from the rotor axe. In axial flux machines flux goes through the axe direction. Also shape of the motor is rather disc type (Figure 2-12).

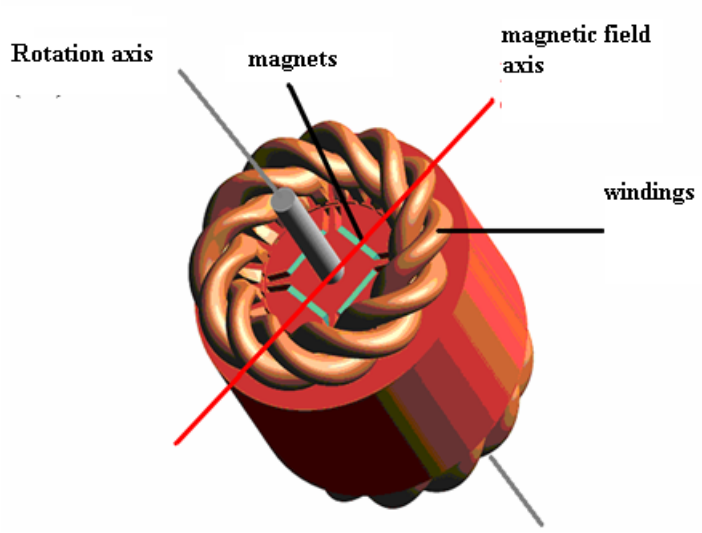

Figure 2-11 Radial flux brushless dc motors

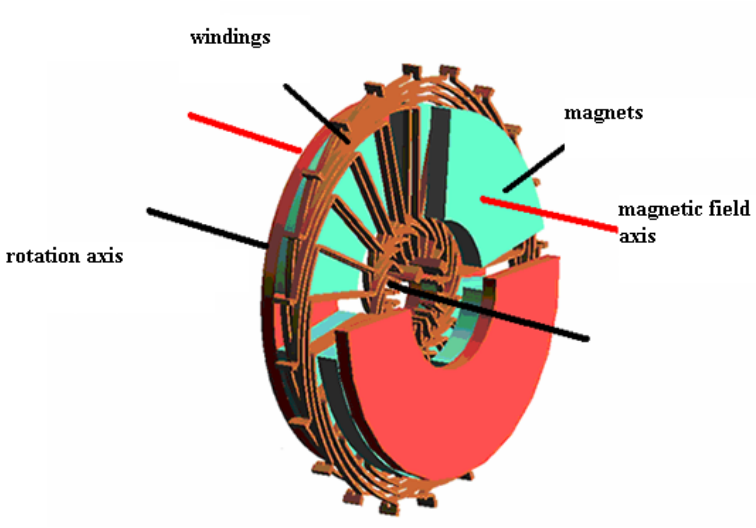

Figure 2-12 Axial flux brushless dc motors

Axial flux machines can be designed as rotor is outside the stator. With this type of design disc type loads can be coupled with the motor. Some times motor is completely inserted into load (i.e. power transmission components [9]). These motors are widely used low torque servo applications. This type of motors are used where small axial space and large radial space is needed.

Main drawback of axial flux machines are presence of two air gaps(In RF type motors there is only one air gap). Mechanical design should be carefully done in AF motors.

2.2.4 General Control of Brushless Motors

For speed control applications brushless motors are controlled through two control loops. First loop compares the actual speed with reference speed and calculates the required current. Since current is proportional to electromagnetic torque current control is used. Using calculated reference current and measured current, reference voltage magnitude is calculated (Figure 2-13 and Figure 2-14).

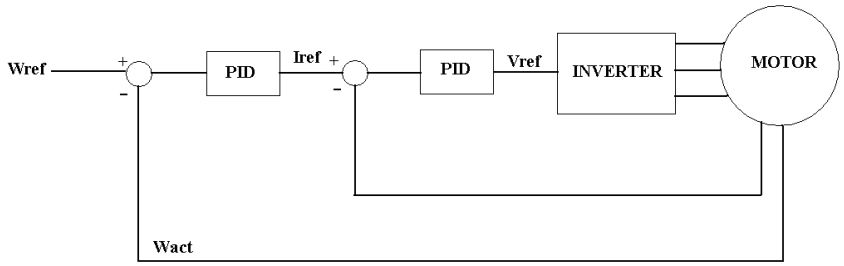

Figure 2-13: Control loops of BLDC motors-1

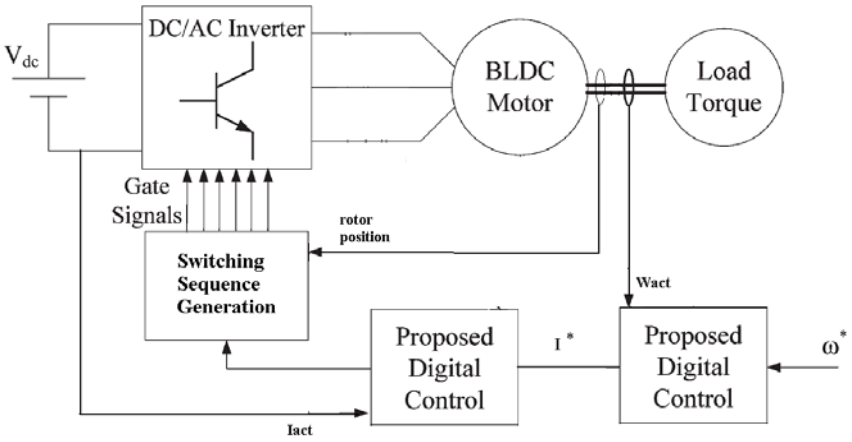

Figure 2-14: Control loops of BLDC motors-2

Reference voltage is applied by the proper switching of the inverter switches. Measured and calculated quantities can be both in stator referenced frame or rotor synchronous frame quantities. In rotor reference frame electrical quantities become constant values and do not change with rotor position or speed. So control in synchronous frame reduces the delay in control architecture.

Brushless DC motors may be classified with their back emf waveform. Back emf waveform of machines can be trapezoidal or sinusoidal. Motors with sinusoidal back emf sometimes called permanent magnet synchronous or ac motors.

Generation of back emf voltage is related with the rotor flux linkage with stator windings. Magnitude of emf is dependent on the rotor speed. Shape of the back emf is related to rotor magnet shape design and stator winding design.

Brushless dc motors waveform of the back emf is typically trapezoidal. This result form nearly constant flux density along the rotor surface. A constant torque can be obtained by controlling the current to be distributed to the individual phases so as to coincide with the back emf as shown in Figure 2-15. Note that it is only necessary to keep the 120^0 current pulse centered on the back emf wave [5] and this method is called as square wave exciation.

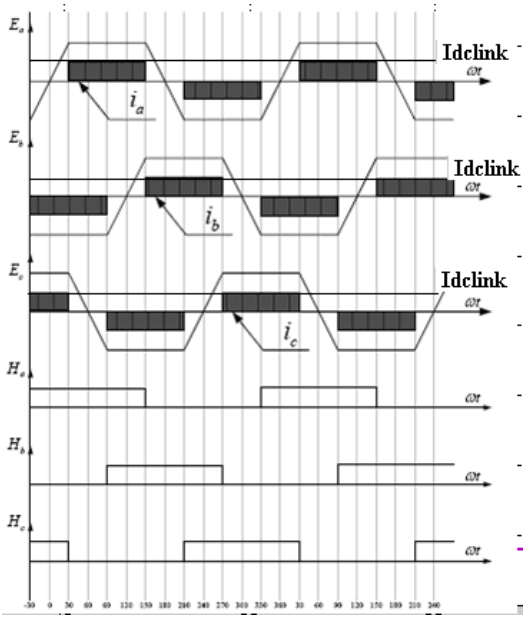

Figure 2-15: Square wave excitation back emf-current-hall sensor

Control of the motor is much simpler than sinusoidal excitation since only indication of the center of the back emf wave is required. Most common method is the use of three Hall sensors to provide timing pulses for the three phases. Magnitude of torque can be adjusted by controlling the dc link current.

BLDC motors of this type are field oriented in the sense that field flux and stator currents (or Magneto Motive Force) are held to a fixed relative spatial position [5]. Conduction angle for each phase current is 120^0. In ideal case using 3 phases uniform torque is maintained through 360^0 rotation. But current can not go to zero while at the end of the conduction because of phase inductance (Figure 2-16) and some torque ripple is observed in this type of control (Figure 2-17).

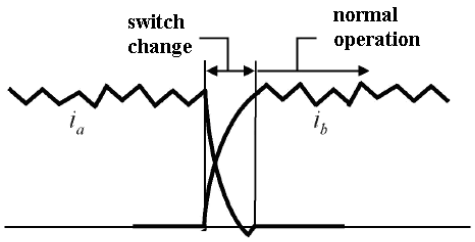

Figure 2-16: Phase current waveform

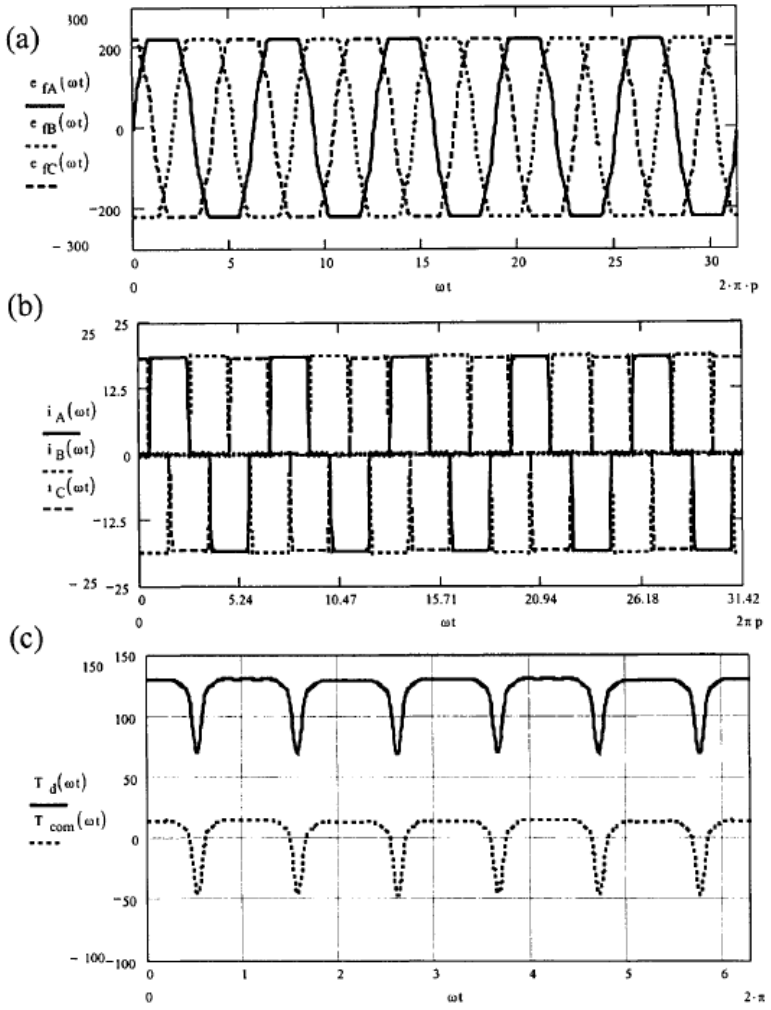

Figure 2-17: Square wave excitation back emf- current torque [8]

Brushless dc motors with sinusoidal back emf waveforms are usually controlled with sinusoidal currents. Shape of back emf waveform is dependent on winding configuration and magnet shape. In order to have sinusoidal back emf fractional pitch windings and shape of the magnets can be optimized. Main advantage in sinusoidal excitation is to have uniform torque characteristic. Since 3 phases are excited at the same time and current waveforms are sinus torque is more smooth and no ripples very smaller than trapezoidal back emf and square wave excitation case.

In order to obtain sinusoidal current waveforms motor voltages should be applied in a proper way. In sinusoidal excitation case reference currents are time varying. Usually dq axis is used in order to control these motors. In order to have maximum torque from the motor most common method is field oriented control .

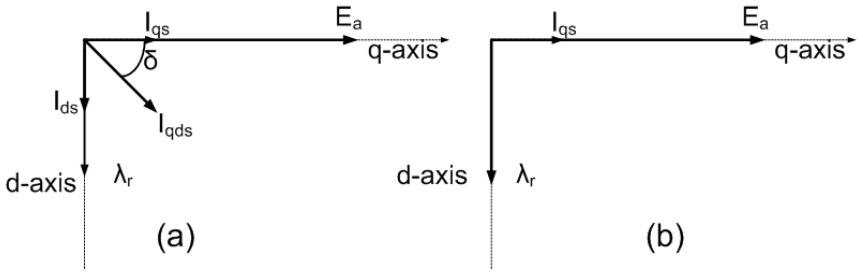

Figure 2-18 (a) Phasor diagram of BLDC motor, (b) field oriented case

Field orientation is defined as angle between stator currents and back emf voltage is zero (Figure 2-18 (a) Phasor diagram of BLDC motor, (b) field oriented case). Since PM creates flux at d axis there is no need to have a current component at d axis, all stator currents are used to create q axis current and torque is maximized in this control structure. In order to create currents at q-axis there phase currents should be controlled. Relation between the motor currents and dq axis motor currents are shown in Eq. (2.7). In trapezoidal back emf machines six different rotor positions are enough to maintain square current waveforms. But in sinusoidal excitation case more resolution in the motor position information is required in order to make the transformation form dq reference frame. More complex control techniques and high resolution sensors (encoders etc) should be used for proper excitation of sinusoidal back emf motors [6]. Back emf, current waveforms and resultant torques in sinusoidal brushless machines are shown in Figure 2-19.

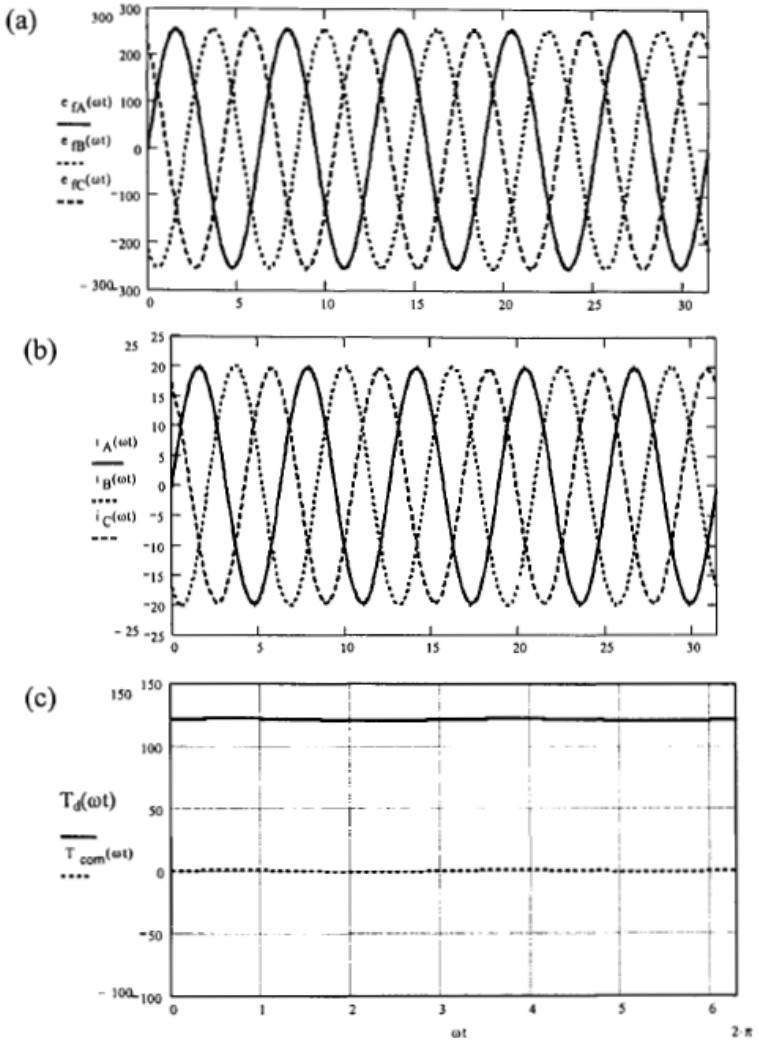

Figure 2-19: Sinusoidal excitation back emf- current torque [8]

CHAPTER 3

SELECTION OF MOTOR AND MATERIALS FOR CMG APPLICATIONS

3.1 Introduction

In this chapter definition of problems in existing CMG prototype is presented. Performance requirements are defined for particular CMG application. Then a summary of materials are included in materials overview part and some materials are selected in order to use in the design process. For suitable motor selection an overview of literature is presented. At last part of this chapter torque equations will be studied in terms of motor dimensions and general design inputs such as electrical loading and air gap magnetic flux density.

3.2 Definition of the Problem

As stated in Chapter 2, this thesis is focused on the wheel motor design of CMG. Gimbal motor is rotating with relatively low (1-10 RPM) speed so power consumption is less then the wheel motor. Wheel motor is determining power consumption volume and mass of the CMG. Wheel motor is operating at very high and constant speed. After a short acceleration time of 1-2 minutes, only load factor is the wheel friction torques (windage and bearing frictions).

Figure 3-1 shows the prototype which is already built. This thesis is mainly focusing on the improvement of the prototype's performance in terms of mass, volume and efficiency.

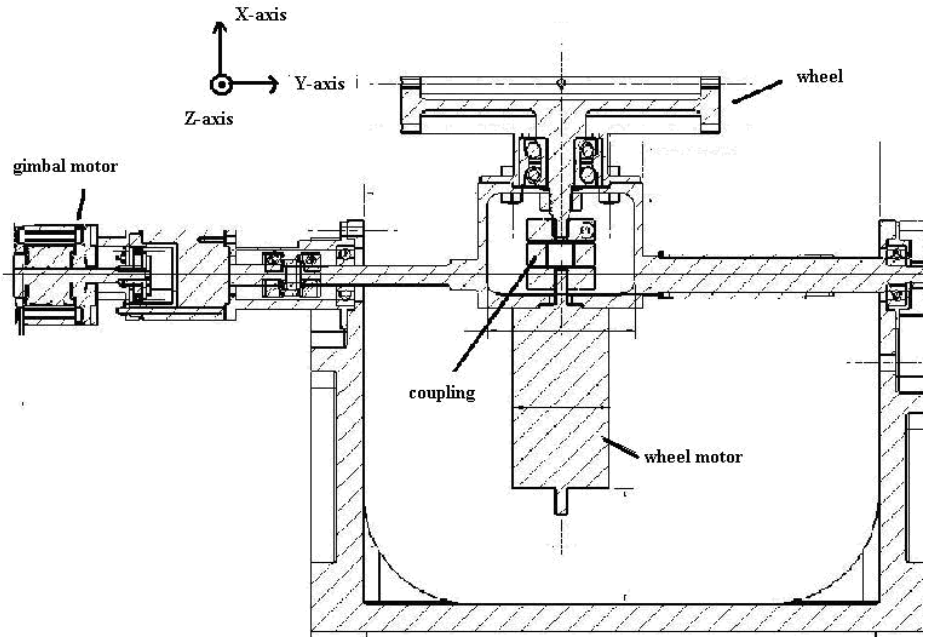

Figure 3-1: CMG prototype

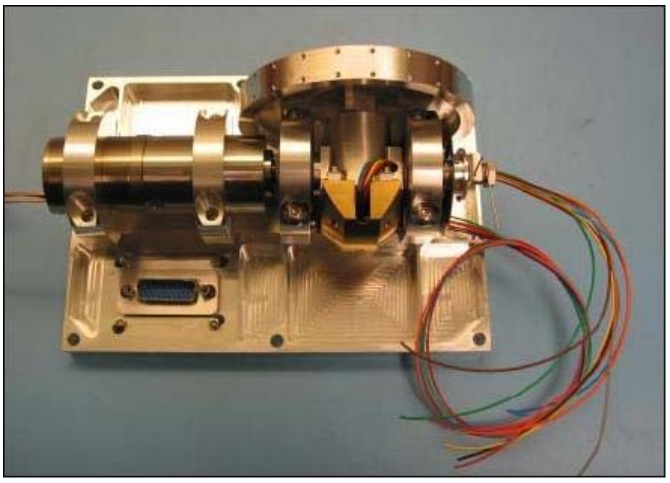

Figure 3-2: CMG built by SSTL

Figure 3-2 shows another CMG developed by SSTL. Although different solutions exist all fundamental working principle is same.

As stated before main power consumption is due to the wheel motor owing to its high speed requirement. (%80 of total power consumption)

Problems in CMG prototype is raising from the commercially available motor usage. Inertia and the speed of the wheel are determined by CMG's satellite level requirements. In order to reach high speeds commercial motors are usually servo type. In order to reach high speeds and have quick response to load changes servo motor are long in axial direction to have low inertia (sausage type). These motors are connected to wheel with a coupling since diameter of bearings is small and usually not designed for large inertial loads. This solution results in balancing problems because there are 3 bearing points and the bearings have long distances between each other.

This type of design also increases the power consumption in CMG gimbal motor. Due to the sausage type motor usage mass is distributed along the X-axis. Gimbal motor is rotating along the Y axis. Sausage type motors causes higher inertia values along the Y axis. Torque obtained from the CMG is dependent on inertia of the wheel, angular speed of the wheel and angular speed of gimbal (Eq. (2.2)). Inertia at Y axis has no contribution to the output torque. Gimbal motor has variable speed characteristics between 1-10 RPM (Figure 3-3) and the rotation axis of gimbal motor is Y axis. High inertia results in high acceleration and deceleration torque in gimbal motor control. So power consumption of gimbal motor is high due to high inertia in Y axis. Furthermore high volume and mass is required for proper geometrical design as seen in Figure 3-1.

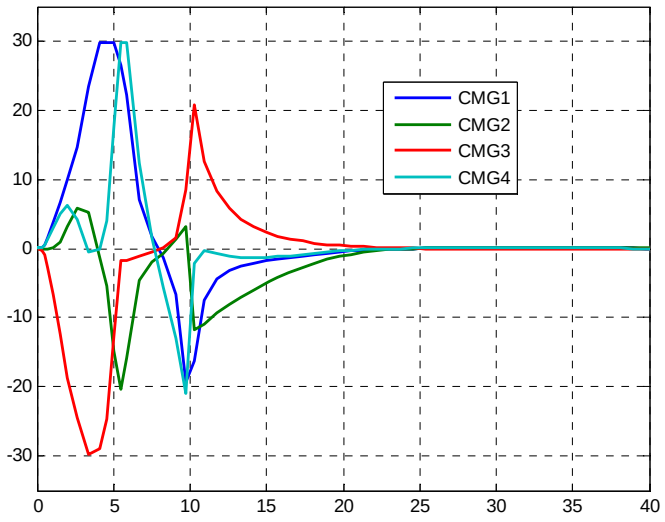

Figure 3-3: CMG cluster gimbal motor speeds (deg/sec vs sec)

Second problem of using commercial motor is the design constrains of motors. Commercial motors are usually designed for different type of load conditions. For example for CMG wheel motor application there is no requirements for high starting torque. Wheel should increase to its maximum speed around 2 minutes and there are no additional load conditions due to external disturbances. Only disturbance is due to friction torques. Commercial motors are usually designed for dynamic load conditions so they can be over designed in terms of mass and volume. It is again difficult to find the exact torque and speed requirements match with a commercially available motor. Also operating point may not match with the motors design constraints so efficiency can be lower.

Problems in current design can summarized as follows

- Balance problem due to 3 bearing points
- High mass and volume due to geometrical design for installation of sausage type wheel motor

- High inertia in gimbal motor rotation axis, high power consumption in gimbal motor
- Mass and power consumption increase in wheel motor due to the difference between wheel motor requirements and of commercial motor design constrains

3.3 Definition of the Problem and Design Requirements

3.3.1 Functional Requirements

Target system is selected as existing CMG prototype for the design of wheel motor .As stated in Eq. 2.2, wheel speed and wheel inertia has an effect on CMG torque production. Requirements coming from CMG level are defined in Table 3-1.

Table 3-1: CMG system level performance requirements

Parameter	Value
Inertia of rotating part (wheel + rotor) (kgm^2)	4.83×10^{-4}
Mechanical speed of the motor RPM	10000
Acceleration time	35 seconds - 2 minutes

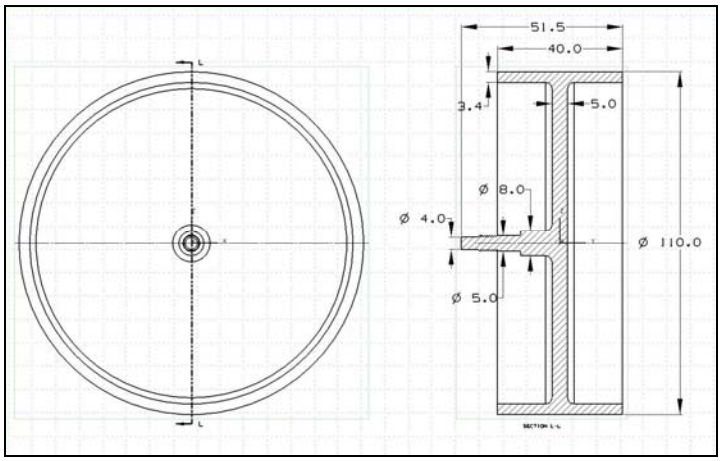

Figure 3-4: Mechanical details of wheel (dimensions are in mm)

In the prototype system wheel mechanical design is optimised to have high inertia with low mass (Figure 3-4). In this thesis, there are two main points, first is study of a new motor to have less axial length and second is study of whether there is a possibility to integrate the wheel and motor system together. This wheel can be modified in order to integrate the wheel and motor. This may increase the mass of the wheel, but in already designed CMG mass of motor also included to total system (390g). In order to make an integrated wheel motor wheel shape and mass can be changed. Only critical value is the total rotating inertia of the wheel because this parameter is coming from CMG performance requirements.

In addition to CMG level requirements an important parameter for motor design is the amount of torque that the motor should supply in order to keep constant nominal speed. After the acceleration time motor is operating at constant speed and only load torque observed is the load torque based on friction. In CMG prototype three different types of motor and mechanical coupling and bearing are used. For each combination different friction torque values are observed (Figure 3-5).

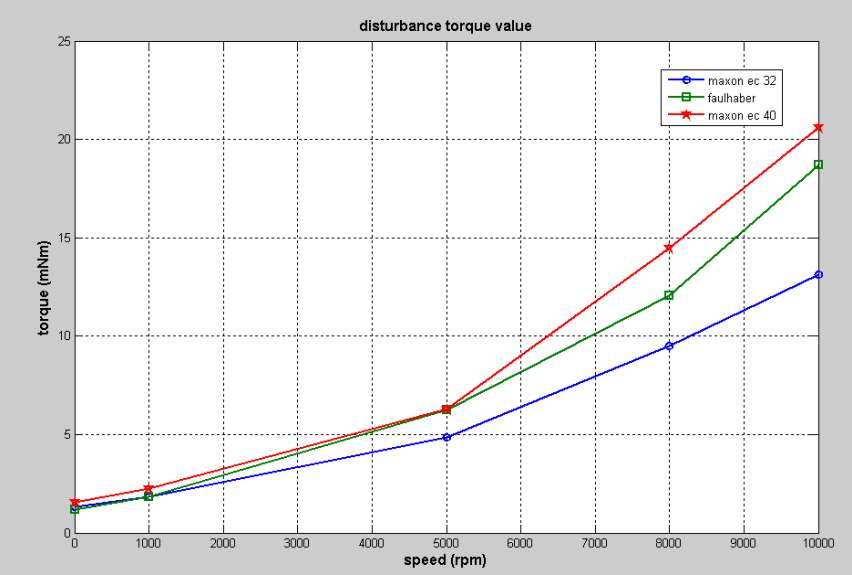

Figure 3-5: Friction torque values for different type of motors

These disturbance torques are coming from bearings and the air friction. Difference between the motors are arising from the coupling and bearings used. Also these values are determined after the bearings are warmed up; while bearings are cold some margin should be added for toque requirement. In addition to constant speed disturbance torques acceleration torque should be considered for determining the torque requirement. Acceleration constraint for the wheel is quite long. Motor should raise its nominal speed under 2 minutes. So necessary acceleration torque application time is very small but it should be also taken into consideration. This issue will be explained later in this chapter.

Table 3-2 summarizes the wheel motor system requirements and values achieved in existing CMG prototype which is using MAXON EC32 type brushless dc motor.

Table 3-2: Summary of parameters in CMG prototype

Parameters	Value in CMG prototype
Inertia of the wheel kg/m^2	4.83 x10^{-4}
Angular speed of the wheel (RPM)	10000 RPM max
Acceleration time	35-120 seconds
Mass of the wheel and wheel motor (g)	503 (263 motor+ 240 wheel)
Efficiency of the motor	% 78
Operating temperature range(C^0)	-20 to +65
Operating voltage (V)	18-33
Torque requirement	32mNm nominal (50mNm max)
Application type	Constant speed, continuous operation
Special Requirement	Ability to operate under 360^0 rotation along an axis which is perpendicular to motor rotation axis.

3.3.1.1 Determination of Motor Torque Characteristics

In order to start to motor design first required torque characteristic should be defined. This torque speed curve should be enough to increase wheel speed to 10000 RPM less than 2 minutes. In this part friction or load torque of motor will be studied and additionally required torque speed curve to have enough acceleration characteristic is determined.

Since it is the starting point we will use the parameters of the Maxon EC32 118892 data. Since this motor is used in CMG prototype and successful we will define the motor torque requirements based on this motor. As it can be seen from Figure 3-5, friction or load torque of motor is changing based on selected bearing type and whether the bearings are warmed or not. As design input Maxon EC32 motor worst case characteristic is taken (Figure 3-6). This friction torque is measured when bearings are not warmed up.

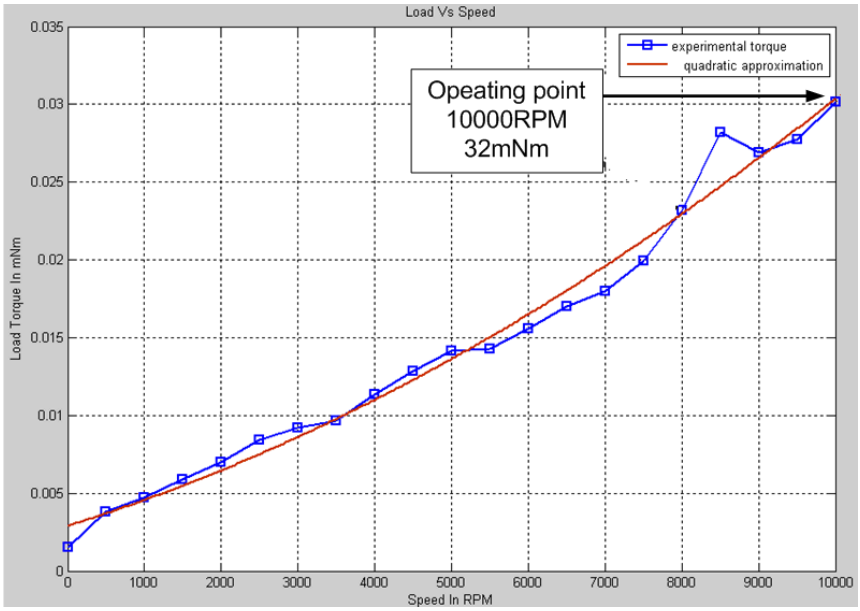

Figure 3-6: Motor load torque due to friction

Since measurements are done from the current and torque is calculated from motor torque constant, load (friction) torque is approximated a quadratic approximation in order to use in determination of acceleration.

As mentioned before motor should reach a speed of 10000 RPM in less than 2 minutes and motor should keep its speed constant at 10000RPM.

In order to determine motor torque characteristic acceleration requirement should be taken into consideration. Motor torque characteristic is expressed in the equation Eq. (3.1).

$$Tm = T_{acc} + T_{load} = J_{wheel}\frac{dw_m}{dt} + T_{load} \tag{3.1}$$

T_{acc} acceleration component of motor torque in Nm

J_{wheel} inertia of the wheel kg/m^2

T_m required motor torque

w_m mechanical speed of motor

Using Eq. (3.1) it should be determined that how the motor torque profile is to be applied to reach acceleration in 2 minutes. Since CMG is not operational in this starting period shorter acceleration times less than 35 seconds is not recommended from the satellite level. It should be taken into consideration that a control algorithm is to be used for acceleration and compensator delays should be added to the acceleration time.

Torque profile should be applied such as motor will reach its max speed in 35-120 seconds. There are two ways to obtain the acceleration time. First way is to change the peak torque of the motor, and second is to change the peak torque application time. If we apply more torque required volume and mass of the motor will also increase and this is not preferred since main aim is reducing the mass and volume. Second alternative is limiting the peak torque and changing the application time of peak torque, this choice should be studied whether temperature of windings stays in a reasonable value.

Figure 3-7 shows a block diagram which is prepared in Matlab Simulink software using Eq. (3.1). Different motor torque vs. speed characteristics are loaded into the Lookup motor torque block. This block takes the motor speed and gives a motor torque value. 5 different motor torques vs. speed curves are applied into motor speed transfer function. Speed transfer function is a simple integrator with a coefficient of 1/inertia of wheel. In the same manner Load calc block computes the motor friction torque using the motor speed instantaneously according to motor load (friction) profile at Figure 3-6. The difference between motor torque and load torque is acceleration torque and applied to an integral block (speed transfer function block) to calculate the instantaneous motor speed according to Eq (3.1). Figure 3-8 shows two different motor torque-speed profiles which are applied to motor. These profiles are applied to have settling time at two limits of acceleration time (maximum and minimum acceleration duration).

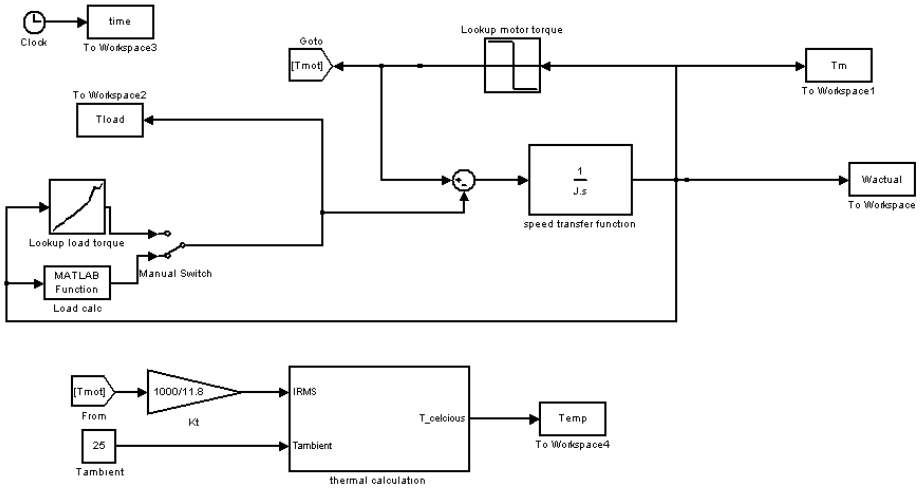

Figure 3-7: Motor torque profile calculation clock diagram

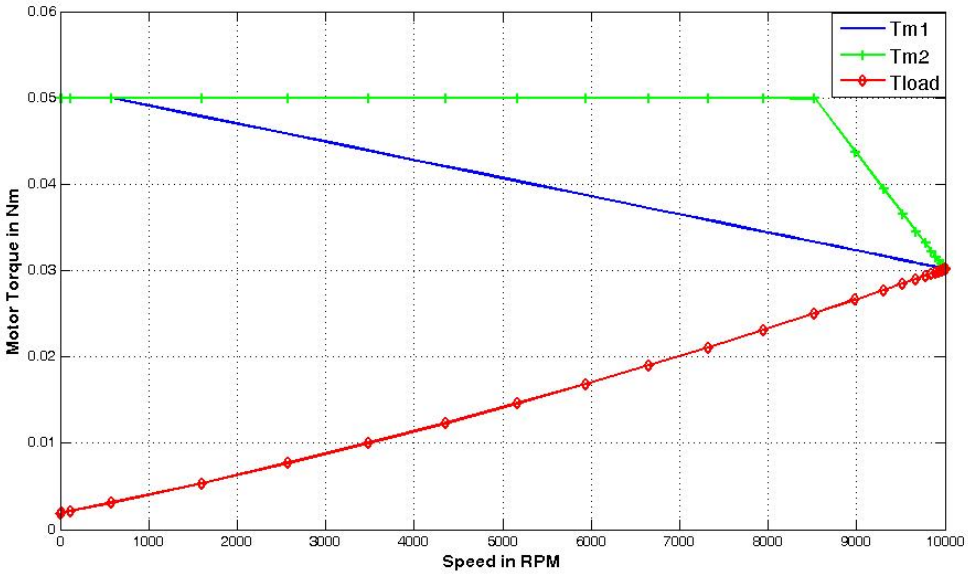

Figure 3-8: Motor torque profiles and motor load torque

Different motor torque profiles results different motor acceleration characteristics. Figure 3-9 gives the acceleration profiles of motor under different motor torque characteristics.

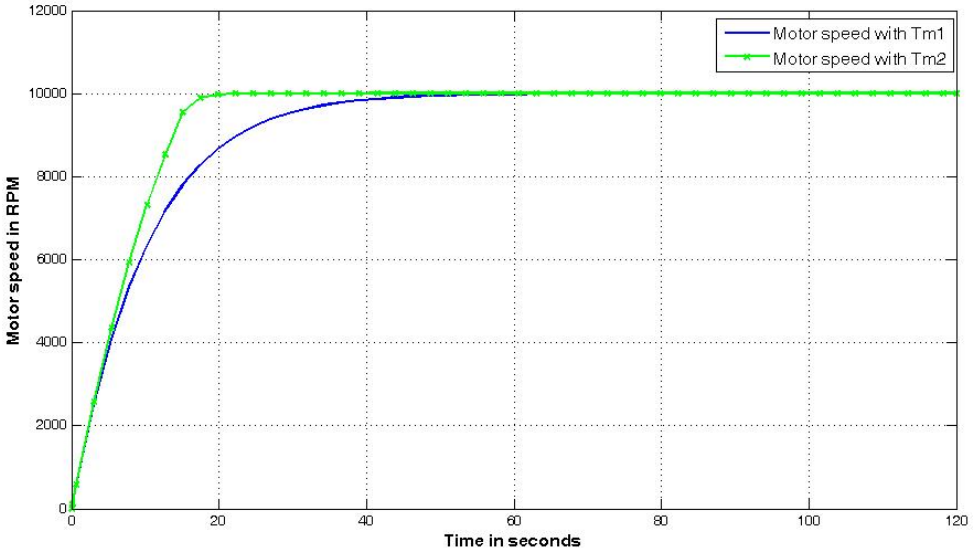

Figure 3-9: Motor speeds vs. time characteristics

As it can be seen from Figure 3-9 both motor torque characteristics have an acceleration time between 20-80 seconds. After reaching 10000 RPM motor torque becomes equal to load torque and speed is constant. In order to control these torque profile may cause any problem related to heating of motor is studied from now on. Temperature rise in different motors will be different based on the properties of motor. But it is assumed that a rough estimate for temperature rise of motors which will be considered in this thesis can be done with the existing Maxon motor characteristics. Most critical issue is whether the coil insulation level can survive under the power dissipation on the coil during acceleration or steady state.

In order to find the motor current torque constant is used which is stated in the data sheet of the Maxon EC32 118892 motor. This motor is used in CMG prototype.

$$T_m = K_t \times I \tag{3.2}$$

K_t is motor torque constant Nm/A(11.8×10^{-3})

I is DC link current and also peak value of the motor phase current under square wave excitation.

By using Eq. (3.2) and defined motor torque profiles expected motor current waveforms are calculated and results are shown in Figure 3-10.

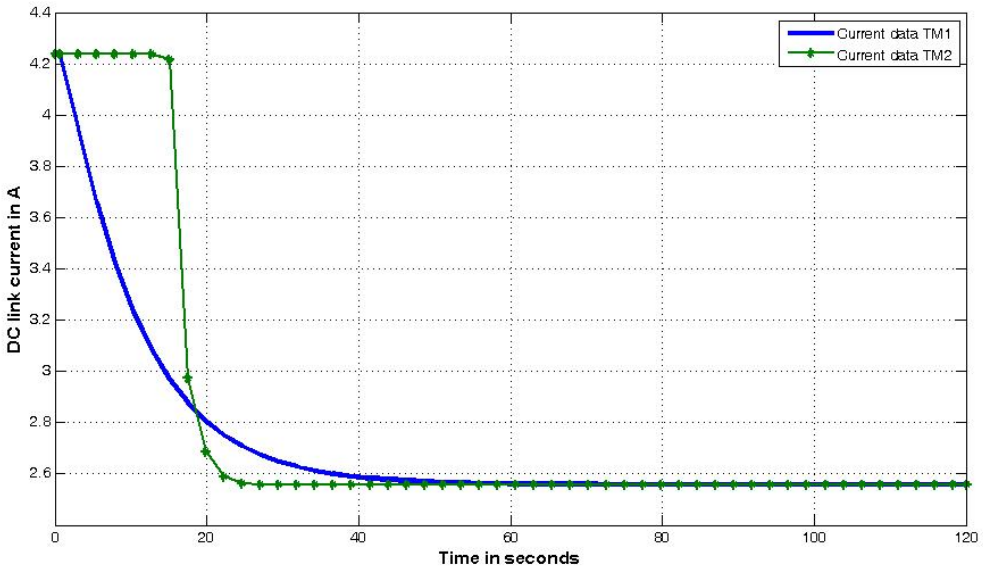

Figure 3-10: Motor current vs. time

In the data sheet of Maxon EC32 motor it is stated that all the parameters are taken square wave excitation.

Figure 2-15 shows the current waveforms under square wave excitation. Each interval motor two phases is conducting and dc link current is passing from the motor active motor phases. Using this information copper loss is calculated using Eq. (3.3).

$$P_{loss} = I^{2} \times R_{phasetophase} \tag{3.3}$$

P_{loss} is motor resistive losses (copper loss)

$R_{phasetophase}$ is motor phase to phase resistance (due to two phase is conducting each interval)

With the help of Eq. (3.3) and current values in Figure 3-10, motor resistive loss values are calculated and results are shown in Figure 3-11.

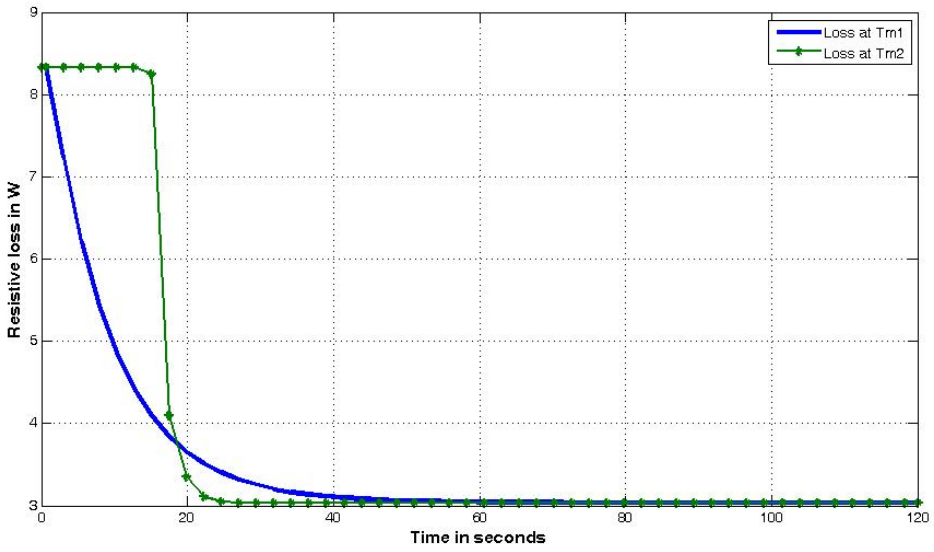

Figure 3-11: Motor Resistive losses vs. time

This motor will be designed to operate at constant speed and continuous duty. Figure 3-11 shows that steady state cupper losses will be constant and equal to 3.05W. At steady state cupper losses will be constant for all motor torque profiles. At acceleration period all motor torque profiles has same average and peak power

consumption. Difference is the duration of power loss which is settling time. Duration of acceleration time has an impact on motor winding temperatures. The transient (acceleration period) and steady state values of winding temperatures should be examined in order to see whether temperature of the winding cause problem on insulation.

In order to calculate the winding temperature vs. time simplified equivalent circuit of motor (Figure 3-12) and thermal balance equation (Eq. (3.4) [12]) is used.

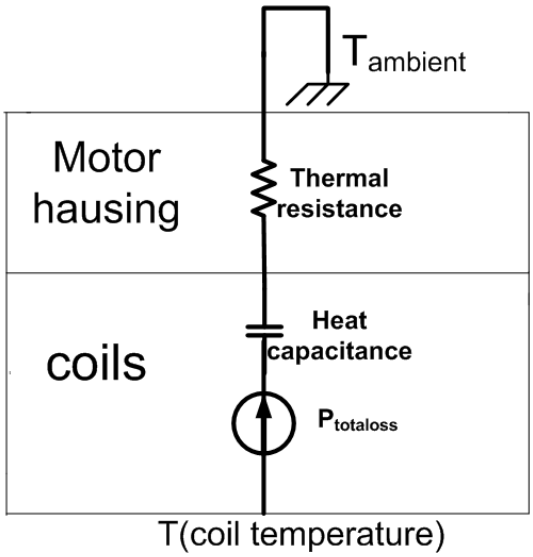

Figure 3-12: Simplified equivalent circuit of motor

$$mc\frac{dT}{dt} = P_{totalloss} - Q$$
$$mc\frac{dT}{dt} = I^2 R_{phasetophase} + P_{core} - (R_{coil-housing}^{-1} + R_{housing-ambient}^{-1})(T - T_{ambient}) \quad (3.4)$$

m is mass of the winding in g.

c is heat capacity of cupper (J/g ^{0}C)

$\frac{dT}{dt}$ is rate of change in the winding temperature ^{0}C

Q is amount of power by conduction and convection to ambient (W)

$R_{coil-housing}$ is thermal resistance coil to motor housing (K/W or ^{0}C/W)

$R_{housing-ambient}$ is thermal resistance motor housing to ambient (K/W or ^{0}C/W)

T is instantaneous coil temperature

$T_{ambient}$ is ambient temperature

P_{core} is total loss on motor

$P_{totaloss}$ is total loss on motor

Mass of the cupper wire should be calculated because we have no information in the data sheet. Eq. (3.5) is used for calculation of mass of the motor winding.

$$m = L\pi(\frac{Dc}{2})^2 d$$

$$R_{phasetophase} = \rho\frac{L}{A} \qquad (3.5)$$

$$L = \frac{R_{phasetophase}A}{\rho}$$

m Mass of the wire in g.

L Length of the wire in m.

ρ Resistivity of the cupper ($8.94\text{x}10^{-6}$ g/m^3)

A Area of the cupper

Dc diameter of the cupper (AWG 22 wire diameter is $0.644\text{x}10^{-3}$ m from data sheet)

d density of cupper $8.94\text{x}10^{-6}$ g/m^3

Mass of the coils (phase to phase) is calculated as 25.58g. Core loss is another required parameter and it is difficult to measure exact value since materials used in Maxon EC 32 is not known. It is assumed that core material is cogent power no 12 non oriented steel and mass of the stator is 130 g (1/3 of total motor weight). Using the core loss approximation defined in 4.3.3, core loss is calculated over speed range.

By using power dissipation information (resistive and core losses) and parameters summarized in Table 3-3 Equation (3.4) is simulated in Matlab Simulink software.

Table 3-3: Parameters used in thermal equation

Parameter	Value	Reference
m	25.58g	Calculated value using copper constants
c	0.385 J/g ^{0}C	Physical property of copper
$R_{coil-housing}$	2.5 (K/W or ^{0}C/W)	From the data sheet of Maxon EC32
$R_{housing-ambient}$	5.4 (K/W or ^{0}C/W)	From the data sheet of Maxon EC32
$T_{ambient}$	65^{0}C	Worst case ambient temperature

Calculated coil temperature values are shown in Figure 3-13. Since steady state current consumption is same and steady state temperature values are same for different motor torque characteristics. Only difference is observed at acceleration period.

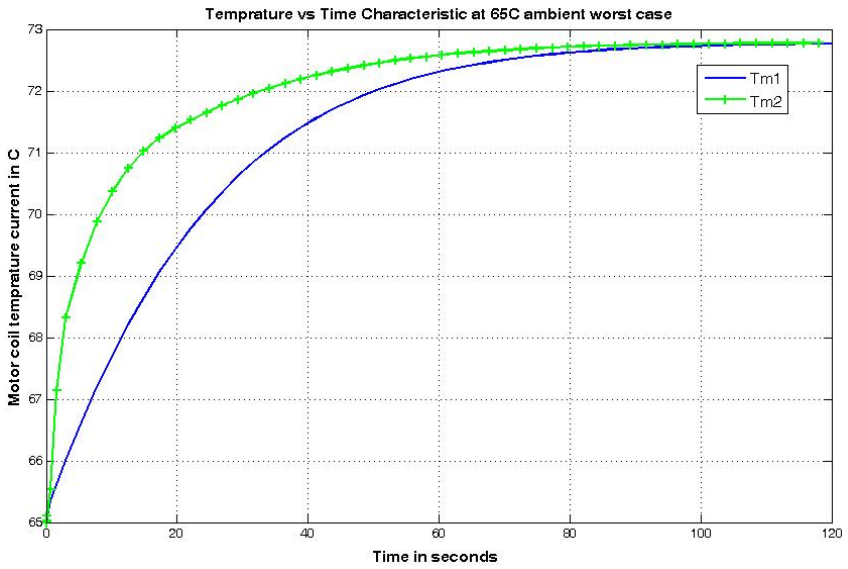

Figure 3-13: Motor coil temperatures vs. time at 65 ^{0}C

Motor winding isolation should be capable of withstand the temperature rise at worst case. Maxon EC 32 maximum permissible winding temperature is 125 ^{0}C, both motor torque profiles are convenient from the temperature point of view. Table 3-4 summarizes five different motor torque characteristics.

Table 3-4: Summary of motor torque profiles

Parameters	Tm1	Tm2
Max. torque	50mNm	50mNm
Max. torque application time	0.65s	12.5s
Settling time	74s	26s
Max Resistive loss	8.33W	8.33W
Resistive loss at steady state	3W	3W
Core loss at 10000RPM	1.52W	1.52W
Maximum temperature of winding at 25 ^{0}C	32.8^{0}C	32.8^{0}C
Maximum temperature of winding at 65 ^{0}C	72.8 ^{0}C	72.8 ^{0}C

Obtained results show any motor torque profile between Tm1 and Tm2 have a settling time less than 120 seconds and motor temperature remains in safe side. Also peak value of motor torque profile can be less than 50mNm, but bearing performance at -20 ^{0}C is not known. Bearing friction can be more at low temperature especially if CMG is not used for long time. In order to keep margin for low temperatures motor peak torque is kept at 50mNm and a motor torque profile which has 60 seconds settling time is selected as design input value (Figure 3-14).

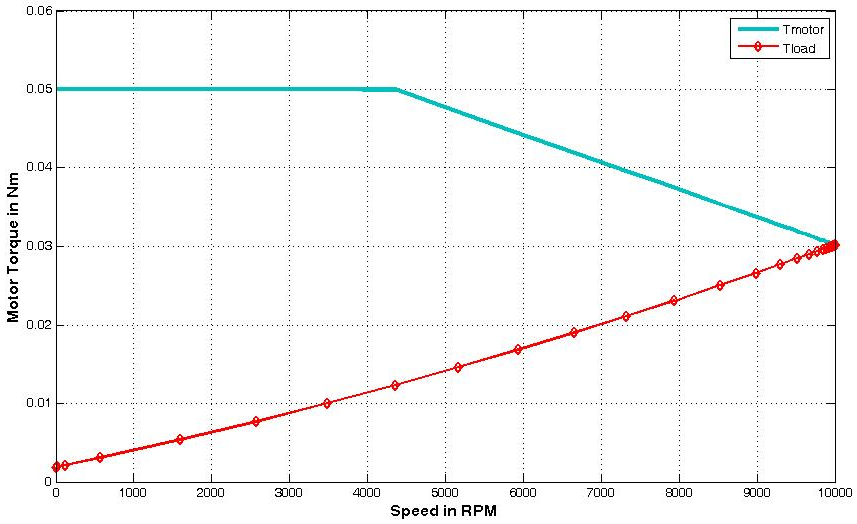

Figure 3-14: Selected motor torque profile and motor load torque

3.4 Material Definitions and Selections

3.4.1 Permanent Magnets

3.4.1.1 Overview

Permanent magnets are materials which can produce magnetic field in the air gap of machines. Due to this capability there is no need to field winding also electrical

loss in field winding is eliminated. External energy is used only changing the energy in the magnetic field not in maintaining it. All magnetic materials are described with their B-H curves (Figure 3-15). PM are called hard magnetic materials, meaning that materials that has wide hysteresis loop on their B-H curve.

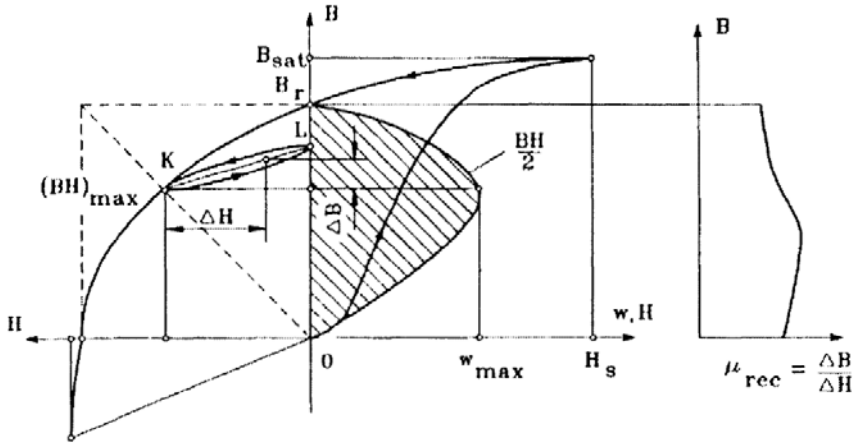

Figure 3-15: B-H curve of a PM [8]

Upper left quadrant of the B-H curve is used (demagnetization curve) while evaluating the PM. If reverse magnetic field intensity is applied to a previously excited magnetic material, the magnetic flux density drops down to point K in Figure 3-15. If reverse field is removed, magnetic flux density rises up to point L again. This reversal magnetic field reduces the remanence or remanent magnetism. If we repeat this action a minor hysteresis loop occurs, and this loop can be approximated by a straight line with a slope called recoil permeability.

If applied reverse magnetic field intensity does not exceed the magnetic field density at point K, PM can be assumed as reasonably permanent. If it exceeds point K, magnetic field density can not return to point L, result will be a new recoil line is established with a lower magnetic field.

In electrical motors PM magnets are used with a magnetic circuit. Due to contribution of ferromagnetic material there exists an additional flux density B_i.

$$B = \mu_0 H + B_i \tag{3.6}$$

Details of magnetic circuit will be examined in Chapter 4. Some basic parameters of PM B-H curves are explained below.

Saturation magnetic flux density B_{sat} corresponds to saturation magnetic field intensity H_s, at this point all magnetic moments are aligned with external field.

Remanent flux density B_r or remanence is the magnetic flux density corresponding to zero magnetic field intensity. High remanence means magnet can support high magnetic flux density in the air gap of the magnetic circuit.

Coercive field strength H_c or coercivity is the value of magnetic field intensity that brings the magnetic field density to zero. High coercivity means thinner magnet can be used to withstand the demagnetization field.

3.4.1.2 Properties and Types of Permanent Magnets

There are three types of PMs used in electrical motors.

- Alnicos(AL, Ni, Co, Fe)
- Ceramics ferrites ($BaOx6Fe_2O_3$ and $SrOx6Fe_2O_3$)
- Rare-Earth PMs (Samarium cobalt and neodymium boron)

B-H curves of these three types at 20 ^{0}C are shown in Figure 3-16.

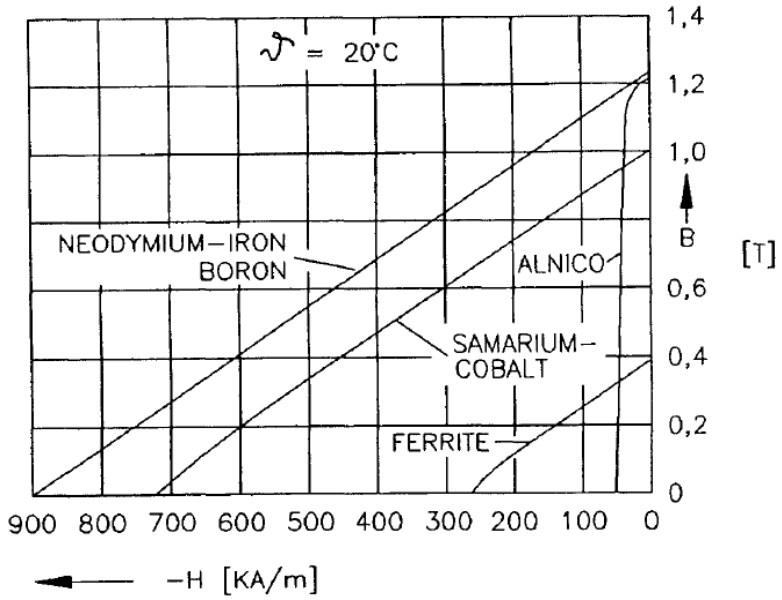

Figure 3-16: B-H curves of different type PMs [8]

Alnicos and ferrites are relatively old technology materials used in the past. After 1970s great process has been achieved with the Rare earth permanent magnets. Rare-Earth PMs (Samarium cobalt and Neodymium boron (after 1980s)) have higher remanent flux and coercivity with respect to previous PMs. SaCo has better BH characteristic but problem is its cost is high because of used Sa and Co. Neodymium boron has high coercivity and higher remanent flux than SaCo and it is cheaper. Main drawback of this PM is the temperature sensitivity (Figure 3-17) and weakness due to corrosion.

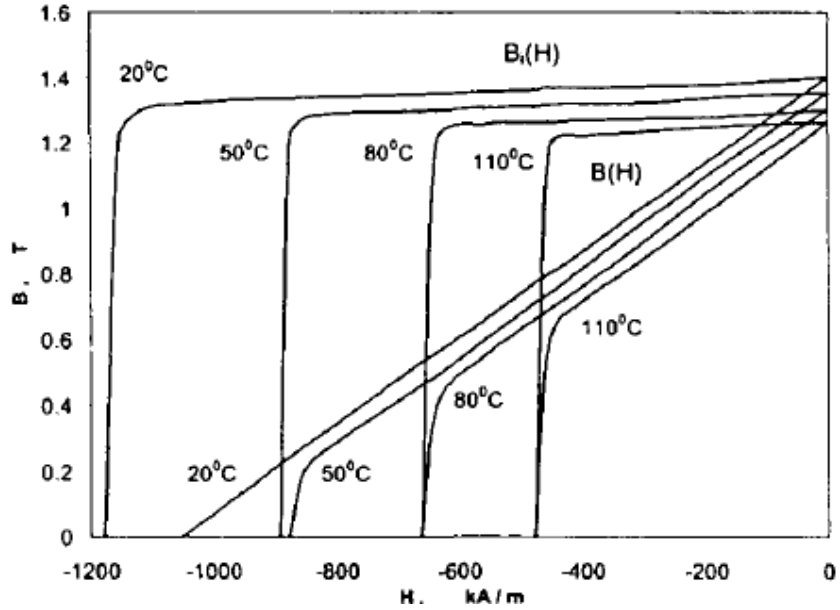

Figure 3-17: Temperature dependence of Neodymium boron [8]

B-H characteristic of PMs are dependent on temperature. B_r and H_c are decrease with increasing temperature and Eq. (3.7) shows the relation of B_r and H_c with temperature.

$$B_r = B_{r20}(1+\frac{\alpha_B}{100}(T_m - 20))$$
$$H_c = H_{c20}(1+\frac{\alpha_h}{100}(T_m - 20)) \quad (3.7)$$

α_B and α_c are temperature coefficients (% chance in per ^{0}C rise in temperature) of coercive field strength and remenant flux density

H_{c20}, B_{r20} are coercive field strength and remenant flux density values at 20 ^{0}C

3.4.1.3 Selection of Permanent Magnet

In order to make a permanent magnet selection for CMG motor application main selection criteria is the thermal characteristic of PM. As stated before rare earth magnets have better BH characteristics than alnicos and ferrites. Selection is done between two types of PM SaCo and NeB.

Although Neodymium boron has better BH characteristics then other types it has strong temperature dependence, since motor in this thesis should operate in a time varying temperature cycle (-20 to 65 ^{0}C) a better thermal characteristic is needed. CMG is operating in a continuous temperature interval of 85 ^{0}C. NeB Br value is changing two times more than SaCo. Since air gap magnetic field density is reduced with temperature (%12.5 for NeB Table 3-5) motor may not give enough torque but since design in this thesis is done with enough margins this situation is acceptable. Second issue is the temperature limits of magnets. PM materials has two temperature limits. First limit is Curie temperature defined as permanent magnets loose all of its magnetic properties (Br and H is 0). This temperatures are very high for SaCo (800 ^{0}C) and NeB(330 ^{0}C). In nominal operating conditions CMG is not face with such high temperatures if satellite thermal control system does not have an anomaly. Second limit is defined as maximum continuous service temperature. This temperature limit is defined as maximum temperature that PM characteristic is same if temperature is rise form certain temperature to another and reduce to initial temperature again. Another words if PM temperature becomes larger than service temperature for a definite time its magnetic properties changes and it will not have same BH curve even temperature reduces below the service temperature. Maximum service temperature of NeB is around 100-110 ^{0}C and this value can be seen on satellite for small tie intervals during early phases of satellite mission (launch and satellite initialization phases). SaCo has a maximum service temperature of 300-350 ^{0}C .

Table 3-5: PM properties

Property	Alnico	Ferrites	Samarium cobalt	Neodymium boron
B_r	1.22	0.4	1-1.10	1.21-1.35
H_c	50	250	720-820	900-1040
α_B in % / ^{0}C	-0.02%	-0.20%	-0.03%to-0.045%	-0.09% to -0.15%
Change in Br in CMG operating interval (-20 to 65 ^{0}C)	%1.7	%17	%2.25-%3.4	%7.65 to12.75
α_c in % / ^{0}C	-0.02%	-0.27%	-0.14% to -0.40%	-0.40% to -0.80%
Max. continuous service Temperature ^{0}C	520	400	300-350	100-120

SaCo magnets have a better thermal characteristic. Another advantage of SaCo is its high resistance against corrosion. NeB magnets are sensitive against corrosion and surface of NeB magnets should be coated against corrosion, especially for space applications more complex surface treatments and material selection should be done for NeB magnets. Table 3-6 shows two samples of commercial PM samples of SaCo and NeB. As summarized before Vacomax 225 samarium cobalt has better thermal performance, also its thermal conductivity is larger which means heat removal is easier than Vacodym 633HR.

While selecting magnets another important selection criteria is radiation resistance. Amount of radiation in aerospace applications are dependent on orbit and shield around the material such as satellite structure and hausing thickness of CMG. Since shield thickness is not known it is difficult to determine a radiation level. But SaCo magnets are insensitive to radiation and in [21] radiation test results of Vacomax 225 is studied and results shows that SaCo magnets are in sensitive to radiation whereas NeB looses its performance depending on the amount of radiation.

In conclusion Vacomax 225 is selected as reference material to be used in design process of this thesis.

Table 3-6: Properties of some Commercial PMs

Property	Vacomax 225 HR-Sm_2Co_{17}	Vacodym 633 HR NdFeB
Remanent flux density B_r, T	1.03 to 1.10	1.29 to 1.35
Coercivity, H_c kA/m	720 to 820	980 to 1040
Relative recoil magnetic permeability	1.06 to 1.34	1.03 to 1.05
Temperature coefficient of B_r, at 20 to 100°C,	-0.030	-0.095
Curie temperature ^{0}C	Approximately 800	330
Maximum continuous service temperature ^{0}C	350	110
Thermal conductivity, W/(m ^0C)	Approximately 12	9

3.4.2 Ferromagnets

3.4.2.1 Overview

In addition to permanent magnets another important material used in electrical motors is ferromagnets. In order to understand how ferromagnets are used in electrical machines Figure 3-18 [10] can be used.

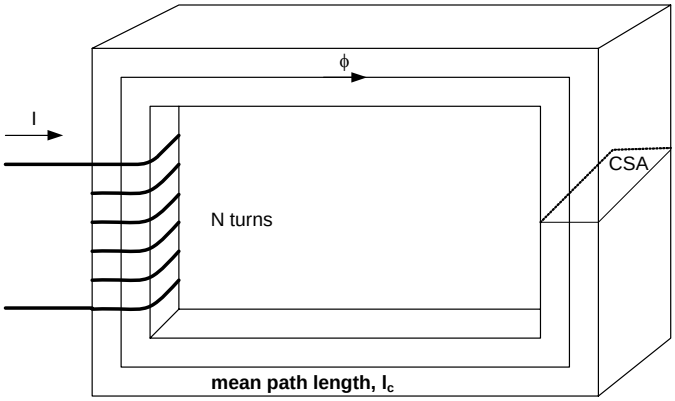

Figure 3-18: Ferromagnetic material with excitation

In Electrical machines a current excitation is used to create a magnetic field. The magnetic field intensity created by a current excitation can be expressed by amperes law.

$$\oint H.dl = I \tag{3.8}$$

If a N turn coil is excited in Figure 3-18 N times current in the coil creates a magnetic field intensity. If core is made from a ferromagnetic material flux occurs inside ferromagnet and resultant magnetic field intensity can be expressed as in Eq. (3.9).

$$H = \frac{Ni}{l_c} \tag{3.9}$$

Magnetic field intensity can also be expressed as an effort to establishment of magnetic field. Magnitude of magnetic field density depends on how much the core ferromagnet let and a coefficient which is called permeability is defined for this concept. Relation between magnetic field intensity and magnetic flux density in a ferromagnet is defined in Eq. (3.10).

$$B = \mu H \tag{3.10}$$

B is magnetic flux density (webers per square meter, Tesla (T))

μ is magnetic permeability of material (Henrys per meter)

H is magnetic field intensity (ampere-turns per meter)

Permeability of free space is a constant and its value is $4\pi x10^{-7}$H/m. Any permeability of other materials compared to permeability of free space is called relative permeability.

$$\mu_r = \frac{\mu}{\mu_0} \tag{3.11}$$

where: μ_o is permeability of free space. Most of the ferromagnet materials have large relative permeability's, for example steels are used in modern electrical machines have relative permeability values 2000-6000. This is the main reason that magnetic field occurs inside the ferromagnet instead of air.

Up to this point some internal parameters of ferromagnet is defined. Last important point is the definition of magnetic circuit composed of air gaps and permanent magnets in the magnetic path.

Since flux density is defined of flux density the flux in the ferromagnetic material is defined using Eq (3.12).

$$\phi = \int BdA \tag{3.12}$$

$$\phi = BA$$

A is cross-sectional area of the ferromagnetic core. In order to understand better we can make an analogy with the classical electrical circuit with magnetic circuit (Figure 3-19).

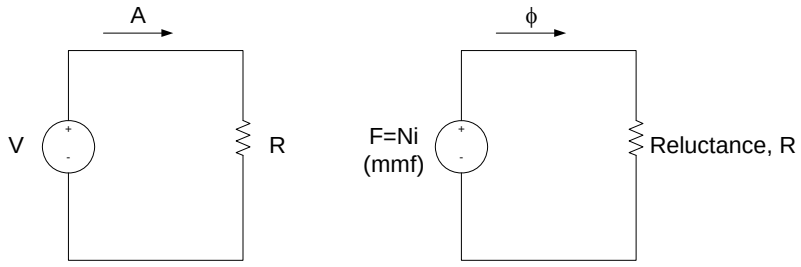

Figure 3-19: Analogy between magnetic circuit and electrical circuit

In electrical circuit voltage produces the current and we can define NI parameter as magneto motive force that drives the magnetic field inside the magnetic circuit. Current in electrical circuit is analogues to flux in the magnetic circuit. Resistance in the electrical circuit can be expressed as reluctance in the magnetic circuit.

Using Eq. (3.13) we can define the reluctance value in magnetic circuit.

$$\phi = BA = \frac{\mu NIA}{l} = F\frac{\mu A}{l} \tag{3.13}$$

$$F = \phi R$$

$$R = \frac{l}{\mu A}$$

Reluctance is valid for the entire path along the magnetic circuit. If we have an air gap or different type of material on the magnetic flux path l on the magnetic circuit, in order to calculate its reluctance A, l and μ are selected for the geometry and and material. Usually only have air gap and permanent magnets are existing on the electrical motors magnetic circuit. While calculating the air gap reluctance, μ_o is used, air gap length and air gap area are taken into consideration. Since permanent magnet materials have relative permeability close to 1, permanent magnets cause large reluctance in the air gap too.

As defined in the permanent magnets part we have some definite constrains such as Br an Hc on the operation of magnetic circuit, ferromagnets also have some definite limitations on its B-H curves. It is already defined that if a magneto motive force is applied to a magnetic circuit a flux is established proportional due to reluctance of magnetic circuit. If geometry is assumed to be constant only determining factor is permeability of ferromagnet and air gap. Air gap permeability is constant independent of applied magneto motive force but it is not same with steels or other ferromagnets.

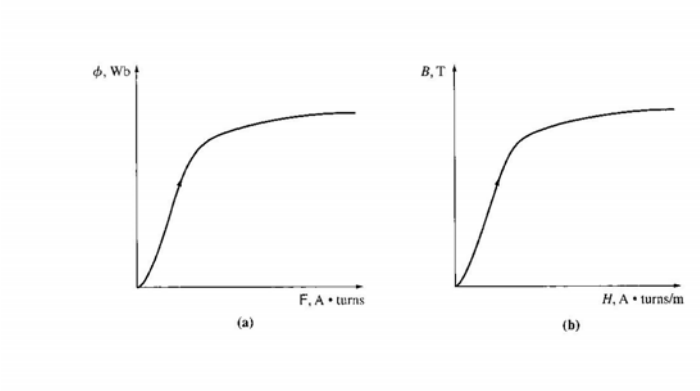

Figure 3-20: Flux vs MMF and B H curve of ferromagnets

Figure 3-20 shows typical curves of ferromagnets up to a specific point permeance of ferromagnets are large and constant and after some point it drops rapidly and ferromagnetic core is assumed to be saturated. After saturation point increasing MMF or another saying current can not produce flux any more. While considering the motor magnetic circuit saturation level of ferromagnetic material should be taken into account.

There are also some loss definitions in ferromagnetic materials. These losses are usually difficult do calculate. General explanations on these losses are below.

Hysteresis Losses

In order to understand the hysteresis loss, the structure of the iron should be understood. Ferromagnets composed of atoms. There are different domains inside the ferromagnet and atoms alignments are randomly distributed. Since these domain distribution is random there are no flux occurs inside a ferromagnet (Figure 3-21).

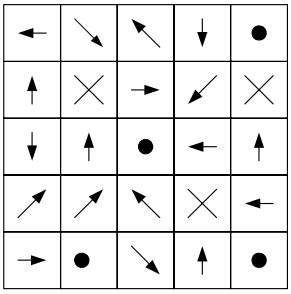

Figure 3-21: Ferromagnet domains before excitation [10]

If an external excitation applied to ferromagnet the domains align with the applied magnetic field direction. When excitation is removed random orientation occurs again but with a different distribution. Some of the domain can not easily re align and some residual flux occurs on the ferromagnet (Figure 3-21).

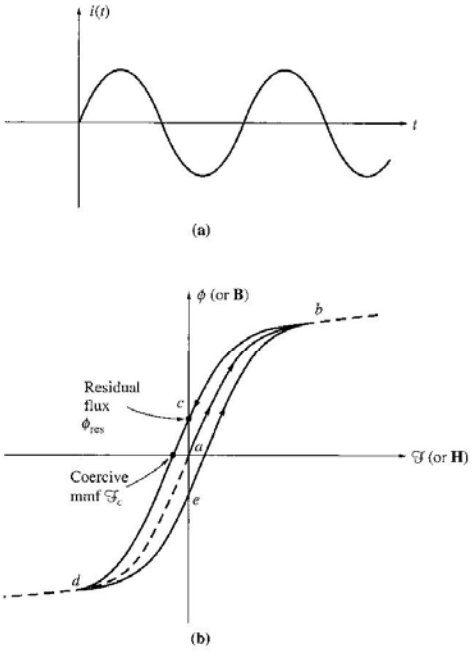

Figure 3-22: Hysteresis curve of ferromagnets

Figure 3-22 shows the excitation characteristics of ferromagnets. If an external magnetic field is applied magnetic field occurs in the way of ab, if external field is removed magnetic field density remove to point c not b. in order to bring the flux density 0 a negative mmf should be applied which is called coercive MMF. Coercive MMF is opposite direction to the applied MMF. If we continuously excite the ferromagnet BH curve follows the b-c-d-e-b path and area inside the BH curve is called hysteresis loss.

Amount of hysteresis loss is depending on the applied MMF magnitude. If larger MMF is applied to ferromagnet, larger hysteresis losses occur. It is very difficult to formulate the hysteresis losses but approximated equations will be explained in chapter 4.

Eddy current losses

Second losses related with the ferromagnets are called eddy current losses. Faradays law states that if a time varying magnetic field is applied inside a wire loop it induces a voltage across the terminals of the wire.

This rule is valid inside the ferromagnet also. Since ferromagnet is under time varying magnetic flux in motor, magnetic circuit and it is made of steels or ferrites it creates small current loops on the ferromagnet core and this currents create resistive losses on the ferromagnet. In order to reduce the current loop lengths ferromagnets are made from laminated steels and a insulating resin in used to glue laminations. It is again difficult to formulate the eddy current losses but approximations will be defined in Chapter 4.

Eddy current and core losses are called core losses of motor magnetic circuit.

3.4.2.2 Selection of Ferromagnet/core

Most common ferromagnet types are non oriented steels and steels are graded by AISI (American Iron and Steel Industry). Different steel standards are shown in Figure 3-23.

Europe IEC 404-8-4 (1986)	U.S.A. AISI	Japan JIS 2552 (1986)	Russia GOST 21427 0-75
250-35-A5	M-15	35A250	2413
270-35-A5	M-19	35A270	2412
300-35-A5	M-22	35A300	2411
330-35-A5	M-36	—	—
270-50-A5	—	50A270	—
290-50-A5	M-15	50A290	2413
310-50-A5	M-19	50A310	2412
330-50-A5	M-27	—	—
350-50-A5	M-36	50A350	2411
400-50-A5	M-43	50A400	2312
470-50-A5	—	50A470	2311
530-50-A5	M-45	—	2212
600-50-A5	—	50A600	2112
700-50-A5	M-47	50A700	—
800-50-A5	—	50A800	2111
350-65-A5	M-19	—	—
400-65-A5	M-27	—	—
470-65-A5	M-43	—	—
530-65-A5	—	—	2312
600-65-A5	M-45	—	2212
700-65-A5	—	—	2211
800-65-A5	—	65A800	2112
1000-65-A5	—	65A1000	—

Figure 3-23: Steel classification in different standards [9]

For small power motor application M-27, M-36 and M-43 are suggested types of steels [9]. While selecting the ferromagnet main selection criteria is amount of loss because these materials has large operating temperature range so temperature (maximum continuous service temperature of 230 ^{0}C and curie temperature of 800 ^{0}C) is not critical. Since core losses are difficult to measure and determine manufacturers usually give core loss values in W/kg (Table 3-7).

Table 3-7: Core loss data for different core materials (Non oriented steels core loss (W/kg))

Magnetic flux density in T	Non oriented steels core loss (W/kg)			
	Armco DI-MAX M-27 (0.36mm)	Cogent power No12 (0.2mm)		
	60Hz	50Hz	400Hz	2.5kHz
0.1		0.02	0.16	1.65
0.2	0.09	0.08	0.71	6.83
0.3		0.16	1.55	15.2
0.4		0.26	2.57	25.4
0.5	0.47	0.37	3.75	37.7
0.6		0.48	5.05	52
0.7	0.81	0.62	6.49	66.1
0.8		0.76	8.09	83.1
0.9		0.32	9.84	103
1	1.46	1.09	11.8	156
1.1		1.31	14.1	
1.2		1.56	16.7	
1.3	2.39	1.89	19.9	
1.4		2.29	24	
1.5	3.37	2.74	28.5	
1.6	4	3.14		
1.7	4.55	3.49		
1.8	4.95	3.78		
1.9				
2				

Generally M 27 is used for fractional HP applications. But they are usually available for 50-60 Hz applications, for frequencies higher than 50-60 Hz thinner steels should be used(less than 2 mm). Cogent power (United Kingdom) can manufacture thin steels for special motors. No12, No18 and No 20 type steels are capable of operating up to 2.5 KHz. The motor in this thesis is designed to operate at 10000RPM and electrical frequency will be between 166(2 pole)-498 Hz (6 pole) or even more depends on number of poles. These steels has a maximum operating temperature of 230 ^{0}C and a maximum intermittent temperature of 850 ^{0}C. Typical mass density is 7650 kg/m^3. Table 3-7 shows core loss values for different frequencies and magnetic field density.

Table 3-8: Alternative core materials

Magnetic flux density in T	Amorphous ferromagnetic alloyscore loss (W/kg)		Soft magnetic powder composites core loss (W/kg)					
	Honeywell-Metglas 2605Co		TSC Ferrite International-Ac-cucore			Höganas-Somaloy 500		
	50Hz	60Hz	60Hz	100 Hz	400 Hz	50Hz	100 Hz	300 Hz
0.1	0.0071	0.009	0.132	0.242	1.058			
0.2	0.024	0.03	0.419	0.683	3.263			
0.3			0.072	1.323	6.217			
0.4	0.063	0.08	1.212	2.072	9.811	1.5	3	12
0.5			1.742	2.976	14.08	1.9	3.6	17
0.6	0.125	0.16	2.315	3.968	18.85	2.7	6	21
0.7			2.954	5.07	24.29			
0.8	0.196	0.25	3.660	6.305	30.49	4.6	10	32
0.9			4.431	7.650	37.34			
1	0.274	0.35	5.247	9.039	44.48	6.8	16	48
1.1			6.129	10.58	52.91			
1.2			7.033	12.21	61.37			
1.3			7.981	13.84	70.15			
1.4			8.929	15.56	79.16			
1.5			9.96	17.39	90.30			
1.6			10.86	19.08	99.67			
1.7			11.7	20.63	109.8			
1.8			12.12	21.4				
1.9								
2						30	50	170

Other alternatives are also available for low power and high speed applications. One alternative is amorphous ferromagnetic alloys. These materials have very low hysteresis loss and better cooling performance (Table 3-8). They have better core loss performance but major drawback is they are very expensive, long

manufacturing process and availability is limited. Also maximum service temperature for these materials is 125-150 ^{0}C. Last alternative for motor ferromagnet is soft magnetic powder composites. Main idea behind this powder production is to adopt difficult geometries. But their core losses are higher than thin steels (Table 3-8).

In conclusion Cogent Power no 12 type non oriented steel is selected as reference material to be used in design process of this thesis.

3.5 Literature Overview

It is already discussed in Chapter 2 brushless dc motors are most convenient and widely used in aerospace wheel applications due to their high torque/volume and mass/volume properties. In addition they have no maintenance requirements which are very critical in aerospace applications.

As stated before main discussion of this thesis will be based on 2 topics. First a RF motor with short axial length will be discussed. Short axial length means distance between bearings will be smaller so balance problems can be reduced (Figure 3-24 (a)). Second study concept is increasing the inertia of motor so that volume and mass of the motor plus wheel system can be reduced (Figure 3-24 (a)). To realize second point AF topologies are studied. Bearing distance in these motors are smaller than RF motors and balance problems can be reduced more.

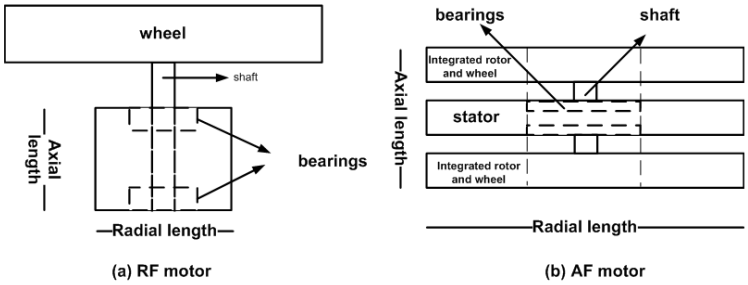

Figure 3-24 wheel system structure with (a) RF motor and (b) AF motor

A sample design will be done based analytical equations and results will be compared in terms of

- torque/volume
- torque/mass ratio
- efficiency

Effect of pole number is also studied. RF topology is selected as a conventional slotted type surface mounted magnets because of simple design structure.

AF motors can be designed in quite different manners, and usually used in limited axial length and large radial length applications (like in CMG case). First decision is to have single or two rotor topologies (Figure 3-25). If two rotor is used motor weight will be symmetrically distributed on the perpendicular axis to its rotation axis and this is an advantage to have low inertia at CMG gimbal axis (y-axis in Figure 3-25) resulting in low torque requirement in gimbal motor. Also with two rotor topology more inertia contribution based on two rotating disc can be achieved.

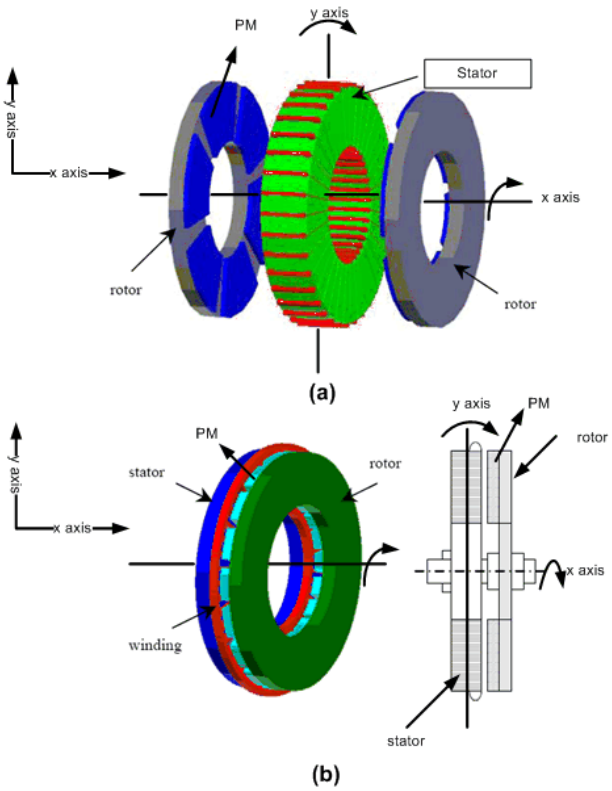

Figure 3-25: (a) two rotor AF topology, (b) single rotor AF topology [17]

Af motors can be designed in very different configurations also, inner rotating rotator topologies are also common but, in such case two stationary core are existing and this in not an advantage in CMG application(Figure 3-26).

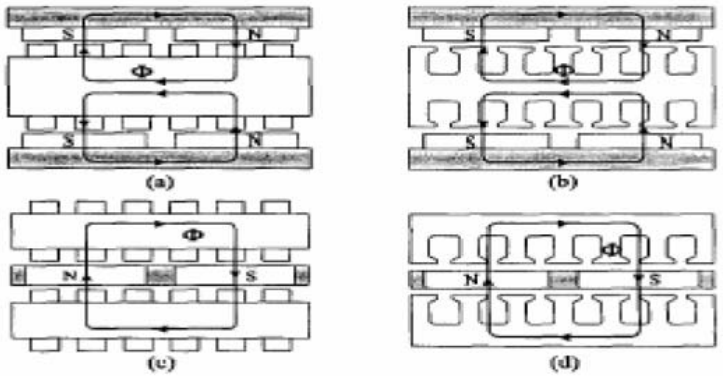

Figure 3-26: Different AF motor topologies, a- slotless single stator two rotor outer rotating rotor, b- - slotted single stator two rotor outer rotating rotor , c- slotless two stator one rotor inner rotating rotor, d- slotted two stator one rotor inner rotating rotor [19]

Another selection is decided on the magnet insertion type. In order to have short end windings (since end winding do not contribute torque only create loss) NN type topology is selected.

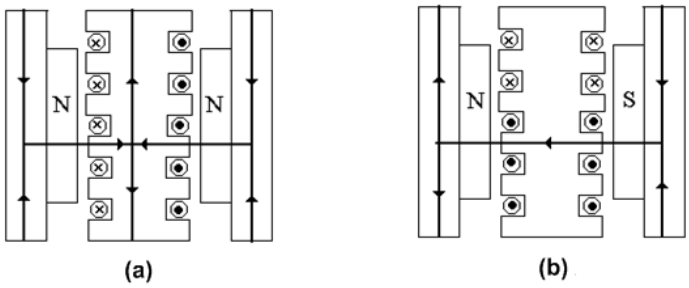

Figure 3-27: a-NN and b-NS magnet configurations [12]

There are various studies done on comparison of these two topologies. In reference 4 a radial flux and [15] different type axial flux motor topology are compared in terms of required copper, steel, and magnet weights, copper and iron loss, moment of inertia, torque per unit moment of inertia, power per unit active weight, and power per unit active volume for five different power levels (0.25kW

– 10kW and 1000-2000RPM). The results are differs at different power ratings and different speeds. But in general AF motors have larger torque/mass, torque/volume and efficiency point of view over the power and speed range of 0.25kW – 10kW and 1000-2000RPM.

In [16] radial and axial flux topologies are compared in terms of torque capacity. Different pole numbers and different geometries are studied. Comparisons are made under, equal overall motor volume, equal losses per wasting surface unit, equal air gap, teeth, and yokes flux density, equal rotational speed (1000RPM).
An obtained results under defined constrains show that, AF motors have larger torque/volume performance under large pole numbers pole numbers.

In [17] a surface mounted dual rotor axial and radial flux machined are studied in terms of material weights and costs, copper and iron losses, torque and power per unit active volume, torque per unit active material weight, magnet material effect, losses per unit air gap area, and machine efficiency. Power range in these applications is 2.2kW – 32 kW and speed is 1800 RPM. Effect of pole number is also investigated. Results can be summarized as in larger power scales and high pole numbers AF motors have large torque density and efficiency.

In [18] and [19] axial and radial flux machines are compared in terms of efficiency torque per volume and torque per mass. Speed range is 0-12500RPM and torque range is between 0.3 Nm to 2.5Nm for a washing machine application. These study requirements are close to the requirements of this thesis since speed range is close to CMG requirements and design process is based on a defined torque speed profile. Obtained results were for large number of poles AF motors have better performance in terms of torque/mass, torque/volume and efficiency.

All of the works previously done is based on different motor torque and speed ranges also for different speed ranges. It is difficult to reach an exact decision on performance of two topologies since all applications and motor types are different

in the literature. Since the motor in this thesis is designed to operate at very high speed (10000RPM) and in small torque range (0-50mNm), radial and axial flux motors will be studied again to compare the performances in terms of efficiency torque/mass and torque/ volume.

3.6 Derivation of Basic Equations of BLDC Motors

In this part since torque is the determining factor, equations of RF and AF motor will be studied in order to find resulting torque in terms of motor dimensions. Equations will be studied in terms of square wave and sinusoidal current excitations for both motor. Main aim is to define a torque expression in terms of motor dimensions and general motor design inputs such as electrical loading and air gap magnetic flux density.

3.6.1 RF Motor Equations

3.6.1.1 RF Motor Equations under Square Wave Excitations

Figure 2-15shows a typical square wave excitation of motor. In each commutating interval only two phases is exciting and peak value of phase current is equal to dc link current. Instantaneously converted power to electromechanical energy and electromechanical torque is expressed in Eq (3.14).

$$P = 2E_{ph}I_p = w_m T$$
$$T = \frac{2E_{ph}I_p}{w_m} \tag{3.14}$$

E_{ph} is flattop value of phase back emf

I_p is dc link current or peak value of phase current

w_m is mechanical speed of motor

T is electromechanical torque

Back emf in RF motor can be calculated using the flux linkage equations of the motor coils (Figure 3-28).

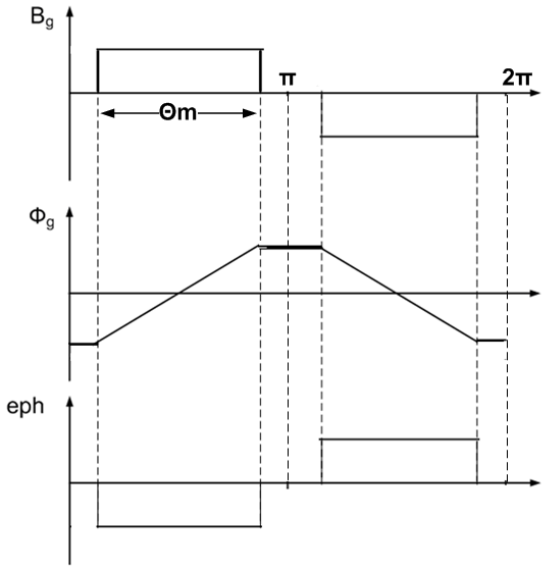

Figure 3-28: Flux linkage, back emf

Back emf can be calculated using Eq (3.15) [11]

$$
\begin{aligned}
e &= -\frac{d\lambda}{dt} = -\frac{d\lambda}{d\theta} \times \frac{d\theta}{dt} = -w_e \frac{d\lambda}{d\theta} \\
\lambda &= N_{ph} \Phi_g \\
\Phi_g &= B_g A_g = B_g R_i \theta_m L = B_g R_i \frac{2\pi}{P} \frac{\theta_m}{\pi} L \\
E_{ph} &= \frac{P}{2} w_m \frac{2N_{ph} \Phi g}{\theta_m} = \frac{P}{2} w_m \frac{2N_{ph}}{\theta_m} B_g R_i \frac{2\theta_m}{P} L \\
E_{ph} &= N_{ph} B_g L D_i w_m
\end{aligned}
\tag{3.15}
$$

N_{ph} is number of turns per phase

B_g is flattop value of air gap magnetic flux density

L is axial length of motor

D_i is inner diameter of motor

λ is flux linkage

Peak value of phase current can be expressed in terms of electrical loading Eq. (3.16).

$$q = \frac{2mN_{ph}I_{RMS}}{\pi D_i}$$

$$I_{RMS} = \sqrt{\frac{2}{3}} I_p \tag{3.16}$$

$$q = \frac{2mN_{ph}}{\pi D_i} \times \sqrt{\frac{2}{3}} I_p$$

I_{RMS} is rms value of motor phase current

I_p is peak value of motor phase current (dc link current)

q is electrical loading value

Using (3.15) and (3.16) electromechanical torque of motor can be expressed in terms of flat top value of air gap magnetic flux density, electrical loading, inner diameter and axial length of motor (3.17) [19].

$$T = \frac{\pi}{\sqrt{6}} B_g q D_i^{\,2} L \tag{3.17}$$

Torque in RF motor can also be calculated using basic force equation acting on the motor coils (3.18)

$$T = 2FR_i \tag{3.18}$$

2 due to two phase is conducting at the same time, force in (3.18) is calculated using Eq. (3.19).

$$F = BI_p L = B_g 2N_{ph} I_p L \tag{3.19}$$

Combining (3.19), (3.18) and (3.16), same torque equation can be obtained in Eq. (3.17).

3.6.1.2 RF Motor Equations under Sinusoidal Wave Excitations

In sinusoidal excitation case all there phase in conduction I each commutation interval and it is assumed that all the phase currents are sinusoidal.

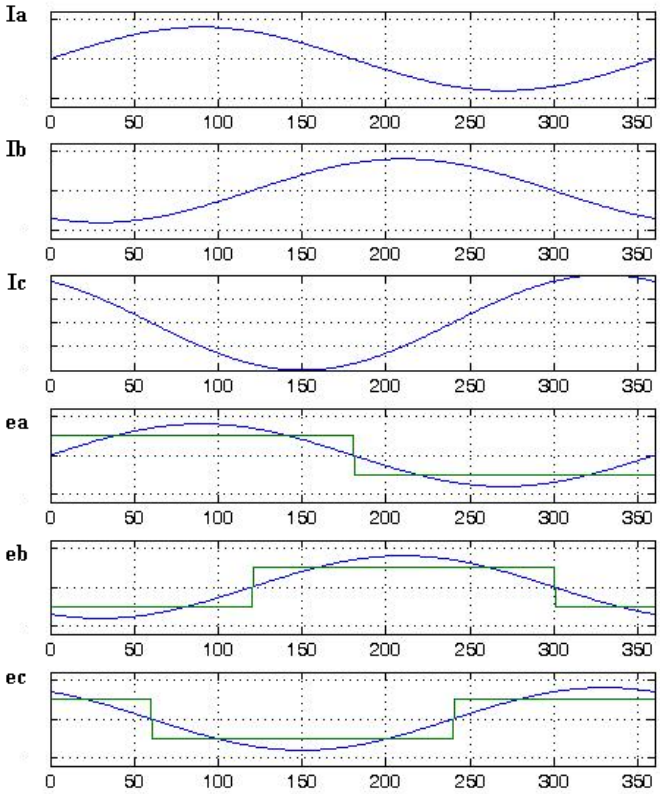

Figure 3-29: Back emf and motor current waveforms under sinus excitation

Only fundamental component of back emf voltage is assumed to create torque with applied phase currents.

Since three phases are conducting at the same time electromechanical torque can calculated using Eq. (3.20)

$$T = \frac{3e_{rms} I_{RMS}}{w_m} \tag{3.20}$$

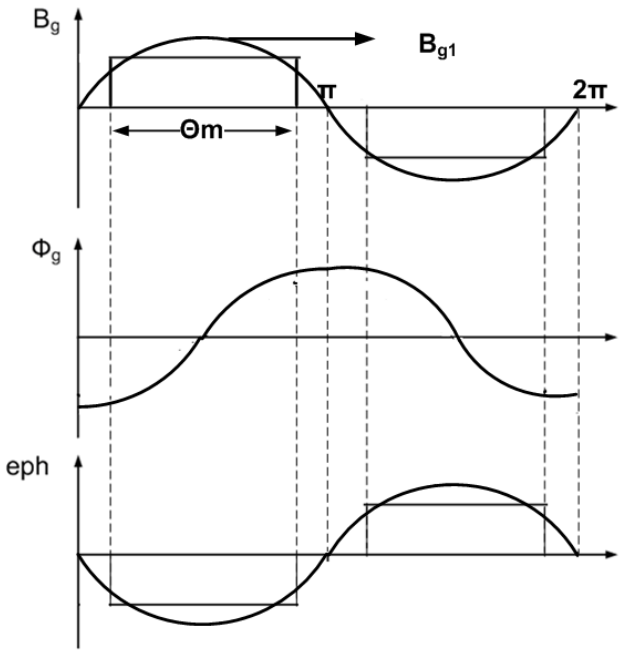

Figure 3-30: Flux linkage, back emf

Assuming only average of fundamental component of air gap magnetic flux density creates fundamental component of back emf voltage, rms value of back emf voltage can be calculated using Eq. (3.21).

$$\hat{e} = -\frac{d\lambda}{dt} = -\frac{d\lambda}{d\theta} \times \frac{d\theta}{dt} = -w_e \frac{d\lambda}{d\theta}$$

$$\frac{d\lambda}{d\theta} = N_{ph} A_g \frac{1}{\pi} \int_0^{\pi} \hat{B}_{g1} \sin(\theta_m) d\theta = N_{ph} A_g B_{gav} \tag{3.21}$$

$$\hat{e} = \frac{P}{2} w_m N_{ph} B_{gav} R_i \frac{2\pi}{P} L$$

$$\hat{e} = \frac{\pi}{2} w_m N_{ph} B_{gav} D_i L$$

$$e_{rms} = \frac{e}{\sqrt{2}} = \frac{\pi}{2\sqrt{2}} N_{ph} B_{gav} D_i L w_m$$

e_{rms} is the rms value of phase back emf voltage and B_{gav} is average of fundamental component of air gap magnetic flux density and dependent on the selection of magnet angle θ_m.

Using Eq (3.21) and (3.20) torque can be expressed as in Eq (3.22).

$$T = \frac{3\pi}{2\sqrt{2}} N_{ph} B_{gav} D_i L I_{RMS} \tag{3.22}$$

With the help of electrical loading equation Eq (3.23), Eq (3.22) can be rewritten as Eq (3.24)

$$q = \frac{2mN_{ph} I_{RMS}}{\pi D_i} \tag{3.23}$$

m is number of phase.

$$T = \frac{\pi^2}{4\sqrt{2}} B_{gav} q D_i{}^2 L \tag{3.24}$$

3.6.2 AF Motor Equations

3.6.2.1 AF Motor Equations under Square Wave Excitations

In AF motor under square wave excitation same excitation characteristic in 3.6.1.1 is valid. Only changing parameters are areas of poles due to different geometry.

For electromechanical torque Eq. (3.14) is valid again. Back emf voltage can be calculated using Eq. (3.25).

$$E_{ph} = -\frac{d\lambda}{dt} = -\frac{d\lambda}{d\theta} \times \frac{d\theta}{dt} = -w_e \frac{d\lambda}{d\theta}$$

$$\lambda = N_{ph} \Phi_g$$

$$\Phi_g = B_g A_g = B_g \frac{\pi (R_o{}^2 - R_i{}^2)}{P} \frac{\theta_m}{\pi}$$

$$E_{ph} = \frac{P}{2} w_m \frac{2N_{ph} \Phi g}{\theta_m} = \frac{P}{2} w_m \frac{2N_{ph}}{\theta_m} B_g \frac{\theta_m (R_o{}^2 - R_i{}^2)}{P} \tag{3.25}$$

$$K_r = \frac{R_i}{R_o}$$

$$E_{ph} = N_{ph} B_g R_o{}^2 (1 - K_r{}^2) w_m$$

R_i, R_o are inner radius and outer radius of AF motor respectively

Torque equation is rewritten using Eq (3.25) in Eq (3.26).

$$T = \frac{2N_{ph}B_g R_o{}^2(1-K_r{}^2)w_m I_p}{w_m} = 2N_{ph}B_g R_o{}^2(1-K_r{}^2)I_p \tag{3.26}$$

Using electrical loading equation at inner diameter of the AF motor(Eq. (3.28)) and relation between the phase current and peak value of the phase current (Eq. (3.27)), torque equation in terms of electrical loading at inner peripheral of motor and flattop value of air gap magnetic flux density is expressed in Eq. (3.29).

$$I_{RMS} = \sqrt{\frac{2}{3}} I_p \tag{3.27}$$

$$q_i = \frac{mN_{ph}I_{RMS}}{\pi D_i} \tag{3.28}$$

$$T = \frac{2\sqrt{2}}{\sqrt{3}}\pi B_g q_i R_o{}^3 K_r(1-K_r{}^2) \tag{3.29}$$

Torque in AF motor can also calculated using basic force acting on coil.

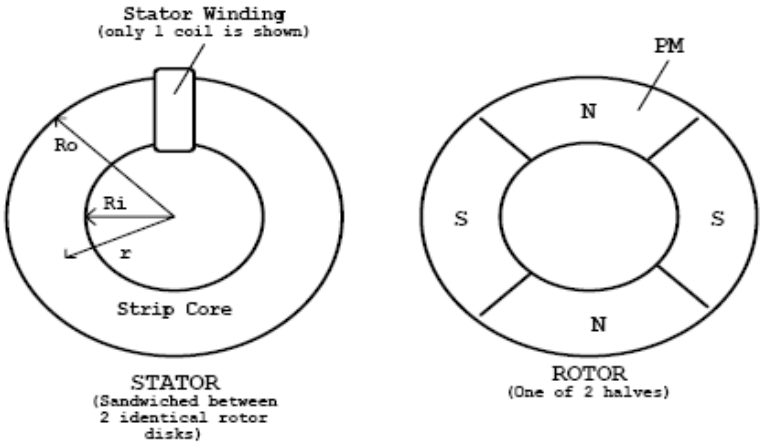

Figure 3-31: AF motor from top view

Torque on dr length of the coil at the statator can be calculated using Eq. (3.30) [19].

$$dT = dFr = B_g I_p drr \tag{3.30}$$

Electrical loading on dr length of the coil can be calculated using Eq. (3.31)

$$q(r) = \frac{q_i \times R_i}{r} \tag{3.31}$$

Using Eq. (3.27) and (3.31), torque on d length of coil can be expressed as in Eq. (3.32) [19]

$$I_p = 2\pi \times r \times \sqrt{\frac{2}{3}} q(r)$$

$$dT = B_g \times 2\pi \times r \times \sqrt{\frac{2}{3}} q(r) \times dr \times r = B_g 2\pi r^2 \sqrt{\frac{2}{3}} q(r) dr \tag{3.32}$$

$$dT = B_g 2\pi r^2 \sqrt{\frac{2}{3}} \frac{q_i \times R_i}{r} dr = 2\sqrt{\frac{2}{3}} \pi B_g q_i R_i r dr$$

$$T = \int_{R_i}^{R_g} 2\sqrt{\frac{2}{3}} \pi B_g q_i R_i r dr = \sqrt{\frac{2}{3}} \pi B_g q_i R_i (R_o^2 - R_i^2)$$

Since there is two faces on AF motor torque should be multiplied by two, resulting torque is same as in Eq. (3.29).

3.6.2.2 AF Motor Equations under Sinusoidal Wave Excitations

Equations again similar as in RF case, only changing factor is area of gap due to different geometry of motor.

Assuming again only fundamental component of air gap magnetic flux density create torque peak value of back emf can be calculated using Eq. (3.33).

$$\hat{e} = \frac{P}{2} w_m N_{ph} B_{gav} \frac{\pi (R_o^2 - R_i^2)}{P}$$

$$\hat{e} = \frac{\pi}{2} N_{ph} B_{gav} (R_o^2 - R_i^2) w_m$$

$$K_r = \frac{R_i}{R_o} \tag{3.33}$$

$$\hat{e} = \frac{\pi}{2} N_{ph} B_{gav} R_o^2 (1 - K_r^2) w_m$$

Torque can be calculated using Eq. (3.20). Rms value of the back emf voltage can be calculated using Eq. (3.34)

$$e_{rms} = \frac{\hat{e}}{\sqrt{2}} = \frac{\pi}{2\sqrt{2}} N_{ph} B_{gav} R_o^{\ 2} (1 - K_r^{\ 2}) w_m \tag{3.34}$$

Eq. (3.20) can be rewritten using (3.34).

$$T = \frac{3\pi}{2\sqrt{2}} N_{ph} B_{gav} R_o^{\ 2} (1 - K_r^{\ 2}) I_{RMS} \tag{3.35}$$

Using (3.35) and (3.28) torque in sinusoidal excitation case can be expressed as in Eq (3.36).

$$T = \frac{\pi^2}{\sqrt{2}} B_{gav} q_i R_o^{\ 3} K_r (1 - K_r^{\ 2}) \tag{3.36}$$

Up to this point, equations for both AF and RF motors are stated. In next chapter design process will be studied based on required motor torque, electrical loading and air gap magnetic flux density.

3.7 Conclusion

Table 3-9 summarizes the derived torque equations for RF and AF motors for both excitations. Torque equations are derived in terms of motor dimensions, and general motor design parameters which are electrical loading and magnetic loading (air gap magnetic flux density) of the motor.

Table 3-9: Summary of torque equations

Excitation type/motor type	RF motor	AF motor
Square wave excitation	$T = \frac{\pi}{\sqrt{6}} B_g q D_i^{\ 2} L$	$T = \frac{2\sqrt{2}}{\sqrt{3}} \pi B_g q_i R_o^{\ 3} K_r (1 - K_r^{\ 2})$
Sinusoidal excitation	$T = \frac{\pi^2}{4\sqrt{2}} B_{gav} q D_i^{\ 2} L$	$T = \frac{\pi^2}{\sqrt{2}} B_{gav} q_i R_o^{\ 3} K_r (1 - K_r^{\ 2})$

Electrical loading of the motor is dependent on output power and rotational speed (details will be discussed in Chapter 4), and it is related with the heating of motor. Since both motor will have same output power and speed electrical loading Is assumed to be same for both excitations. Using equations in Table 3-9 an initial estimation can be calculated for different excitations. Assuming same electrical loading for both excitations and same motor dimensions amount of torque can be obtained from the motor is dependent on air gap magnetic flux density. Air gap magnetic flux density shape is dependent on magnet angle and magnet thickness.

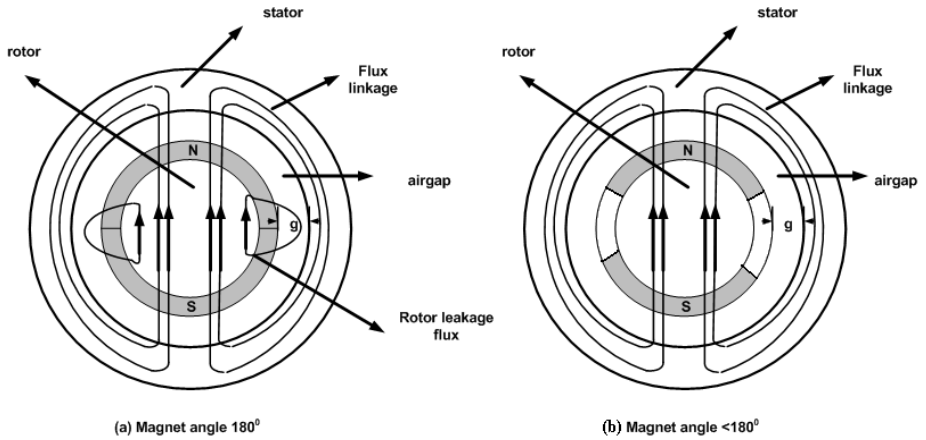

Figure 3-32: Effect of rotor magnet angle (a) 180^0 magnet angle (b) magnet angle<180^0

Magnet angle is rarely selected as 180^0. This is mainly due to the fact that if magnet angle is selected 180^0, magnet flux at the edges of magnet can not pass air gap and linkage the stator coils (magnets are wasted if 180^0 magnet angle is selected [20]).

Figure 3-33 shows pole pitch of the motor (t_p) and magnet dimensions.

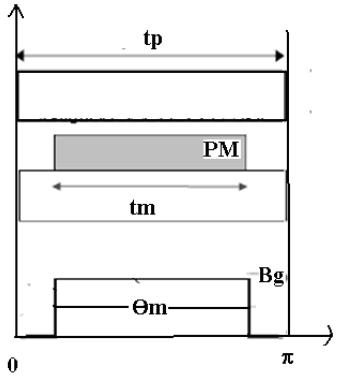

Figure 3-33: Pole pitch of the motor, magnet span and resulting air gap magnetic field shape (tm magnet pitch mechanical, θ_m magnet angle)

Magnet angle θ_m strongly determines the shape air gap magnetic field density. Fundamental component of air gap magnetic field density is the most important part of air gap magnetic field density in sinusoidal excitation case. Peak value of the fundamental component of the air gap magnetic field density can be calculated using Eq. (3.37) [12].

$$\hat{B}_{g1} = \frac{4}{\pi} B_g \sin(\frac{\theta_m}{2}) \tag{3.37}$$

Having larger fundamental component will result in large air gap magnetic field density and more torque. If magnet span is selected as 180^0C degree largest fundamental component is obtained but in this case air gap harmonics are quite large and cause to much ripple and noise problems. Usually in order to reduce the harmonic contend magnet angle is selected as 120 ^{0}C; this makes the third and the most problematic harmonic 0. More advanced magnet shaping can be done in order to reduce the fifth or higher harmonics but in this thesis simply 120 degree magnet span is assumed. Also for square wave excitation case 120^0 magnet angle is enough for 120^0 back emf voltage (Figure 3-28). After deciding the magnet angle last important value is flat top value (B_g) of air gap magnetic flux density.

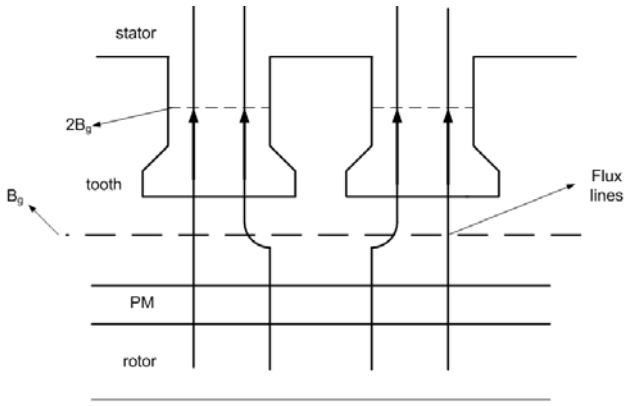

Figure 3-34 Flux paths in RF motor

Flat top value of back emf is limited by the stator saturation at teeth or stator core when slotless structures used (in AF case) (Figure 3-34). Since same materials are used in both excitation cases flat top value of air gap magnetic flux density is assumed to be same in order to make comparison on same basis between excitations. Determination of this value will be studied in detail in Chapter 4. Note that average of fundamental component (Eq. (3.38)) is used in torque equations of sinusoidal excitation and flat top value is used in equations of square wave excitation.

$$Bgav = \frac{2}{\pi}\hat{B}_{g1} = \frac{6}{\pi^2}B_g \sin(\frac{\theta m}{2})$$
$$Bgav = 0.7B_g \tag{3.38}$$

For same electrical loading, same flat top value of air gap magnetic flux density and same motor dimensions, torque of motors for different excitations can be calculated using equations in Table 3-7 and Eq. (3.38). T_{sq} (torque in square wave excitation)/ T_{sin} (torque in sinusoidal excitation) is calculated as 1.049, another words amount of torque for both excitations are very close but 5 % more torque can be obtained in square wave excitation from same volume of the motor. Next chapter dimensions, values of electrical loading, magnetic loading etc will be studied numerically in detail and results will be compared in terms of motor volume, mass and efficiency point of view.

CHAPTER 4

DESIGN CALCULATIONS OF RF AND AF MOTORS

In this part of thesis in order to have better performance in CMG wheel motor system design of the AF and RF motors will be done according to the equations derived in Chapter 3. Design criteria's are based on the performance requirements defined in Chapter 3 and the design calculations defined here after.

For RF motor, design is studied based on conventional surface mounted slotted type permanent magnet motor. AF motor, design is studied on the basis of slotless two rotating disc and two air gap motor is studied. Motor dimensions and performance is determined and performance of designed motor is to be compared between each other. Also effect of pole number on motor design and performance is studied. After determining the main electrical and geometrical design practical considerations on motor is studied.

4.1 Introduction

In RF motor design process first the magnetic circuit of RF motor is studied. Than design parameters (torque, electrical loading, air gap magnetic flux density) are defined. Using the equations derived in Chapter 3 and determined design parameters dimensions of motor are calculated. Based on calculated dimensions and design inputs, electrical parameters (number of turns per phase, phase

resistance, phase inductance, required motor current, and required voltage levels) are calculated. Finally mass and volume the motor is calculated and performance comparisons are made. Practical problems of manufacturing are studied at the end of this part.

During design process first two main design processes are studied based on square wave and sinusoidal excitations on a 2-pole RF motor. Then effect of excitation difference on motor is compared. For one excitation type the effect of pole number a 6pole design process is studied.

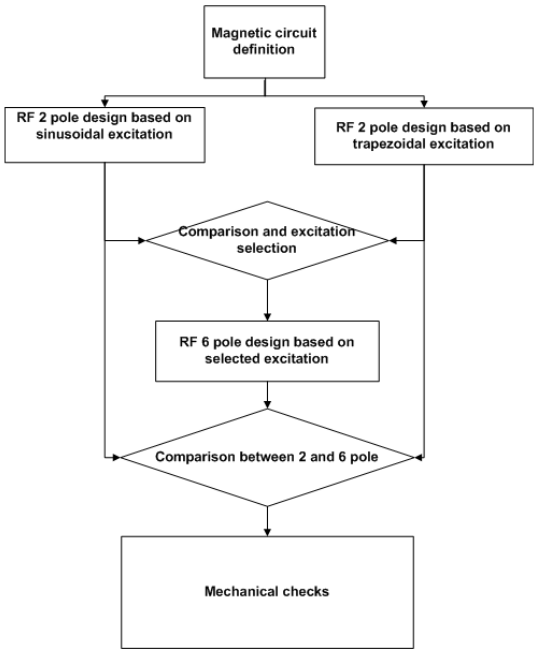

Figure 4-1: RF Design flow

4.2 Magnetic Circuit of RF Motor

In PM motors performance of the motor is strongly dependent on the magnetic circuit design. In Chapter 3, for a defined magnetic flux density, electrical loading and torque requirement dimension calculation equations are derived. What remaining is the magnetic circuit calculation details in order to start with feasible design input (such as air gap magnetic field distribution and proper magnet thickness).

Magnetic circuit is dependent on the geometry and the selected magnet BH curve. Details and definitions of BH curve are stated in Chapter 3. In order to start to calculate dimensions of motor, required magnet thickness and air gap magnetic flux density should be studied. Operating point of the permanent magnet on its BH curve should be found. Figure 4-2 shows a typical magnet BH curve and load line.

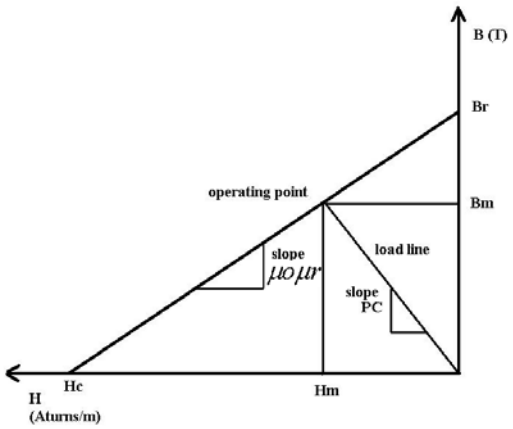

Figure 4-2: BH curve and load line of a typical magnetic circuit

Intersection between load line and magnets natural demagnetization BH curve determines the magnet operating point and air gap magnetic field density (Figure 4-2). Slope of the load line is strongly dependent on magnetic circuit and

magnetic circuit is expressed in terms of reluctances or permeances. Reluctance and permeances are dependent on magnet and air gap dimension and motor dimensions. Here after magnetic circuit of a radial flux motor is an established and necessary equations for determination of operating point (and hence air gap magnetic flux density) are defined. Figure 4-3 shows a typical cross-section of two poles RF slotted PM motor. Using main dimensions and geometrical structure magnetic circuit can be defined.

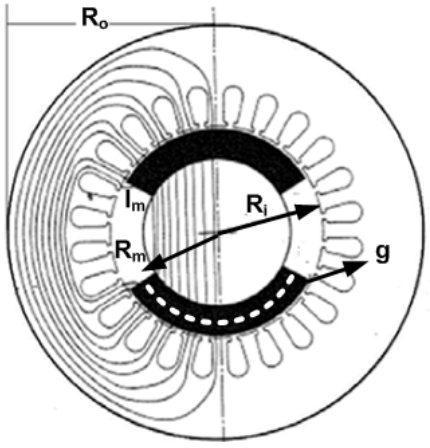

Figure 4-3: Cross-section of 2pole RF motor

In RF motor magnetic flux is created by magnets crosses the air gap and circulates on the rotor and motor. Assuming an infinitely permeable ferromagnetic core in the motor, equivalent magnetic circuit is shown in Figure 4-4.

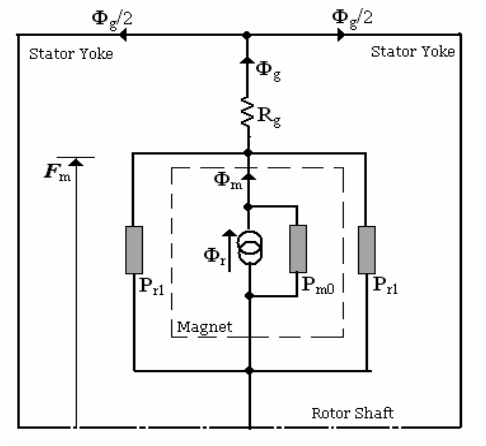

Figure 4-4: Magnetic equivalent circuit of the RF 2 pole motor [11]

Φ_r is the magnetic flux generated by the permanent magnet. PM can be assumed as a magnetic flux generator and some of the flux created by magnet is lost inside the magnet and it is dependent on internal permanence of magnet P_{m0}. flux generated by magnet and internal permanence is expressed in Eq. (4.1).

$$\Phi_r = B_r A_m$$
$$P_{m0} = \frac{\mu_0 \mu_{rec} A_m}{l_m} \tag{4.1}$$

Φ_r is flux generated by permanent magnet, B_r is the magnet remenant flux density, μ_0 is permeability of free space, μ_{rec} is relative permeability of PM with respect to permeability of free space, l_m is magnet thickness and A_m is the area of the magnet.

Since magnet angle is determined as 120^0 , area of the magnet can be calculated using Eq. (4.2) [11]. Note that average radius of the magnet is used in Eq. (4.2)

$$A_m = \frac{\frac{2}{3}\pi\left(R_i - g - \frac{l_m}{2}\right)}{pp} L \tag{4.2}$$

R_i is the inner radius of motor shown in Figure 4-2, g is the air gap distance, lm is the magnet thickness and pp is number of pole pair, L is axial length. 2/3 coefficients is coming from the 120 ^{0}C magnet angle.

After determining the PM internal permeance another loss factor rotor leakage should be defined. Not all of the magnetic flux can pass the air gap due to the leakage fluxes and it is very difficult to determine the exact value. In [11] leakage permeance is 5-10% of magnets internal permeance (P_{mo}). P_{r1} is assumed to 10% of P_{mo} and modified magnet internal permanence is assumed as in Eq. (4.3).

$$P_m = P_{mo} + P_{r1} = P_{mo} \times 1.1 \tag{4.3}$$

Next issue is to determine the air gap reluctance R_g in the magnetic circuit. R_g is expressed in Eq. (4.4).

$$R_g = \frac{g'}{\mu_0 A_g} \tag{4.4}$$

Where $g' = K_c g$, and g' is the equivalent air gap due to slotting and to have the effect of slotting carters coefficient is used and it is assumed to 1.05 in this thesis.

Reluctance of air gap is also dependent of the air gap area and it is calculated according to the Eq (4.5).

$$A_g = \left(\frac{\frac{2}{3}\pi\left(R_i - \frac{g}{2}\right)}{pp} + 2g \right)\left(L + 2g\right) \tag{4.5}$$

Flux passing to air gap is not uniform at the edges of magnet due to fringing effect. In order to make an approximation to fringing effect, a distance of air gap g is added to each edges of the magnet in calculation of air gap.

All the parameters in the magnetic circuit are defined in Eq. (4.1) to (4.5). Eq. (4.6) shows the calculation of air gap magnetic field density from the magnetic circuit equations.

$$F_m = \frac{\phi_r - \phi_g}{P_m} = \phi_g R_g$$

$$\phi_g = \frac{\phi_r}{1 + P_m R_g} \tag{4.6}$$

$$B_g A_g = \frac{B_r A_m}{1 + P_m R_g}$$

$$B_g = \frac{C}{1 + P_m R_g} B_r, C = \frac{A_m}{A_g}$$

It can be seen from the magnetic circuit magnet operating point is different from the Br value based on magnets internal permeance and leakage permeance, Eq. (4.7) shows the calculation of Bm by solving the magnetic circuit.

$$\begin{aligned} F_m &= \frac{\phi_r - \phi_m}{P_{mo}} + \frac{\phi_m - \phi_g}{P_{r1}} = \phi_g R_g \\ \phi_r &= B_r A_m \\ \phi_m &= B_m A_m \\ B_m &= \frac{1 + P_{r1} R_g}{1 + P_m R_g} B_r \end{aligned} \tag{4.7}$$

Now B_m value is determined for a given geometry, using the slope of the BH curve magnetizing force H_m can be calculated using the Eq. (4.8).

$$-H_m = \frac{B_r - B_m}{\mu_o \mu_{rec}} \tag{4.8}$$

By using Eq (4.7) into (4.8) load line characteristics can be found as Eq. (4.9).

$$\begin{aligned} B_m &= PC x H_m \\ PC &= \mu_o \mu_{rec} \frac{1 + P_{r1} R_g}{P_{mo} R_g} \end{aligned} \tag{4.9}$$

Up to this point magnetic circuit of RF motor is studied. For defined dimensions and defined magnet properties resulting air gap magnetic flux density value can be calculated using Eq. (4.6). In next part design considerations is done based on equations stated in Chapter 3 and magnetic circuit equations stated here.

4.3 Design of 2 pole RF motor under sinusoidal excitation

Up to now magnetic circuit equations are stated in previous part and dimension equations are already determined in Chapter 3. In this part of thesis dimensioning and design of the motor is started based on the Eq. (4.11) for sinusoidal excitation.

$$T_p = \frac{\pi^2}{4\sqrt{2}} B_{gav} q D_i^{\,2} L \tag{4.11}$$

Before starting the design definitions of input parameters (such as electrical and magnetic loading, torque requirement, air gap) will be done and validity of designed values and motor performances will be studied in this part.

T is the peak torque coming from the motor performance requirements and it is 50mNm (Figure 3-14). Another parameter to be defined is electrical loading value in motor inner peripheral. This parameter is related to the heating of machine. In reference [22] q value is defined for given output power/speed ratio. Motor maximum speed is defined as 10000RPM and the rated output power at operating point is defined in Eq. (4.12).

$$P_{out} = T_{load} x w_m \tag{4.12}$$

For 10000 RPM (1047 rad/sec) and 32mNm load torque output power is calculated as 33 W.

For 10000 RPM speed and 33W output power range typical electrical loading value is around 8000-10000Aturn/m (Figure 4-5).

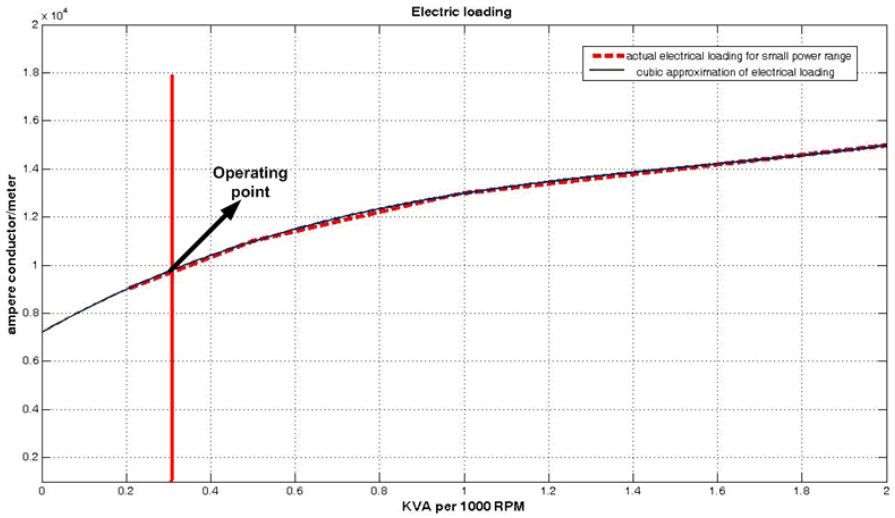

Figure 4-5: Electrical loading curve

These graphs are valid for motors that operate in earth environment. Since designed motor will operate in vacuum environment, heat removal by convection is not realized. In order to have a design margin selected electrical value should be lower than 8000-10000Aturn/m. As a design parameter electrical loading value is selected as 6000Aturn/m.

D_i and L are parameters to be defined in the sizing equations. In servo applications L is selected as long and D_i is selected small (D_i/L ratio is around 2/5). By choosing low D_i/L ratio inertia of the motor is made small and active winding to end winding ratio also become smaller. Low inertia means higher response in load changes and low active winding to end winding ratio means low resistive losses since end winding could not create torque. On the other had in our application long axial length L cause longer CMG in X axis and volume of the CMG and the inertia on Y axis increases (Figure 3-1).

Designed motor in CMG will operate in constant speed so there is no need to have low inertia on the contrary high inertia is required in order to store angular momentum. If rotor inertia becomes significant attached wheel volume and mass can be smaller.

In [22], in order to determine an optimum D_i/L ratio a design range is given in terms of core length/pole pitch for different number of poles (Figure 4-6).

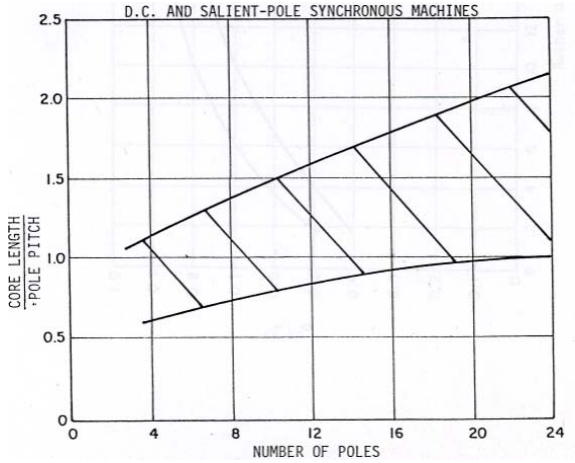

Figure 4-6: Core length /pole pitch for different number of poles

Pole pitch (PP) is defined as Eq. (4.13).

$$PP = \frac{\pi D_i}{p} \tag{4.13}$$

D_i is inner diameter of motor and ratio between pole pitch and core length should between 0.5 and 0.9, so D_i/L ratio interval can be calculated using Eq. (4.13) for 2 pole motor and is shown in Eq. (4.14).

$$\begin{aligned} 0.5 \le \frac{pL}{\pi D_i} \le 0.9 \\ 0.7 \le \frac{D_i}{L} \le 1.27 \end{aligned} \tag{4.14}$$

D_i/L ratio is selected as 1 for 2 pole RF motor. Since if D_i becomes larger, end winding resistance will be higher.

Air gap is another important design input to the magnetic circuit equations. 0.5mm air gap thickness is determined for mechanical clearance in RF motor, also in order to keep the magnets mechanically on the rotor some additional treatments

are required and 0.25mm is added to air gap to have enough place for mechanical enhancement (problems of attaching the magnet on the rotor surface will be explained later in this chapter). Total air gap distance is assumed to 0.75mm in RF motor design.

In order to find a reasonable air gap magnetic flux density value an iterative process is necessary in order to check whether this value can be obtainable for a given air gap and reasonable magnet thickness . In order define a proper air gap magnetic flux density magnetic circuit of the motor should be solved.

Sinusoidal excitation case motor dimensions are calculated using average value of fundamental air gap magnetic flux density (3.6.1.2). In order to see whether selected design value can be achievable by given design constrains (motor torque, electrical loading, air gap etc) following calculation and graphical visualization procedure is done in Matlab.

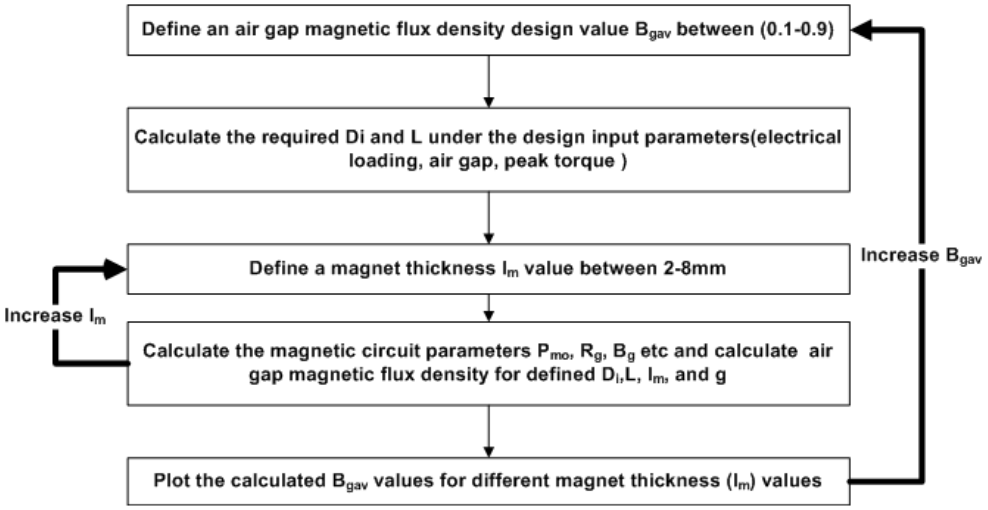

Figure 4-7: B_{gav} design value selection flow

Bgav design value is selected between the interval 0.1T to 1T and magnet thickness interval is selected to 2mm to 8mm. Summary of design constrains are shown in Table 2-1. Obtained results are shown in Figure 4-8.

Table 4-1: Design constrains of RF 2-pole Motor (sinus excitation)

Design parameter	Value
Peak torque requirement T_p (mNm)	50
Electrical loading q (Aturn/m)	6000
Inner diameter to axial length ratio (D_i/L)	1
Air gap g (mm)	0.75
B_{gav} design value (T) for sinusoidal excitation	0.1-0.9
Magnet thickness l_m (mm)	2-8 mm

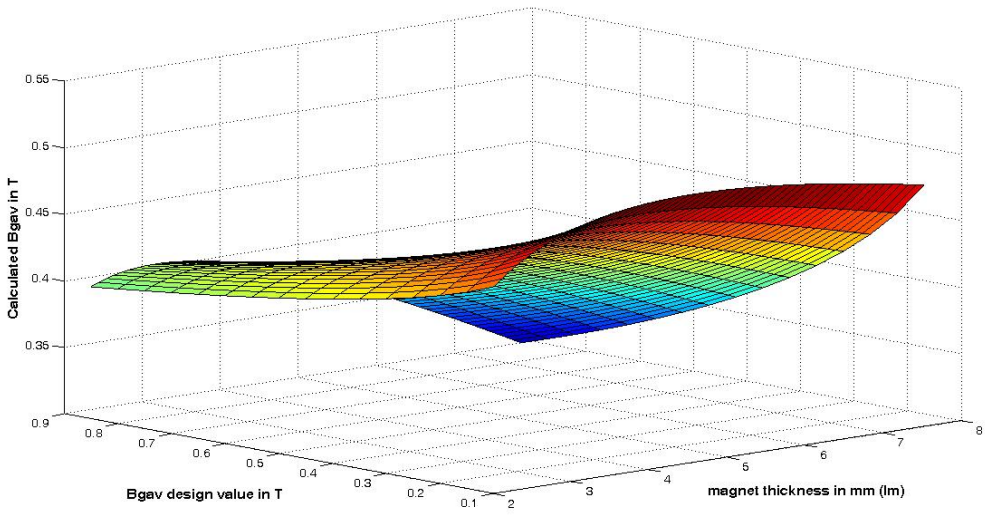

Figure 4-8: Calculated B_{gav} values for different B_{gav} design values and different magnet thickness (sinusoidal excitation)

It can be observed from Figure 4-8 that for sinusoidal excitation for B_{gav} design value higher than 0.43 T is not achievable for defined design constraints. In order to make motor as small as possible, B_{gav} design value is selected as 0.43 T. Since

all design parameters are defined for Eq. (4.12) dimensions of motor can be calculated. Using the parameters in Table 4-2 and Eq. (4.12), inner diameter and axial length values are calculated (Table 4-3)

Table 4-2: Design parameters of RF 2-pole Motor

Design parameter	Value
Peak torque requirement T_p (mNm)	50
Electrical loading q (Aturn/m)	6000
Inner diameter to axial length ratio (D_i/L)	1
Air gap g (mm)	0.75
B_{gav} design value (T) for sinusoidal excitation	0.43

Table 4-3: Inner radius and axial length of RF 2-pole motors

Parameter	
Inner diameter D_i (mm)	22.3
Axial length L (mm)	22.3

Since required dimensions for magnetic circuit are defined (D_i, L), required magnet thickness should be calculated in order to reach desired air gap magnetic field density.

A shaft is required for coupling of the load (wheel) and minimum diameter of 5mm assumed. Di is around 22 mm for both motor and air gap thickness is 0.75mm. Magnet thickness can be between 2-8 mm for both motors. For fixed design constrains magnetic circuit equations is solved and calculated air gap magnetic field densities for different magnet lengths are shown in and Figure 4-9.

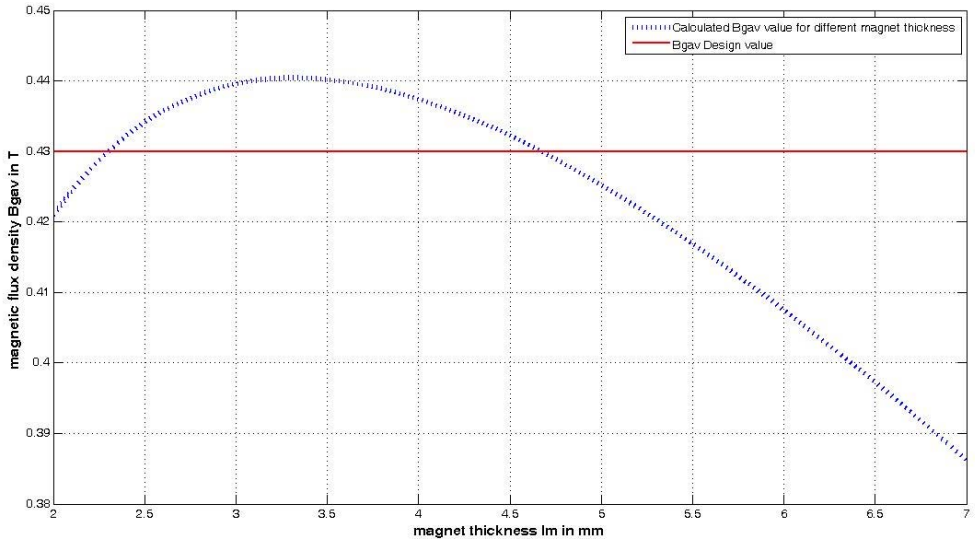

Figure 4-9: Calculated B_{gav} values for different magnet thickness (sinusoidal excitation)

Required average air gap magnetic flux density value (B_{gav}) can not be achieved for magnet thickness values lower than 2.3mm, also for thickness values higher than 4.6 mm resultant air gap magnetic field distribution can not be achieved. This result is coming from the radial shape of the magnet. As magnet thickness (l_m) increase B_{gav} is increasing but after some level, area of the magnet becomes smaller because area of magnet is calculated using average radius of magnet (R_m) in Eq. (4.1) (In Figure 4-10 magnet thickness is smaller in case (b) and since inner radius of motor is same for both cases average radius of magnet is smaller in case (b)). Magnets internal permanence (Eq. (4.1)) is dependent on area of magnet as area begins to decrease permeance of magnet is increasing or another words magnet reluctance is becoming larger and air gap magnetic flux density decreases.

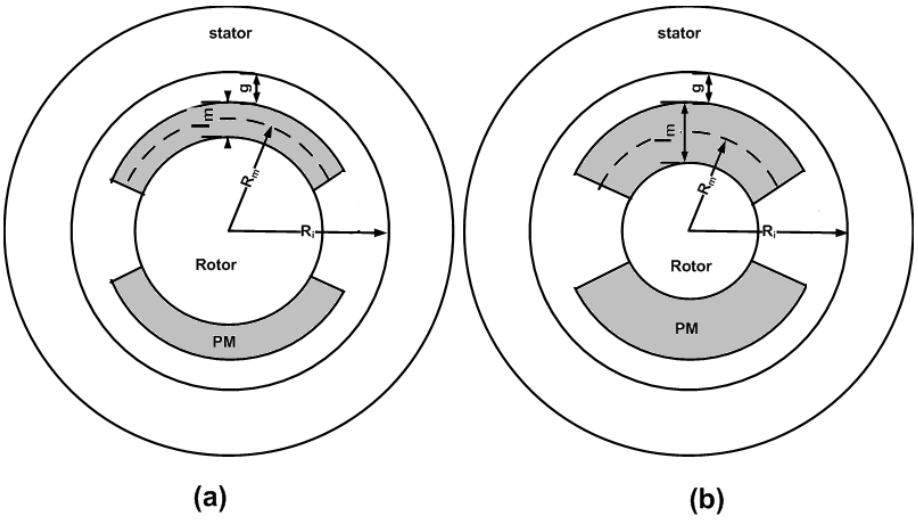

Figure 4-10: Effect of magnet thickness on area of magnet

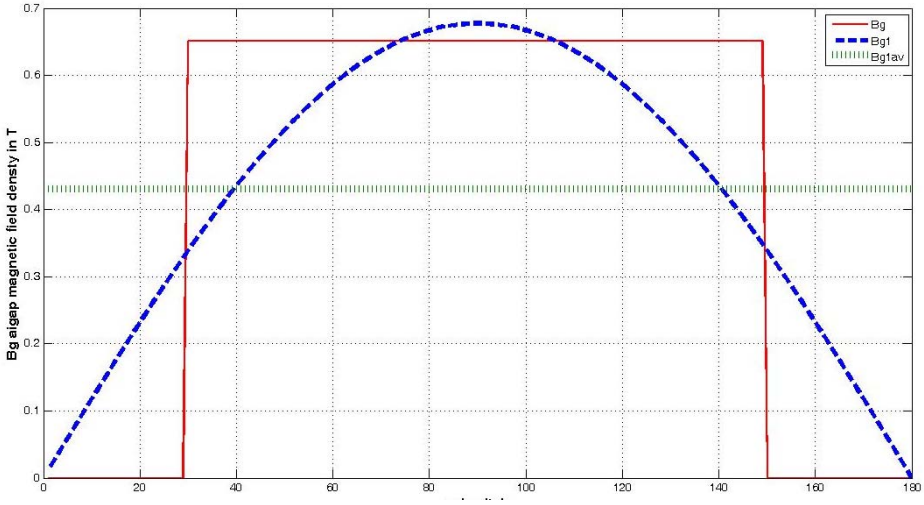

Figure 4-11: Air gap magnetic flux density distribution over pole pitch for sinusoidal excitation

While determination of the magnetic circuit equations stator core is assumed to be infinitely permeable which not the actual case is. In order to have margin for MMF drop on the core, magnet thickness is selected as 3mm. Resulting magnetic flux distribution over pole pitch is shown in Figure 4-11.

After determining the inner diameter, axial length air gap, and magnet thickness, remaining parameter is the outer diameter of the motor. Before calculating the outer diameter slot depth (h_s) should be calculated (Figure 4-12).

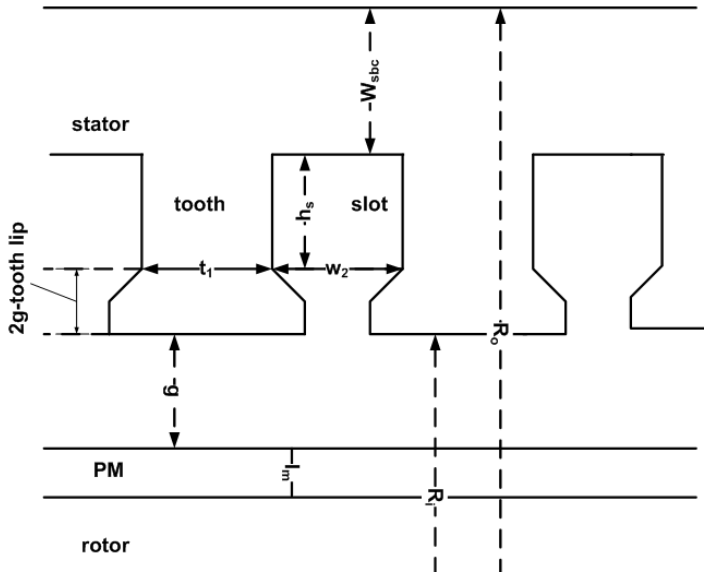

Figure 4-12: RF motor stator dimensions

Total number of conductors placed on the stator is 6 times number of turns per phase and total required conductor area (A_{con}) area can be expressed in Eq (4.17).

$$A_{con} = 6N_{ph}A_{wire} \tag{4.17}$$

A_{wire} is area of one conductor wire and it can be expressed using current density (J) and rms current on the conductor (I_{rms}). While conductors are putted in slots fill factor should be kept in mind for mechanical reasons (K_{cu}). Using Eq. (4.17) fill factor and current density required total slot area in the stator can be expressed as in Eq.(4.18)

$$A_{slot} = \frac{6N_{ph}A_{wire}}{K_{cu}} = \frac{6N_{ph}I_{rms}}{JK_{cu}} \tag{4.18}$$

Required total slot area can also be expressed by mechanical motor dimensions (Figure 4-12) (Eq. (4.19)). Stator slot shape is assumed as parallel sided for simplification of calculations. Rotor tooth width (t_1) is assumed to be equal to slot width (w_2). In fact the teeth are parallel sided.

$$A_{slot} = \frac{\pi(\frac{D_i}{2} + h_s)^2 - \pi(\frac{D_i}{2})^2}{2} \tag{4.19}$$

K_{cu} is copper fill factor and it is assumed to be 0.4, current density *(J)* is assumed to be 7A/mm^2 . Slot depth can be calculated by substituting Eq.(4.20) into Eq. (4.18) and equating A_{slot} equations in Eq. (4.19) and Eq. (4.18).

$$\begin{aligned} q &= \frac{6N_{ph}I_{rms}}{\pi D_i} \\ N_{ph}I_{rms} &= \frac{q\pi D_i}{6} \end{aligned} \tag{4.20}$$

By equating required slot area expressions in Eq (4.19) and Eq. (4.18) resulting 2nd degree polynomial equation can be solved for slot depth h_s (Eq. (4.21)). All parameters in Eq. (4.21) is determined. (fill factor (K_{cu}) 0.4, current density *(J)* 7A/mm^2, remaining parameters are in Table 4-2 and Table 4-3)

$$h_s = \sqrt{D_i^{\,2} + \frac{4D_i q}{K_{cu} J}} - D_i \tag{4.21}$$

Next parameter to be defined before defining the outer diameter is stator back core thickness (W_{sbc}). Stator back core flux density determines the back core area and also back core thickness since axial length of motor is already determined. As it can be seen from the Figure 4-21, half of the flux per pole is passing through stator back core. B_{gav} (Figure 4-11) is already determined and using magnetic equivalent circuit back core flux can be calculated using Eq. (4.22).

$$\begin{aligned} \Phi bc = B_{sbc}A_{bc} &= \frac{\Phi p}{2} = \frac{B_{gav}A_{pole}}{2} \\ A_{bc} &= W_{sbc}L \\ A_{pole} &= \frac{2\pi R_i}{p}L \end{aligned} \tag{4.22}$$

L is already calculated, only the unknown parameter in Eq. (4.22) is the average stator back core flux density (B_{sbc}). Flux density at the back core should be chosen based on the ferromagnetic material properties used in stator. Figure 4-13 shows the BH curve of selected material.

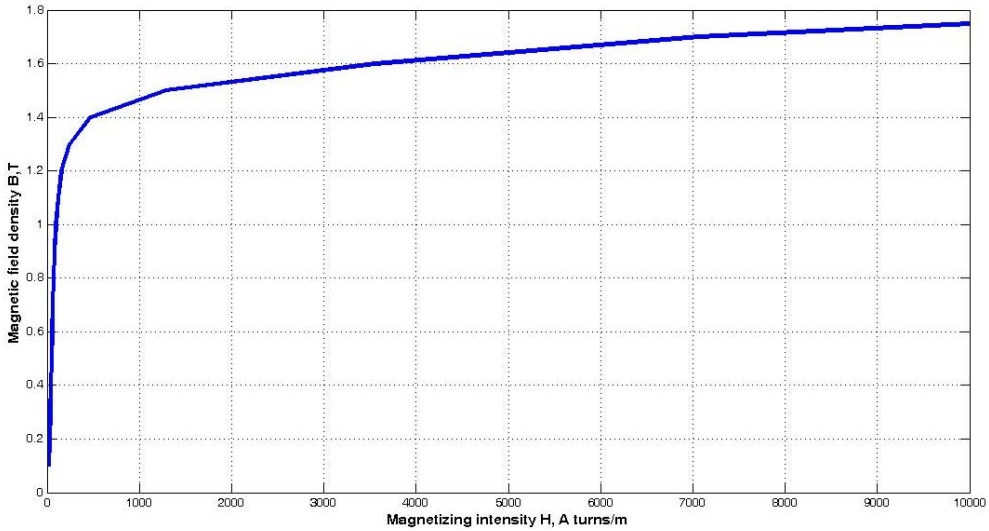

Figure 4-13: BH curve of Cogent power No 12

Selected ferromagnetic material begins to saturate after 1.2 T and MMF drop is acceptable up to 1.4T level. Flux in the stator is time varying and it is assumed to have sinusoidal variation. Peak value of the back core flux density is assumed to 1.4T (B_{sbcp}) and the of it is 0.9T (B_{sbc}, 2/л of peak value). Under the determined parameters W_{sbc} can be calculated using Eq. (4.23).

$$W_{sbc} = \frac{B_{gav} A_{pole}}{2LB_{sbc}} \tag{4.23}$$

In order to keep the coils inside the stator tooth and reduce affect of slots on air gap, a tooth lip of 2 g is added and it has a contribution to outer diameter (Figure 4-12). Outer diameter of the motor can be calculated using Eq. (4.24).

$$D_o = Di + 2hs + 4g + 2W_{sbc} \tag{4.24}$$

Calculated parameters are summarized in Table 4-4.

Table 4-4: Stator dimensions of RF 2-pole motor (sinusoidal excitation)

Parameters	
Outer diameter D_o (mm)	49.9
Slot depth h_s (mm)	3.9
Stator back core thickness W_{sbc} (mm)	8.4

4.3.1 Winding design

To determine the number of turns per phase Eq. (3.21) derived in Chapter 3 is used.

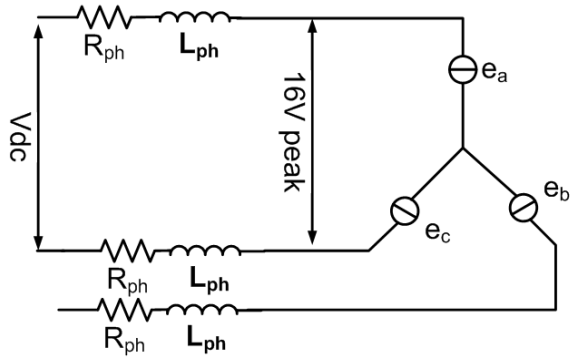

Figure 4-14 Voltages on Y connected motor

In sinus excitation peak value of line to line back emf voltage should not be larger than the minimum available dc link voltage. 2 V is assumed as margin to resistive and transistor voltage drops, and peak value line to line back emf voltage emf voltage should be lower than 16V (Figure 4-14). Ratio between line to line back

emf voltage and phase back emf peak voltage under Y connected phase windings is $\sqrt{3}$. Since in Eq. (3.21) RMS value of the phase back emf is calculated (e_{rms}) and rms value of back emf voltage should be lower than $16/\sqrt{6}$ in sinusoidal excitation case.

Eq. (3.21) can be rewritten in order to find number of turns per phase (Eq. (4.25)).

$$N_{ph} = \frac{2\sqrt{2}e_{rms}}{\pi B_{gav} D_i L w_m} \tag{4.25}$$

w_m is used as maximum speed of the motor and remaining parameters are already calculated, number of turns per phase is calculated and results are shown in Table 4-5. Since number of turn per phase can not be a fractional number values are approximated to exact numbers.

Table 4-5: Number of turns per phase of RF 2-pole Motor (sinus excitation)

Parameter	Sinusoidal excitation
N_{ph} calculated value	26.23
N_{ph} assumed value	27

Total number of slots is assumed to be 18. Number of slots per pole per phase becomes 3. Figure 4-15 shows the winding distribution of stator.

slot number	1	2	3	4	5	6	7	8	9	10	11	12	13	14	15	16	17	18
phase winding	A	A	A	-C	-C	-C	B	B	B	-A	-A	-A	C	C	C	-B	-B	-B
number of turns per slot	9	9	9	9	9	9	9	9	9	9	9	9	9	9	9	9	9	9
poles	pole1									pole2								

Figure 4-15: Winding distribution RF 2 pole motor (sinus exciation)

4.3.2 Equivalent circuit parameters

4.3.2.1 Determination of phase resistance

Basic resistance equation (Eq. (4.26)) can be used to determine the phase resistance.

$$R_{ph} = \frac{\sigma L_{co}}{A_{co}} = \sigma \frac{LMC \times N_{ph}}{A_{cu}}$$
$$Aco = \frac{I_{rms}}{J} \tag{4.26}$$

A_{co} is area of the cupper

LMC is mean length of the conductor turn

σ is resistivity of cupper 1.72×10^{-8} Ωm

$\boldsymbol{J}$ is current density ($7 A/mm^2$)

LMC is dependent on motor geometry and LMC for one conductor is shown in Figure 4-16.

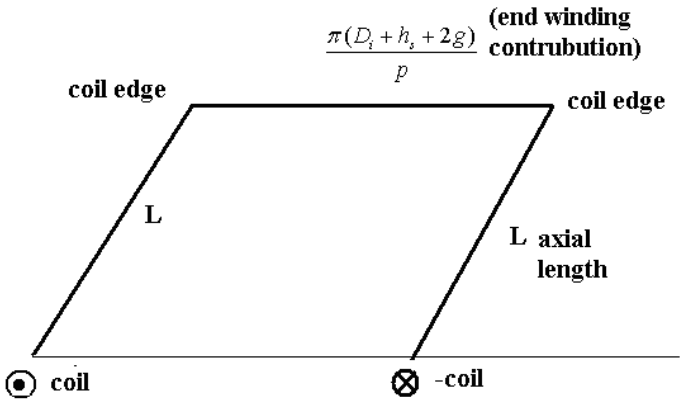

Figure 4-16: LMC of one conductor

LMC of one conductor can be calculated using Eq. (4.27). Since conductors at the edges can not turn directly, an estimate for bending radius effect should be added.

There are several industry standards that give minimum bending radius for many different cable types. National Electrical Code (NEC) and the Insulated Cable Engineers Association (ICEA)) but to make calculations simpler 5-6 times wire diameter is used for single wire. There are 9 conductors in each slot. Estimated value of wire diameter is around 0.7mm, and in order to have margin for bending length at the coil edges 7mm is added to *LMC* calculations.

$$LMC = (2L + \frac{\pi(D_i + h_s + 2g)}{p}) + 2x0.007 \tag{4.27}$$

Remaining parameter in Eq. (4.26) is the area of conductor and it can be approximated using the Eq. (4.19) and resulting area is approximated by known parameters at Eq. (4.28).

$$A_{co} = \frac{q\pi D_i}{6N_{ph}J} \tag{4.28}$$

After defining of the parameters at Eq. (4.26) phase resistance is calculated 120 mΩ .

4.3.2.2 Determination of phase inductance

Phase inductance (*Lph*) is summation of three main inductances. First inductance is phase air gap inductance (L_g), second is slot leakage inductance (L_{lek}), end turn inductance (L_e). Air gap inductance is calculated based on magnetic equivalent circuit per pole pair (Figure 4-17) and Eq. (4.29) [20].

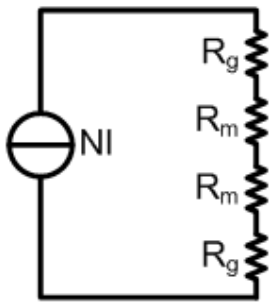

Figure 4-17 Equivalent circuit per pole pair

$$\lambda s = N\Phi_{sbc}$$
$$\lambda s = \frac{L}{I}$$
$$\Phi_{sbc} = \frac{NI}{2Rg + 2Rm}$$
$$Rm = \frac{1}{Pm} \tag{4.29}$$
$$L = \frac{N^2}{2Rg + 2\frac{1}{Pm}}$$
$$L_g = \frac{P}{2}L$$

N is number of turns per phase per pole pair. Remaining parameters are already calculated in magnetic circuit equations and dimension equations.

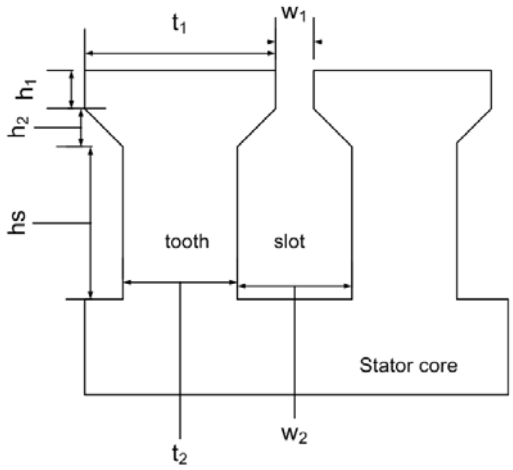

Figure 4-18: Slot geometry

Slot leakage inductance is dependent on the slot geometry. Tooth width is assumed to slot width in order to simplify calculations, and shape of the slot is shown in Figure 4-18 and calculated dimension values are summarized in Table 4-7.

Slot leakage inductance is calculated based on Eq. (4.30) [20].

$$L_{lek} = n_c(2N_c^{\,2})\left[\frac{\mu_o hsL}{3w_2} + \frac{\mu_o h_2 L}{(w_1 + w_2)/2} + \frac{\mu_o h_1 L}{w_1}\right] \tag{4.30}$$

N_c is total number of conductors in slot,

n_c is total number of slots per phase

Last inductance value is end turn inductance. It is calculated according to the Eq. (4.31) [20].

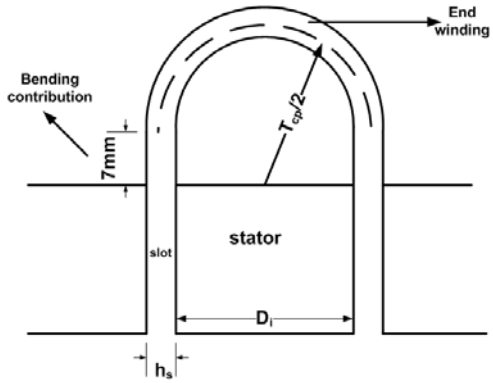

Figure 4-19: End winding

$$L_e = \frac{n_c \mu_o T_{cp} N_c^{\,2}}{8} \ln\left(\frac{T_{cp}\sqrt{\pi}}{\sqrt{2A_{slot}}}\right)$$
$$A_{slot} = w_2 hs + \left[\frac{(w_2 + w_1)}{2} h_2\right] + (h_1 w_1) \tag{4.31}$$

In order to simplify the calculations effect of bending contribution is ignored and T_{cp} is assumed as equal to inner diameter of the motor (D_i). remaining calculated dimensions are shown in Table 4-7. Summary of calculated inductance values are shown in Table 4-6.

Table 4-6: Inductance values for RF 2-pole Motor under sinusoidal excitation

Parameters	
Air gap inductance L_g (μ H)	105.9
Leakage inductance L_{lek} (μ H)	49.2
End turn inductance L_e (μ H)	1.9
Phase inductance L_{ph} (μ H)	157

4.3.3 Calculation of losses

Losses in brushless dc motor are composed of core losses and resistive losses. Core loss composed of two major components one is hysteresis loss and second is eddy current losses as explained in Chapter 3. Core losses are usually difficult to calculate exactly, an approximation under 1 T can be done using Eq. (4.32) ([14], [13]).

$$\begin{aligned} P_c &= P_h + P_e \\ P_h &= k_h f B^n \\ P_e &= k_e f^2 B^2 \end{aligned} \tag{4.32}$$

P_c is total core loss W/kg

P_h is hysteresis losses W/kg

P_e is eddy current losses W/kg

k_h is hysteresis loss coefficient

k_e is eddy current coefficient

f is electrical frequency

B peak magnetic flux density value on the core

Coefficient n usually between 1.5-2.5 and it is assumed as 2 in this thesis [13]. Selected material ARMCO NO12 loss values for different magnetic field density and frequency is expressed in Table 3-7 .

By using two different data from manufacturer data sheet in Table 3-7, at 0.4T at 50 Hz and 0.4T 400hz coefficients are approximated as k_h 0.0314 and k_e 2.18x10^{-5}. Resulting approximated core loss curves and actual data from the core loss curves are shown in Figure 4-20 for different maximum magnetic flux density and frequencies.

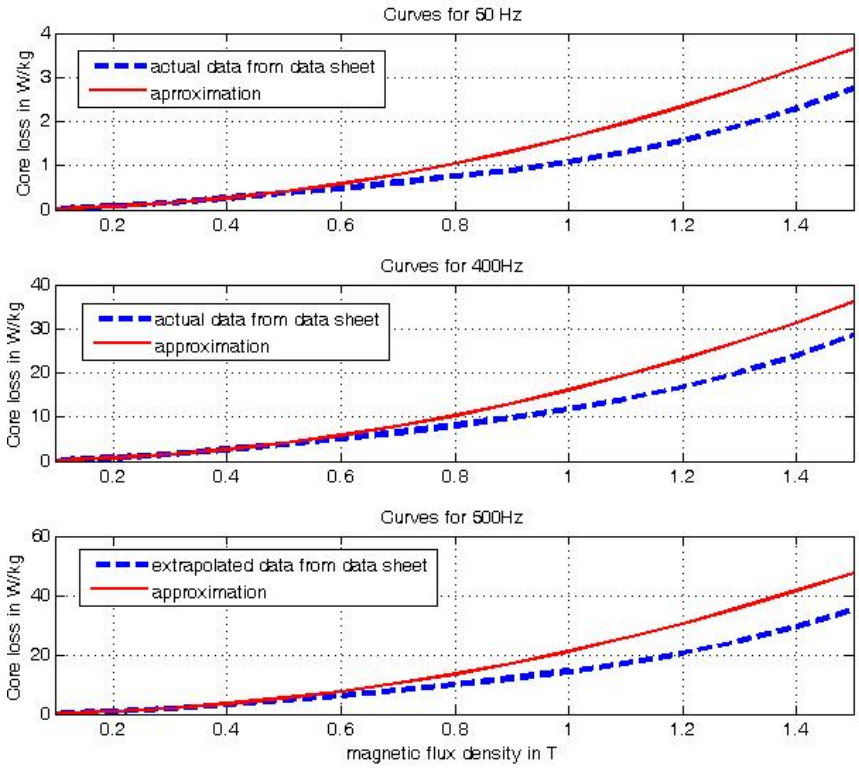

Figure 4-20: Core loss vs magnetic flux density for different frequencies (Cogent power no 12)

For larger magnetic field densities above 1T and larger frequencies, approximation results are larger than the manufacturer data but this difference is assumed as margin to core loss calculations.

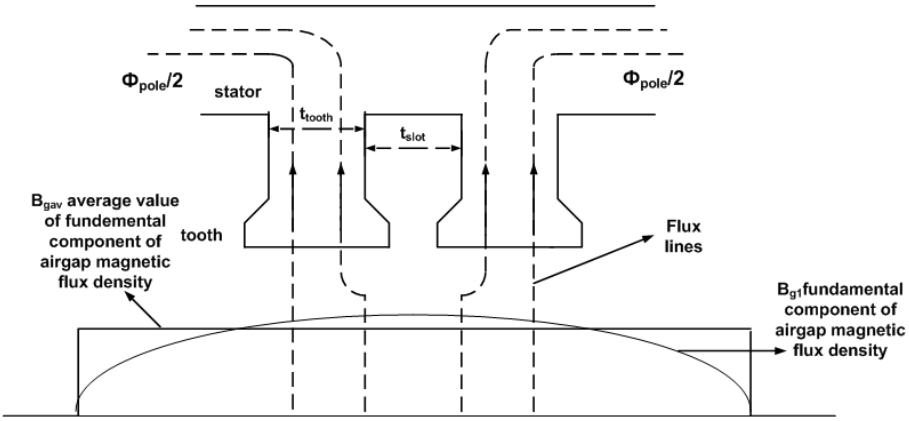

Figure 4-21 Flux distribution on stator (RF motor)

Since flux is stationary at rotor there is no loss on rotor .On the other hand flux density in the stator is time varying so hysteresis and eddy current losses exist. Losses on the stator are composed of losses on stator teeth and losses at stator back core. Core losses are calculated using the maximum flux density on core material. Peak value of flux density in stator back core is determined as 1.4T (B_{sbcp} =2B_{sbc}/л) in 4.3 while determining stator back core thickness. Maximum flux density on stator teeth is dependent on average of fundamental component of air gap flux density (Note that 3rd harmonic is eliminated by 120^0 magnet shape and higher order harmonics are ignored). Assuming equal slot width to tooth width and no flux is passing through slots; average flux density at stator tooth can be calculated using (Eq. 4.33).

$$B_{tooth} = \frac{B_{gav}(t_{slot} + t_{tooth})L}{t_{tooth}L}$$
$$B_{tooth} = \frac{B_{gav}}{2} \tag{4.33}$$

Note B_{gav} is already calculated value is 0.43T (Figure 4-11), so average flux density at stator tooth is 0.86T. Assuming sinusoidal variation at stator teeth peak value of stator teeth flux density becomes 1.35T (B_{toothp}). All parameters in Eq.(4.37) are determined separately for stator back core and stator teeth. Core loss can be calculated in terms of W/kg using Eq. (4.32). Total core loss in the motor

can be calculated using mass of stator back core and stator teeth mass (Eq. (4.34)) and Eq. (4.32). calculation is done in the following way. Electrical frequency and peak flux density values are substituted into Eq.(4.32) and since coefficients k_h (0.0314) and k_e ($2.18\text{x}10^{-5}$) are determined corresponding W/kg core loss value is obtained. Then mass of the core material (tooth and stator back core) is multiplied by obtained value (P_c) so core loss value is calculated at that operating condition.

$$\begin{aligned} P_{core} &= P_c(M_{statorbackcore} + M_{statorteeth}) \\ M_{statorbackcore} &= pi(R_o{}^2 - (R_o - W_{sbc})^2)Ld_{steel} \\ M_{statorteeth} &= n_{st}(t_2 hs + t_1 h_1 + (\frac{t_1 + t_2}{2})h_2)Ld_{steel} \end{aligned} \tag{4.34}$$

d_{steel} is the density of stator steel 7650 kg/m^3 (Cogent Power No 12), $M_{statorbackcore}$ and $M_{statorteeth}$ are mass of stator back core and stator teeth respectively. Dimensions of tooth and stator are shown in Figure 4-18 and dimension values are shown Table 4-7.

In sinusoidal excitation case resistive (copper) losses can be calculated using Eq. (4.35).

$$P_{co} = 3I_{inrms}{}^2 R_{ph} \tag{4.35}$$

In order to calculate total resistive (copper) losses in the motor, the total input current coming into motor should be calculated. Core losses should be taken into account while calculating total power and current coming into motor. Since resistive losses are calculated using phase rms currents, one third of core losses are added to each phase current.

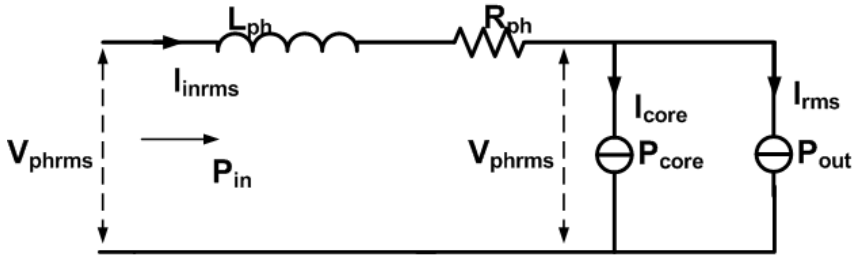

Figure 4-22: Power flow in motor

Assuming vector control is applied to motor total phase rms input current can be calculated using Eq. (4.36).

$$I_{inrms} = I_{rms} + \frac{P_{core}}{3V_{phrms}}$$
$$V_{phrms} = \sqrt{(ZI_{rms})^2 + e_{rms}{}^2} \quad (4.36)$$
$$Z = \sqrt{(wL_{ph})^2 + R_{ph}{}^2}$$

Z is phase impedance, w is electrical speed, L_{ph}, R_{ph} are phase inductance and resistance respectively.

4.3.4 Calculation of motor volume and mass

By ignoring the winding and mechanical fixtures (hausing, bearings and windings), volume and mass of the RF motor can be calculated using Eq. (4.37) and Eq. (4.38) respectively(dimensions are shown in Figure 4-23 and value of dimensions are shown in Table 4-7).

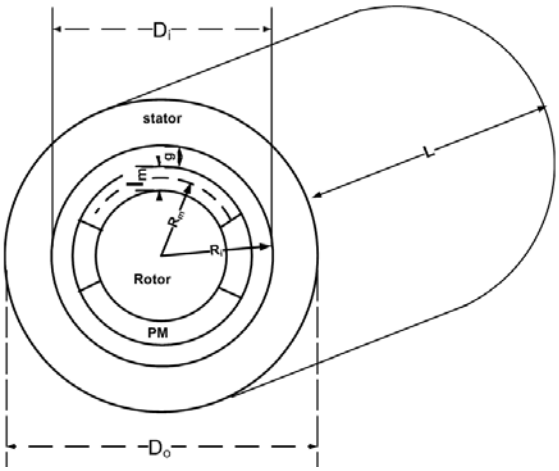

Figure 4-23 RF motor dimensions

$$V_{motor} = \pi R_o{}^2 L \tag{4.37}$$

$$\begin{aligned} M_{motor} &= M_{rotor} + M_{magnet} + M_{stator} \\ M_{rotor} &= \pi (Ri - l_m - g)^2 L d_{steel} \\ M_{magnet} &= \frac{2\pi\left[(Ri-g)^2 - (Ri-g-l_m)^2\right]L}{3} d_{magnet} p \\ M_{stator} &= M_{statorbackcore} + M_{statorteeth} \end{aligned} \tag{4.38}$$

d_{magnet} is density of magnet (8400 kg/m^3), d_{steel} is the density of steel (7650 kg/m^3), $M_{statorteeth}$ and $M_{statorbackcore}$ can be calculated using Eq. (4.34).

Inertia of total rotor composed of two parts one is coming from rotor core and second is magnets and it can be calculated using Eq. (4.39) [24].

$$I_{rotor} = M_{magnet}\left[\frac{(Ri-g)^2 + (Ri-g-l_m)^2}{2}\right] + M_{rotor}\left[\frac{(Ri-g-lm)^2}{2}\right] \tag{4.39}$$

Summary of main dimensions, and calculated volume and mass of the motor is given in Table 4-7.

Table 4-7: Main dimensions, mass and volume

D_i inner diameter (mm)	22.3
D_o outer diameter (mm)	49.9
L axial length (mm)	22.3
g air gap (mm)	0.75
h_s slot depth (mm)	3.9
l_m magnet thickness (mm)	3
h_1 tooth lip-1 (mm)	0.75
h_2 tooth lip-2 (mm)	0.75
w_1 lip opening (mm)	1
$w_2$slot thickness (mm)	2.3
W_{sbc} stator back core thickness (mm)	8.4
t_1 tooth width at air gap (mm)	2.9
t_2 tooth width (mm)	2.3
Inertial of motor (kgm^2)	$2.51x10^{-6}$
Volume of motor (m^3)	$4.36\ x10^{-5}$
Mass of motor (kg)	0.285

4.3.5 Performance of RF motor under sinusoidal excitation

4.3.5.1 Required motor current and electrical loading over speed range

Air gap magnetic field density is assumed to be constant over whole speed range (B_{gav}). Electrical loading and required motor rms phase current values are dependent on motor torque profile in Figure 3-14, they can be calculated over speed range using Eq. (4.40) and (4.41) for sinusoidal excitation since remaining parameters are already calculated constant values. This is done by substituting torque for a given speed value (from Figure 3-14) into Eq. (4.46), electrical

loading value can be calculated and the value of electrical loading is substituted into Eq. (4.41) to find the rms value of phase current for this operating condition.

$$q = \frac{4\sqrt{2}T_m}{\pi^2 B_{gav} D_i^{\,2} L} \tag{4.40}$$

$$I_{rms} = \frac{q\pi D_i}{6N_{ph}} \tag{4.41}$$

Calculated results of electrical loading and required motor current are shown in Figure 4-24 .

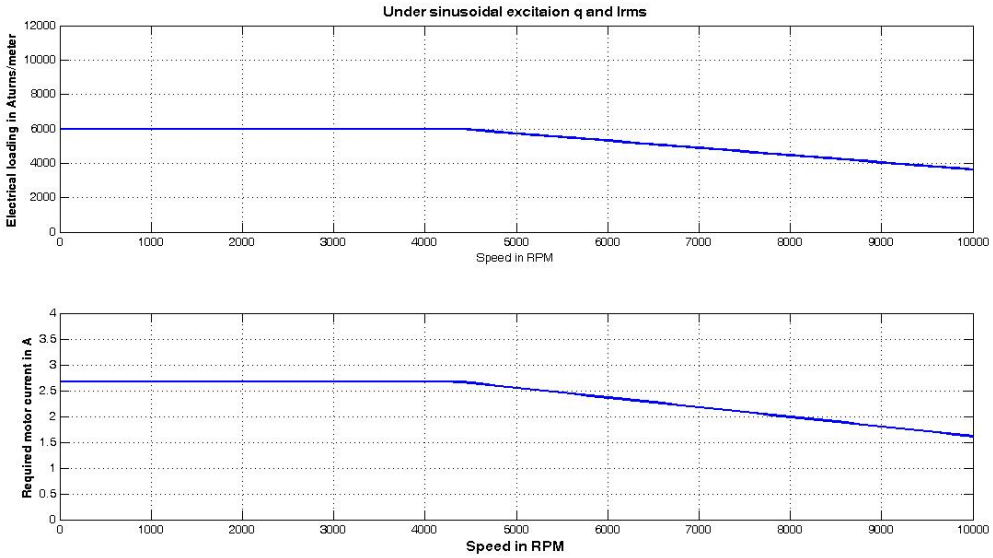

Figure 4-24: Electrical loading and required rms motor current (sinusoidal excitation)

4.3.5.2 Required line to line voltage and back emf voltage over speed range

Note that the current drown from the supply should also provide for the core losses. So the total phase current can be calculated using Eq. (4.36). Rms value of back emf voltage and phase voltage is calculated using Eq. (3.21) and Eq. (4.36) respectively. Peak value of line to line voltage can be calculated as $\sqrt{6}\ V_{phrms.}$ And

this value should be less than available dc link voltage. Calculated results are shown in Figure 4-25.

$$I_{inrms} = I_{rms} + \frac{P_{core}}{3V_{phrms}}$$

$$V_{phrms} = \sqrt{(ZI_{rms})^2 + e_{rms}{}^2} \tag{4.36}$$

$$Z = \sqrt{(wL_{ph})^2 + R_{ph}{}^2}$$

$$e_{RMS} = \frac{e}{\sqrt{2}} = \frac{\pi}{2\sqrt{2}} N_{ph} B_{gav} D_i L w_m \tag{3.21}$$

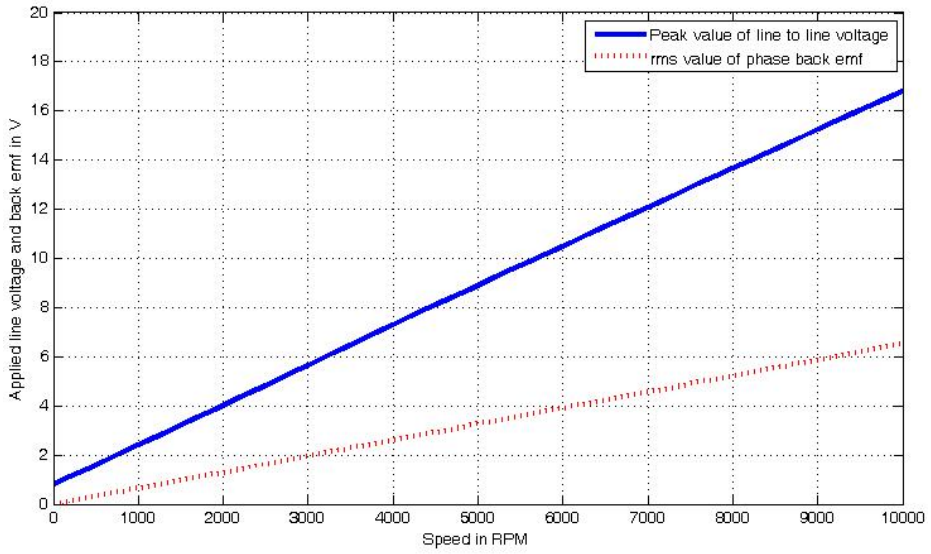

Figure 4-25 Line to line voltage and back emf voltage for RF 2 pole sinusoidal excitation

4.3.6 Losses over speed range

Core losses and resistive losses can be calculated using the equations in 4.3.3 Obtained results is shown in Figure 4-26.

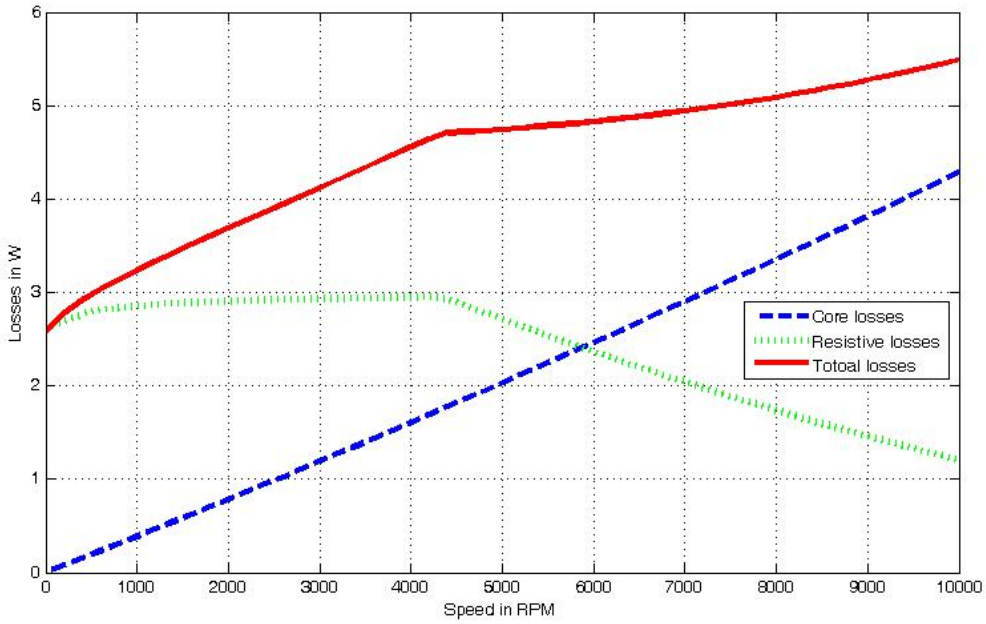

Figure 4-26 Losses in sinusoidal excitation

4.3.7 Efficiency

Efficiency is defined as output power over total input power, and it is calculated based on Eq. (4.42). Figure 4-27 shows the efficiency over whole speed range.

$$\eta = \frac{P_{out}}{P_{in}} = \frac{T_{out} \times \omega_r}{T_{out} \times \omega_r + P_{cu} + P_{core}} \tag{4.42}$$

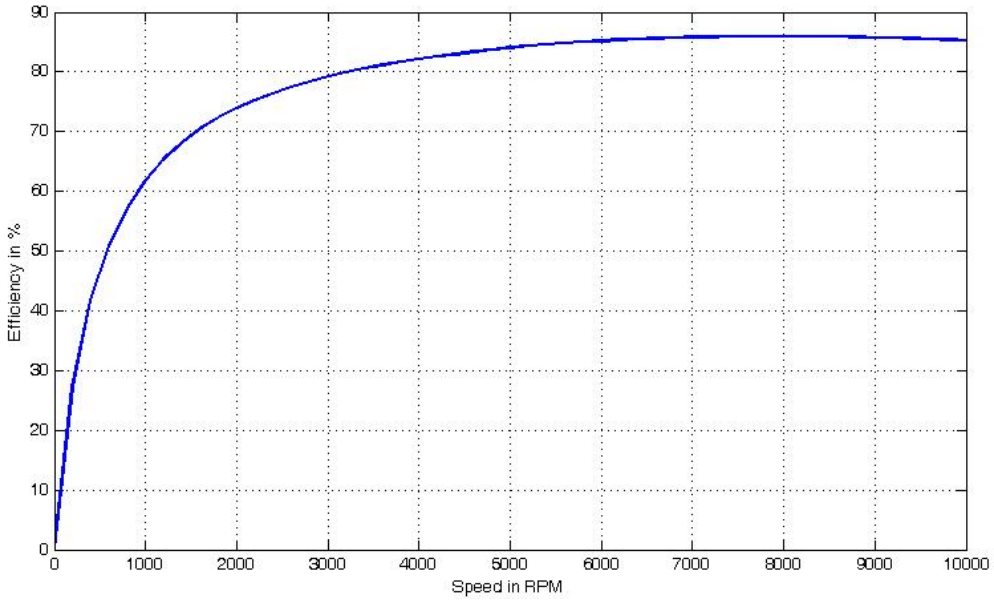

Figure 4-27: Efficiency (sinusoidal excitation)

4.3.8 Evaluation of RF 2 pole motor under sinusoidal excitation

- Motor peak electrical loading value vas determined as 6000Aturn/m. Calculated value of electrical loading is shown in Figure 4-24, and during acceleration period electrical loading value is not more than the limit value. During steady state at 10000RPM electrical loading value is around 3900Aturn/m, this means heating of machine will be less at steady state. Note that during the calculation of electrical loading core loss currents was not added to rms phase current. When core losses are added resulting electrical loading is becoming larger(Figure 4-28). During acceleration period electrical loading becomes larger than the design peak value but duration is less than 60 seconds. At steady state current loading is around 4000 Aturns/m and design will be on the safe side.

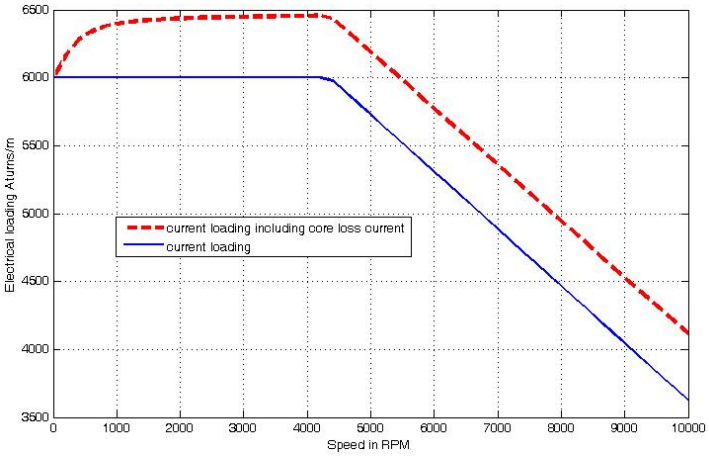

Figure 4-28 Current loading of motor with core loss are added (RF 2 pole-sinus excitation)

- Maximum current density at stator coils is selected as 7A/mm^2. Peak current on stator coil is calculated as 2.7A (Figure 4-24) during acceleration period. Necessary conductor area is calculated using these two values and it is 0.38mm^2. It should be checked whether conductors can be inserted into slots. Using 0.4 fill factor and 9 conductors per slot, 8.4mm^2 slot area is required. Designed slot dimensions are summarized in Table 4-7 and slot area is calculated as 8.87mm^2 using calculated dimensions, so conductors can be inserted into designed slots.
- Figure 4-25 shows the peak line to line voltage and phase back emf rms voltage over speed range. Peak line to line voltage is maximum at 10000 RPM and its value is 16.5V. This value is less than minimum available dc link voltage (18V) if we add the switch voltage drop of 1.4V, so design is in safe side.
- Resistive losses during acceleration period are large due to high current demand, where as core losses are small since frequency is smaller. As speed rises up to steady state current requirement is less and resistive losses become smaller but core losses are becoming higher. Efficiency is dependent on the total losses so as total losses increases efficiency of motor decreases.

4.4 Design of 2 pole RF motor under square wave excitation

Same design procedure in sinusoidal excitation case is applied for square wave excitation. Difference is only the torque equation. Eq. (4.43) is used instead of Eq. (4.11) is used.

$$T_p = \frac{\pi}{\sqrt{6}} B_g q D_i^2 L \tag{4.43}$$

Design parameters peak torque (T_p), electrical loading (q), and D_i/L ratio is same for square wave excitation. In torque equation of square wave excitation flat top value of air gap magnetic flux density (B_g) is to be determined. In order to find a proper air gap flux density value a similar process is done for square wave excitation case (Figure 4-29).

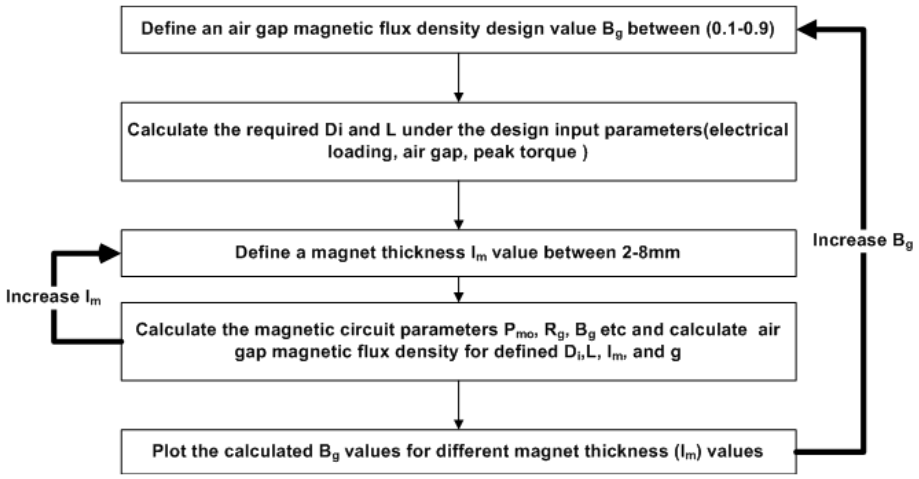

Figure 4-29: B_g design value selection flow

Summary of design constrains are shown in Table 4-8. Obtained results are shown in Figure 4-30.

Table 4-8: Design constrains of RF 2-pole Motor (square wave excitation)

Design parameter	Value
Peak torque requirement T_p (mNm)	50
Electrical loading q (Aturn/m)	6000
Inner diameter to axial length ratio (D_i/L)	1
Air gap g (mm)	0.75
Bg design value (T)	0.1-0.9
Magnet thickness lm (mm)	2-8

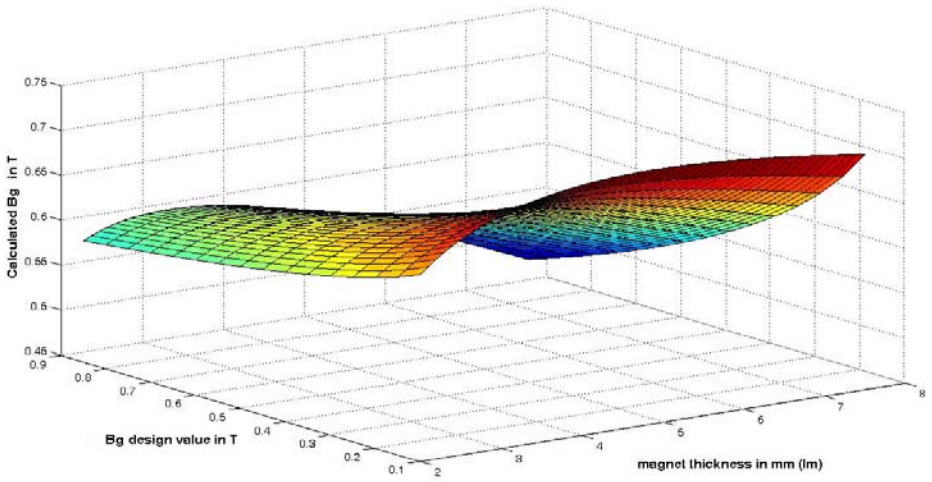

Figure 4-30: Calculated B_g values for different B_g design values and different magnet thickness (Square wave excitation)

For square wave excitation for B_g design values higher than 0.62T can not be reached determined design input parameters (electrical loading, air gap etc). B_g is selected as 0.62T and inner diameter and axial length of motor is calculated using Eq. (4.43). (Table 4-9)

Table 4-9 Inner radius and axial length of RF 2-pole motors (square wave excitation)

Parameter	
Inner diameter D_i (mm)	21.9
Axial length L (mm)	21.9

In order to find necessary magnet thickness same study is done as in sinusoidal excitation case.

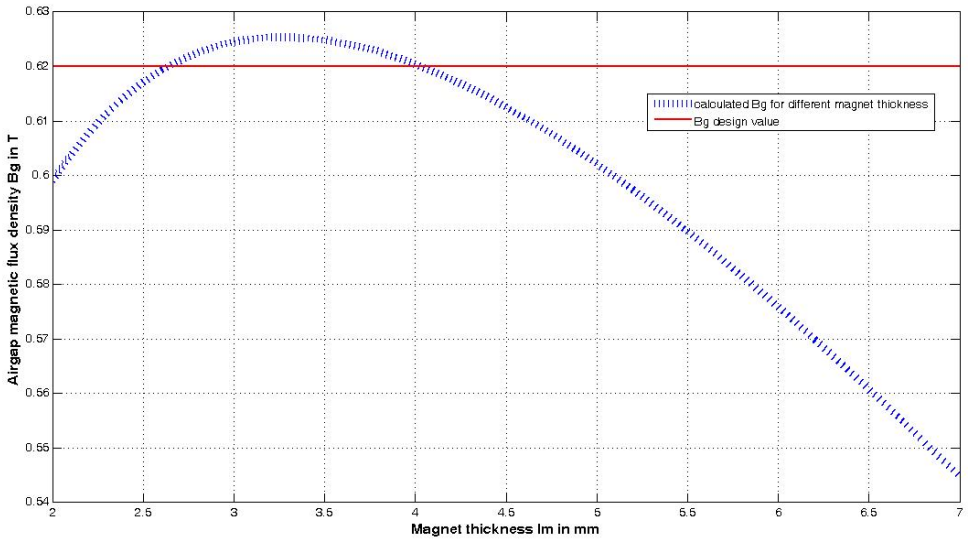

Figure 4-31: Calculated B_g values for different magnet thickness (square wave excitation)

Magnet thickness is selected as 3mm in order to have margin for mmf drop at core(Figure 4-31). Resulting magnetic flux density distribution over pole pitch is shown in Figure 4-32.

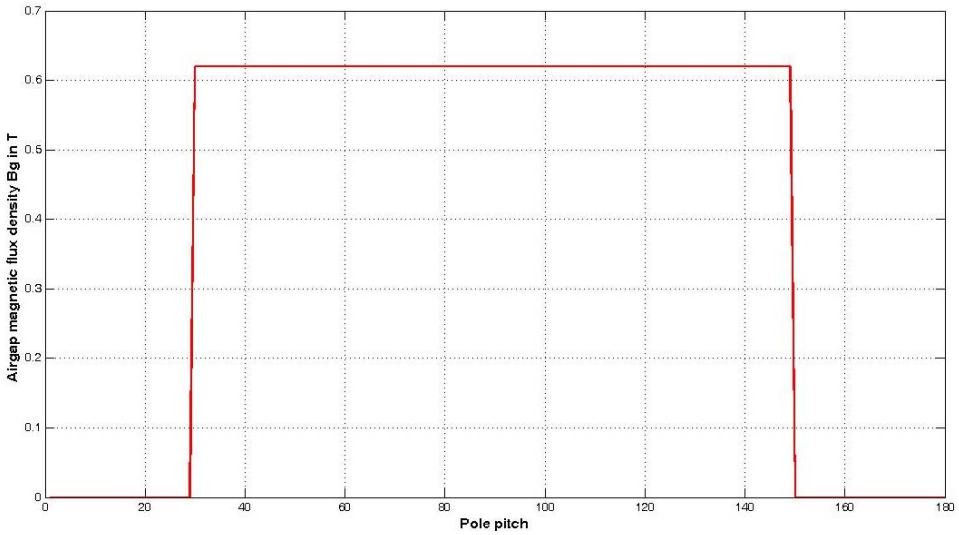

Figure 4-32: Air gap magnetic flux density distribution over pole pitch

Stator dimensions of motor (Figure 4-12) are calculated using the same procedure as in sinusoidal excitation case and results are summarized in Table 4-10 .

Table 4-10: Stator dimensions of RF 2-pole Motor (square wave excitation)

Parameters	
Outer diameter D_o (mm)	49.3
Slot depth h_s (mm)	3.9
Stator back core thickness W_{sbc} (mm)	8.3

4.4.1 Winding design

In square wave excitation only two phases are active for each commutation interval (Figure 2-15) and summation of back emf voltages for active 2 phases should not be larger than minimum available dc link voltage (18V). 2V voltage drop margin for switch voltage drops and resistive voltage drop is assumed and

summation of two phase back emf voltage should be under 16V. Maximum value of phase back emf voltage is assumed to be 8V in square wave excitation.
Eq. (3.15) can be rewritten in order to find number of turns per phase (Eq. (4.44)).

$$N_{ph} = \frac{E_{ph}}{B_g L D_i \omega_m} \tag{4.44}$$

Since all the parameters are defined, number of turns per phase is calculated and results are shown in Table 4-5. Since number of turn per phase can not be a fractional number values are approximated to exact numbers.

Table 4-11: Number of turns per phase of RF 2-pole motor (square wave)

Parameter	Sinusoidal excitation
N_{ph} calculated value	25.73
N_{ph} assumed value	27

Total number of slots is assumed to be 18. Number of slots per pole per phase becomes 3. Figure 4-15 shows the winding distribution of stator.

4.4.2 Equivalent circuit parameters

Same procedure is applied for sinusoidal excitation case and calculated value of phase resistance and phase inductance values are summarized in Table 4-12

Table 4-12: Inductance and resistance values for RF 2-pole motor under square wave excitation

Parameters	
Air gap inductance L_g (μ H)	101.3
Leakage inductance L_{lek} (μ H)	48.6
End turn inductance L_e (μ H)	1.8
Phase inductance L_{ph} (μ H)	151.8
Phase Resistance R_{ph}(mΩ)	116.7

4.4.3 Calculation of losses

Core losses in square wave excitation are calculated using the same formulations in 4.3.3. Note that B_g (flat top value of air gap magnetic flux density) value is calculated as 0.62 T (Figure 4-32). In order to calculate peak flux density average at tooth in Eq. (4.33), average value of fundamental component of air gap flux density is calculated as 0.434T. Resulting peak flux density on stator tooth is 1.36T and stator back core peak flux density is assumed as 1.4T as same in the sinusoidal excitation.

$$\begin{aligned} P_c &= P_h + P_e \\ P_h &= k_h f B^n \\ P_e &= k_e f^2 B^2 \end{aligned} \tag{4.32}$$

$$\begin{aligned} B_{tooth} &= \frac{B_{gav}(t_{slot} + t_{tooth})L}{t_{tooth} L} \\ B_{tooth} &= \frac{B_{gav}}{2} \end{aligned} \tag{4.33}$$

$$\begin{aligned} P_{core} &= P_c(M_{statorbackcore} + M_{statorteeth}) \\ M_{statorbackcore} &= pi(R_o{}^2 - (R_o - W_{sbc})^2)Ld_{steel} \\ M_{statorteeth} &= n_{st}(t_2 hs + t_1 h_1 + (\frac{t_1 + t_2}{2})h_2)Ld_{steel} \end{aligned} \tag{4.34}$$

Necessary dimension parameters for calculating the core losses in Eq. (4.34) are summarized in Table 4-13.

In square wave excitation case in each commutation interval only two phases are excited (Figure 2-15). Dc link voltage and dc link current and resistive losses can be using Eq. (4.45).

$$
\begin{aligned}
I_{inrms} &= I_{rms} + \frac{P_{core}}{3V_{dc}\sqrt{\frac{2}{3}}} \\
V_{dc} &= 2I_{rms}R_{ph} + E_{ph} \\
Idc &= \sqrt{\frac{3}{2}} I_{inrms} \\
P_{co} &= 2I_{dc}{}^{2}R_{ph}
\end{aligned}
\tag{4.45}
$$

4.4.4 Calculation of motor volume and mass

Mass, volume, and inertia of motor under square wave excitation can be calculated using Eq. (4.37) to Eq. (4.30). Summary of main dimensions, and calculated volume and mass of the motor is summarized in Table 4-13

Table 4-13: Main dimensions, mass and volume of RF 2 pole motor (square wave excitation)

D_i inner diameter (mm)	21.9
D_o outer diameter (mm)	49.3
L axial length (mm)	21.9
g air gap (mm)	0.75
h_s slot depth (mm)	3.9
l_m magnet thickness (mm)	3
h_1 tooth lip-1 (mm)	0.75
h_2 tooth lip-2 (mm)	0.75
w_1 lip opening (mm)	1
$w_2$slot thickness (mm)	2.2
W_{sbc} stator back core thickness (mm)	8.3
t_1 tooth width at air gap (mm)	2.8
t_2 tooth width (mm)	2.2
Inertial of motor (kgm^2)	$2.26x10^{-6}$
Volume of motor (m^3)	$4.18\ x10^{-5}$
Mass of motor (kg)	272.6

4.4.5 Performance of RF motor under square wave excitation

4.4.5.1 Required motor current and electrical loading over speed range

Air gap magnetic field density flat top value is assumed to be constant over whole speed range (B_g). Electrical loading and required motor rms phase current values are dependent on motor torque profile in Figure 3-14, they can be calculated over speed range using Eq. (4.46) and (4.41) for square wave excitation since remaining parameters are already calculated constant values. This is done by substituting torque for a given speed value (from Figure 3-14) into Eq. (4.46), electrical loading value can be calculated and the value of electrical loading is substituted into Eq. (4.41) to find the rms value of phase current for this operating condition

$$q = \frac{\sqrt{6}T_m}{\pi D_i L B_g} \tag{4.46}$$

$$I_{rms} = \frac{q\pi D_i}{6N_{ph}} \tag{4.41}$$

Calculated results of electrical loading and required motor rms phase current are shown in Figure 4-33.

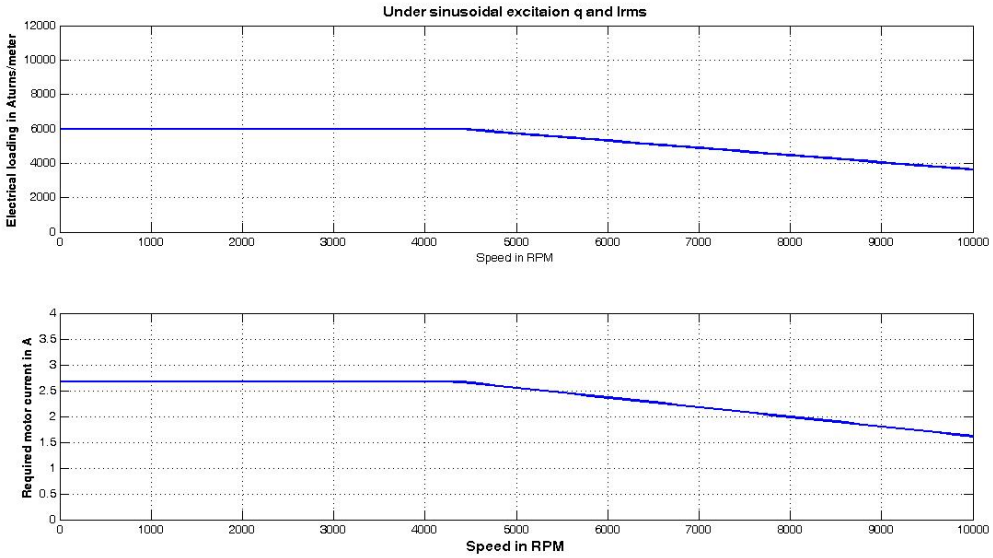

Figure 4-33: Electrical loading and required rms motor current (square wave excitation)

4.4.5.2 Required dc link voltage and back emf voltage over speed range

Back emf voltage and phase voltage is calculated using Eq. (3.15) and Eq. (4.45) respectively. Calculated results are shown in Figure 4-34.

$$I_{inrms} = I_{rms} + \frac{P_{core}}{3V_{dc}\sqrt{\frac{2}{3}}}$$

$$V_{dc} = 2I_{dc}R_{ph} + E_{ph} \tag{4.45}$$

$$Idc = \sqrt{\frac{3}{2}} I_{inrms}$$

$$P_{co} = 2I_{dc}{}^{2}R_{ph}$$

$$E_{ph} = N_{ph}B_g LD_i w_m \tag{3.15}$$

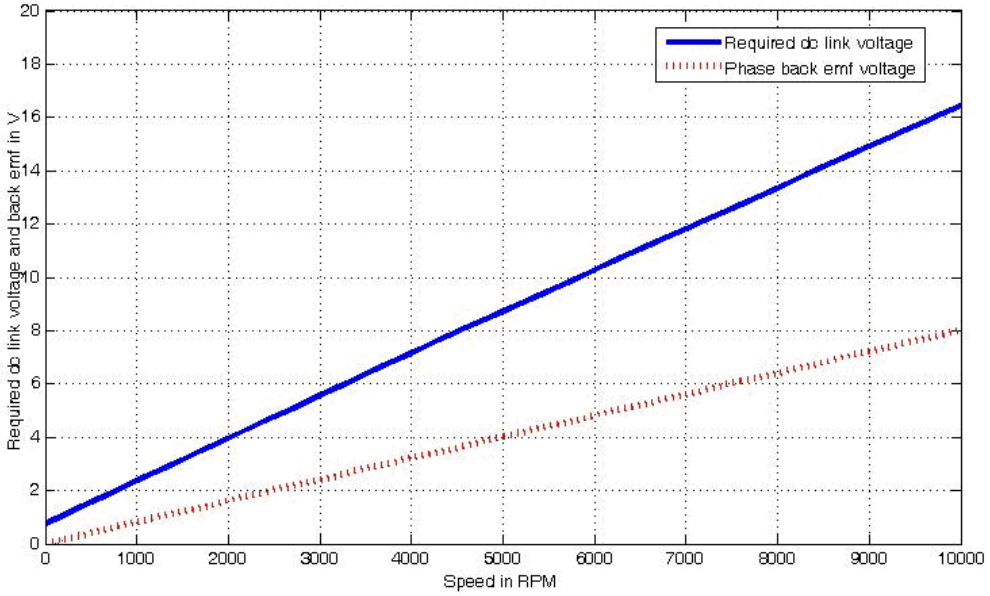

Figure 4-34: Required dc link voltage and back emf voltage for RF 2 pole square wave excitation

4.4.6 Losses over speed range

Core losses and resistive losses can be calculated using defined equations and values in 4.3.3. Obtained results are shown in Figure 4-35.

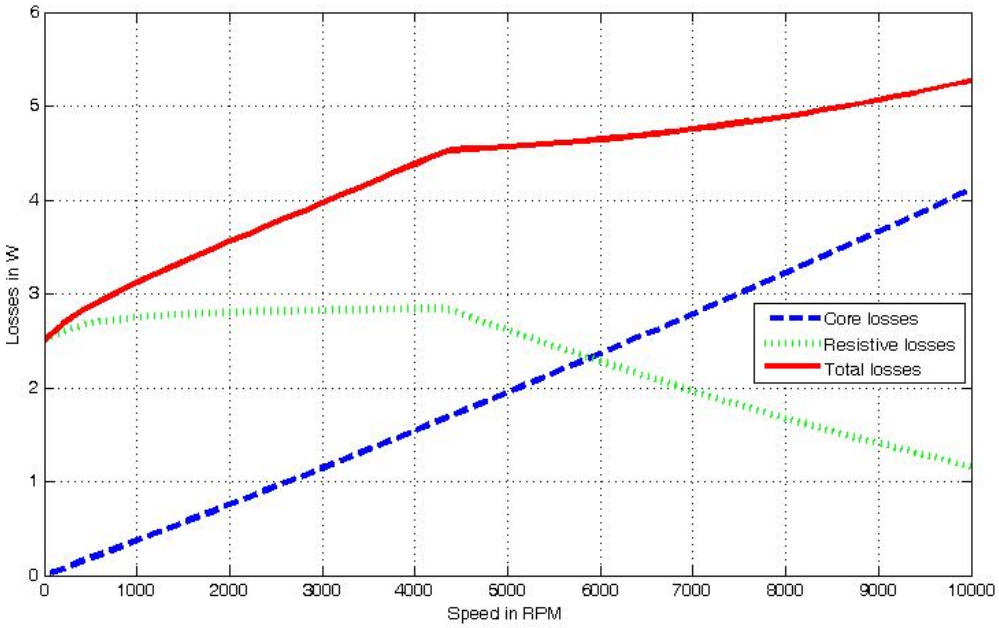

Figure 4-35: Losses in RF 2 pole motor (square wave excitation)

4.4.7 Efficiency

Efficiency is defined as output power over total input power, and it is calculated based on Eq. (4.42). Figure 4-36 shows the efficiency over whole speed range.

$$\eta = \frac{P_{out}}{P_{in}} = \frac{T_{out} \times \omega_r}{T_{out} \times \omega_r + P_{co} + P_{core}} \tag{4.42}$$

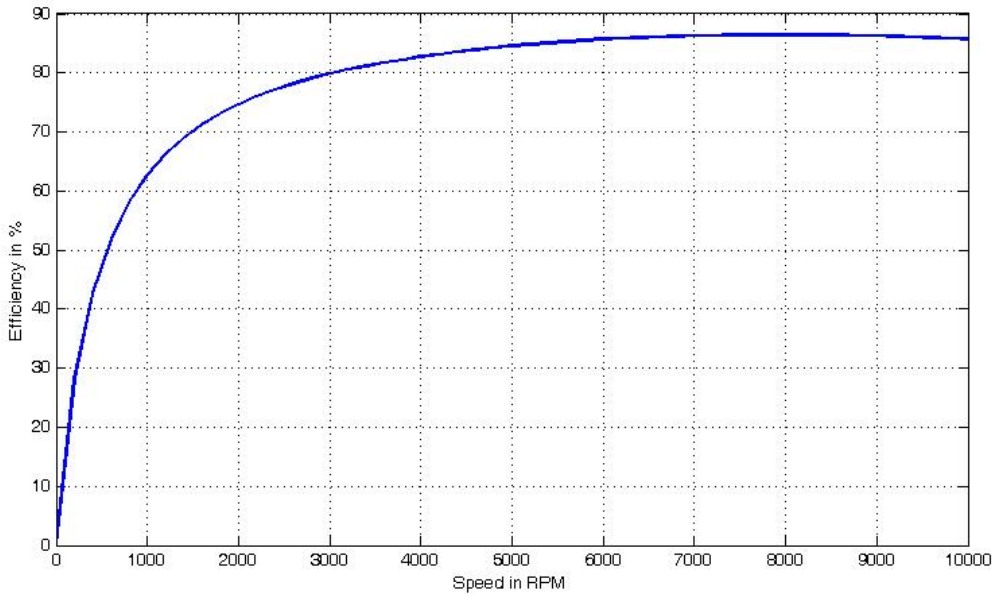

Figure 4-36: Efficiency in RF 2 pole motor (square wave excitation)

4.4.8 Evaluation of RF 2 pole motor under square wave excitation

- Motor peak electrical loading value was determined as 6000Aturn/m in performance calculations, calculated value of electrical loading is shown in Figure 4-33, and during acceleration period electrical loading value is not more than the limit value (6000Aturn/m). During steady state at 10000RPM electrical loading value is around 3900Aturn/m. Note that during the calculation of electrical loading core loss currents was not added to rms phase current. When core losses are added resulting electrical loading is becoming larger (typically %10 larger than the calculated value, results for sinusoidal excitation are shown in Figure 4-28). During acceleration period electrical loading becomes larger than the design peak value but duration is less than 60 seconds. At steady state current loading is around 4000 Aturns/m and design will be on the safe

side Note that electrical this means heating of machine will be less at steady state and design will be safe side in square wave excitation also.

- Maximum current density at stator coils is selected as 7A/mm^2. Peak current on stator coil is calculated as 2.65A (Figure 4-33) during acceleration period. Necessary conductor area is calculated using these two values and it is 0.37 mm^2. It should be checked whether conductors can be inserted into slots. Using 0.4 fill factor and 9 conductors per slot, 8.32 mm^2 slot area is required. Designed slot dimensions are summarized in Table 4-13 and slot area is calculated as 8.58 mm^2 using calculated dimensions, so conductors can be inserted into designed slots.
- Figure 4-34 shows required dc link voltage and phase back emf rms voltage over speed range. Required dc link voltage is maximum at 10000 RPM and its value is 16.4V. This value is less than minimum available dc link voltage (18V) if we add the transistor voltage drop of 1.4V, so design is in safe side.
- Losses and efficiency characteristics of square wave excitation are similar in the case of sinusoidal excitation.

4.5 Comparison of sinusoidal and square wave excitation on 2 pole RF motor design

Table 4-14 summarizes the calculated parameters of RF 2 pole motor under square wave and sinusoidal excitation.

Electrical current loading, peak torque requirement and inner diameter to axial length ratio are assumed to be same for both excitation cases.

- In terms of main dimensions, sinusoidal excitation case has larger dimensions than square wave excitation. For the same torque requirement %5 more motor weight and motor volume is required in sinusoidal excitation case (This result was an expected form section 3.7).

Consequently torque/mass and torque/ volume ratio is higher in square wave excitation case

- Phase resistance and inductance values are larger in sinusoidal excitation case since motor dimensions are larger.
- Efficiency values are again close to each other losses at 10000RPM and 30mNm load torque.
- Last point is regarding to inertia. In CMG system motor will be coupled with a high inertial wheel ($4.87x10^{-3}$) and rotor inertia is a part of total rotating inertia. If inertia values of rotor were large enough, mass and shape of the rotating wheel could be smaller. Calculated values of rotor inertias are too small for both excitation and their contribution is less than 1%.

Under the calculated results there is no significant difference between the dimensioning of motor under sinusoidal and square wave excitations. Dimensioning based on square wave excitation has slightly larger torque/mass and toque/volume ratio.

In sinus excitation current and back emf values are assumed to be sinusoidal and only fundamental values are producing torque where as in square wave case peak values of the current and emf voltages are producing torque. Note that in order to have sinusoidal back emf additional effort on magnet shape and more on winding distribution should be done such as skewing and fractional coil pitch. This effort can result in higher fundamental component in the air gap and performance of the motor can be increased. This work also minimizes the harmonics and reduces the torque ripple due to higher order harmonics. But in this thesis for the sake of simplicity it is assumed that only the fundamental components of current and back emf are producing torque.

Table 4-14: Summary of Calculated Performance Parameters

Parameter	Square wave excitation	Sinusoidal excitation
Core losses at 10 kRPM (W)	4.11	4.28
Resistive losses (W) at 10 kRPM	1.15	1.22
Total losses (W)	5.26	5.5
Efficiency at 10 kRPM	%85.7	%85.2
Mass (g)	272.6	285
Volume (m^3)	4.18×10^{-5}	4.36×10^{-5}
Torque/mass (Nm/kg)	0.183	0.175
Torque/ volume (Nm/m^3)	1196	1146
Inertia (kgm^2)	2.26×10^{-6}	2.51×10^{-6}
Inertia contribution to total required inertia	% 0.46	% 0.51

The major difference is as stated in section 2.2.4 at Figure 2-17 and Figure 2-19, sinusoidal excitation case has very low torque ripple where as square wave excitation case, current distortion (Figure 2-16) in commutation changes produce torque ripple. But thanks to the larger inertia of the wheel torque ripples do not affect the wheel speed due to large mechanical time constant.

While selecting the excitation type sensor and drive requirements should also be considered. Square wave excitation case there 6 different switching states of motor and in each state only two phases are excited with dc link voltage. Only 60 ^{0}C resolution hall sensors are enough for square wave excitation (2.2.4).

In order to have sinusoidal current wave forms more accurate motor position information is required to determine the applied voltage level at each time of switching, so high resolution sensors are required for motor control. Usually optical or magnetic encoders are used to have higher motor position resolution. Also required processing power and complex control algorithms are required in

sinusoidal excitation. Since complex systems are avoided in aerospace applications and there is no significant difference in between motor sizes, dimensioning of motor based on square wave excitation will be considered on the following design studies.

4.6 Design of 6 pole RF motor under square wave excitation

Magnetic circuit of the 6 pole topology is the same as 2 pole topology; the only difference is that there are separate flux paths for each pole (Figure 4-37). Since pole and magnet areas are smaller and air gap flux densities should be calculated again. Since derivations of equations are done for different pole numbers same magnetic circuit and design process will be used for six pole design.

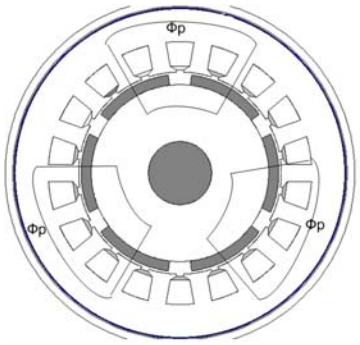

Figure 4-37: Cross-section of RF 6 pole motor

Since number of poles is changed some design parameters should be defined again in Eq. (4.43). Peak torque is determined by system performance requirements and is the same as for 2 pole case (50mNm). Current loading is determined by the power rating and operational speed requirements using Figure 4-5 and since the same requirements are valid for the 6 pole case, current loading value also assumed to be same as 2 pole case. Air gap distance is assumed to be the same as 2 pole case based on mechanical reasons. Important parameter to be

reconsidered for 6 pole case is the ratio of inner diameter to axial length. This is mainly due to required slot pitch limitations. Theoretically we can increase the pole number as much as possible but then there will be a problem about the slot areas. In order to avoid this particular problem data given in Figure 4-6 is used. Data in this figure is created on previous experiences on motor design, so we have to redefine the ratio again. Eq. (4.14) can be rewritten using the new limits from the Figure 4-6 and resulting equation becomes like in Eq. (4.46)

$$0.7 \le \frac{pL}{\pi D_i} \le 1.2$$
$$1.61 \le \frac{D_i}{L} \le 2.7 \tag{4.46}$$

Note that ratio interval limits become larger since we need smaller axial length due to the requirements of CMG and have shorter end winding a suitable ratio 2 is selected.

After defining the input parameters, process is continued with determination of a proper air gap magnetic flux density as stated in the 2-pole design (calculation flow is shown in Figure 4-29). Summary of defined design constrains are summarized in Table 4-15 and obtained results are shown in Figure 4-38.

Table 4-15: Design Constrains for RF 6-pole Motor

Design parameter	
Design parameter	50
Peak torque requirement T_p (mNm)	6000
Electrical loading q (Aturn/m)	2
Inner diameter to axial length ratio (D_i/L)	0.75
Air gap g (mm)	0.1-0.9
Bg design value (T)	2-8 mm

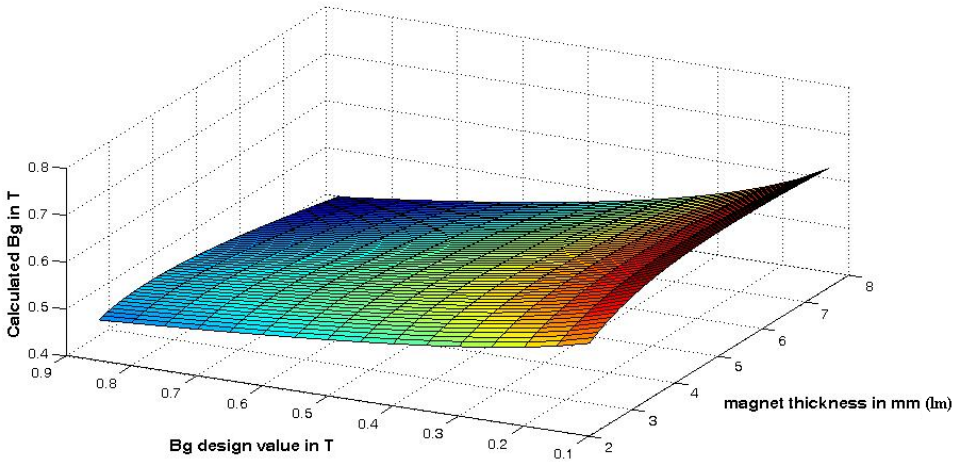

Figure 4-38: Calculated B_g values for different Bg design values and different magnet thickness (RF 6 pole)

Note that if design values are selected above 0.53T, for determined dimensions air gap magnetic field density can not be produced. As a design value 0.53T is selected. Calculated inner diameter and axial length are summarized in Table 4-16.

Table 4-16: Inner Radius and Axial Length of RF 6-pole Motor

Parameter	Value
Inner diameter D_i (mm)	29.1
Axial length L (mm)	14.5

Since required dimensions are defined required magnet thickness can be calculated in order to reach desired air gap magnetic field density. For fixed design constrains magnetic circuit equations can be solved and calculated air gap magnetic field densities for different magnet lengths are shown in Figure 4-39.

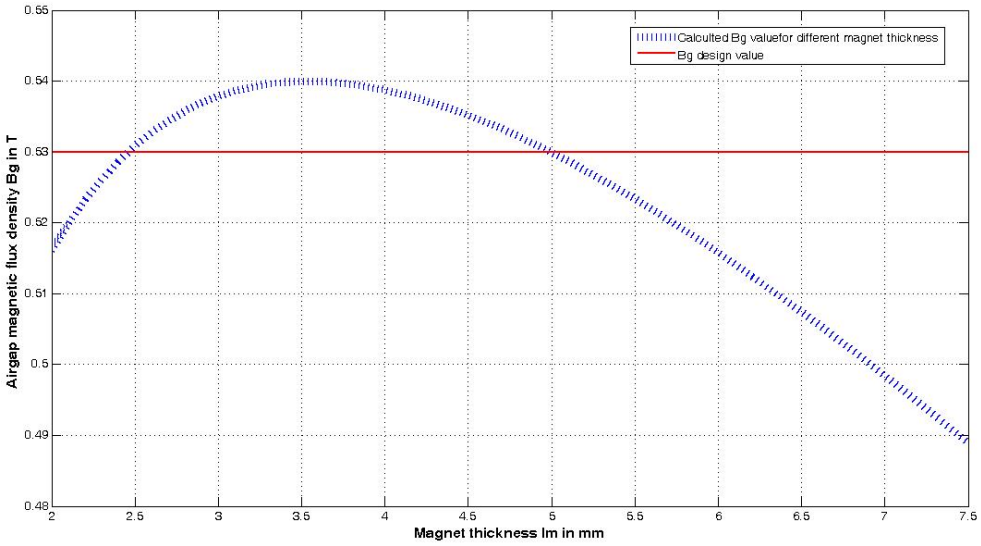

Figure 4-39: Calculated B_g values for different magnet thickness (6pole-square wave excitation)

Magnet thickness is selected as 3mm in the 6 pole case. After determining the inner diameter, axial length, air gap, and magnet thickness, remaining parameters slot depth and outer diameter of the motor are calculated using same equations in 2 pole case (section 4.4) results are summarized in Table 4-17.

Table 4-17: Stator Dimensions of RF 6-pole Motor

Parameter	Value
Outer diameter D_o (mm)	46.3
Slot depth h_s (mm)	4
Stator back core thickness W_{sbc} (mm)	3.1

4.6.1 Winding design

In 6 pole design Eq. (4.44) is used for calculation of number of turns per phase, calculated value is 36. Winding distribution of 6 pole case is shown in Figure 4-40.

$$N_{ph} = \frac{E_{ph}}{B_g L D_i \omega_m} \tag{4.44}$$

slot number	1	2	3	4	5	6	7	8	9	10	11	12	13	14	15	16	17	18
phase winding	A	-C	B	-A	C	-B	A	-C	B	-A	C	-B	A	-C	B	-A	C	-B
number of turns per slot	12	12	12	12	12	12	12	12	12	12	12	12	12	12	12	12	12	12
poles	pole1			pole2			pole3			pole4			pole5			pole6		

Figure 4-40: Winding distribution of RF 6 pole motor

4.6.2 Equivalent circuit parameters

Same procedure is applied for sinusoidal excitation case and calculated value of phase resistance and phase inductance values are summarized in Table 4-18.

Table 4-18: Inductance and resistance values for RF 6-pole Motor under square wave excitation

Parameters	
Air gap inductance L_g (μH)	136.5
Leakage inductance L_{lek} (μH)	91
End turn inductance L_e (μH)	1
Phase inductance L_{ph} (μH)	228.5
Phase Resistance R_{ph}(mΩ)	94.1

4.6.3 Calculation of losses

Calculations of losses are done using same equations in 4.4.3 (Eq. (4.32), Eq. (4.33), Eq. (4.34)). Only difference is the flat top value of air gap magnetic flux density is calculated as 0.53T in 6 pole case. Resulting average flux density is 0.371T over pole pitch and resulting peak flux density as stator tooth is 1.16T. Since same material is used as stator core, stator back core flux density is assumed as 1.4T as in 2 pole case. .Necessary dimensions for calculation of core losses are summarized in Table 4-19.

$$\begin{aligned} P_c &= P_h + P_e \\ P_h &= k_h f B^n \\ P_e &= k_e f^2 B^2 \end{aligned} \tag{4.32}$$

$$\begin{aligned} B_{tooth} &= \frac{B_{gav}(t_{slot} + t_{tooth})L}{t_{tooth} L} \\ B_{tooth} &= \frac{B_{gav}}{2} \end{aligned} \tag{4.33}$$

$$\begin{aligned} P_{core} &= P_c x (M_{statorbackcore} + M_{statorteeth}) \\ M_{statorbackcore} &= pi(R_o{}^2 - (R_o - W_{sbc})^2) L d_{steel} \\ M_{statorteeth} &= n_{st}(t_2 hs + t_1 h_1 + (\frac{t_1 + t_2}{2}) h_2) L d_{steel} \end{aligned} \tag{4.34}$$

$$\begin{aligned} I_{inrms} &= I_{rms} + \frac{P_{core}}{3 V_{dc} \sqrt{\frac{2}{3}}} \\ V_{dc} &= 2 I_{rms} R_{ph} + E_{ph} \\ Idc &= \sqrt{\frac{3}{2}} I_{inrms} \\ P_{co} &= 2 I_{dc}{}^2 R_{ph} \end{aligned} \tag{4.45}$$

4.6.4 Calculation of motor volume and mass

Mass, volume, and inertia of motor under square wave excitation are calculated using Eq. (4.37) to Eq. (4.30). Summary of main dimensions, and calculated volume and mass of the motor is summarized in Table 4-19.

Table 4-19 Main dimensions, mass and volume of RF 6 pole motor (square wave excitation)

D_i inner diameter (mm)	14.5
D_o outer diameter (mm)	23.15
L axial length (mm)	14.5
g air gap (mm)	0.75
h_s slot depth (mm)	4
l_m magnet thickness (mm)	3
h_1 tooth lip-1 (mm)	0.75
h_2 tooth lip-2 (mm)	0.75
w_1 lip opening (mm)	1
$w_2$slot thickness (mm)	2.9
W_{sbc} stator back core thickness (mm)	3.1
t_1 tooth width at air gap (mm)	4
t_2 tooth width (mm)	3.1
Inertial of motor (kgm^2)	$5.23x10^{-6}$
Volume of motor (m^3)	$2.45\ x10^{-5}$
Mass of motor (kg)	146.3

4.6.5 Performance of 6 pole RF motor under square wave excitation

4.6.5.1 Required motor current and electrical loading over speed range

Electrical loading and required motor rms phase current values are calculated using same approach and equations in 4.4.5.1.

$$q = \frac{\sqrt{6}T_m}{\pi D_i L B_g} \tag{4.46}$$

$$I_{rms} = \frac{q\pi D_i}{6N_{ph}} \tag{4.41}$$

Calculated results of electrical loading and required motor rms phase current are shown in Figure 4-41.

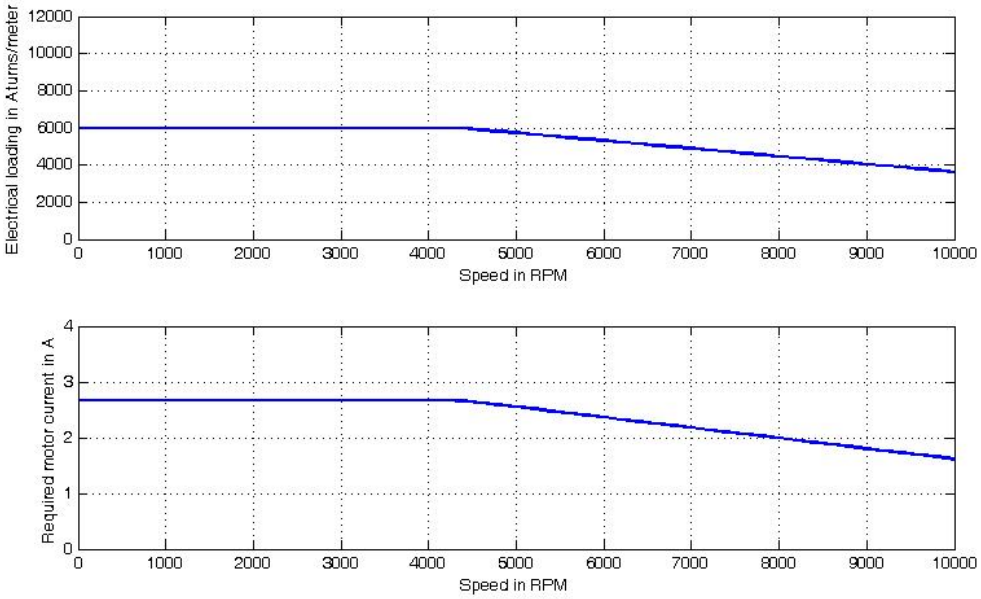

Figure 4-41: Electrical loading and required rms motor current of RF 6 pole motor (square wave excitation)

4.6.5.2 Required dc link voltage and back emf voltage over speed range

Back emf voltage and phase voltage is calculated using Eq. (3.15) and Eq. (4.45) respectively. Calculated results are shown in Figure 4-42.

$$I_{inrms} = I_{rms} + \frac{P_{core}}{3V_{dc}\sqrt{\frac{2}{3}}}$$

$$V_{dc} = 2I_{dc}R_{ph} + E_{ph} \tag{4.45}$$

$$Idc = \sqrt{\frac{3}{2}} I_{inrms}$$

$$P_{co} = 2I_{dc}{}^{2}R_{ph}$$

$$E_{ph} = N_{ph}B_g LD_i w_m \tag{3.15}$$

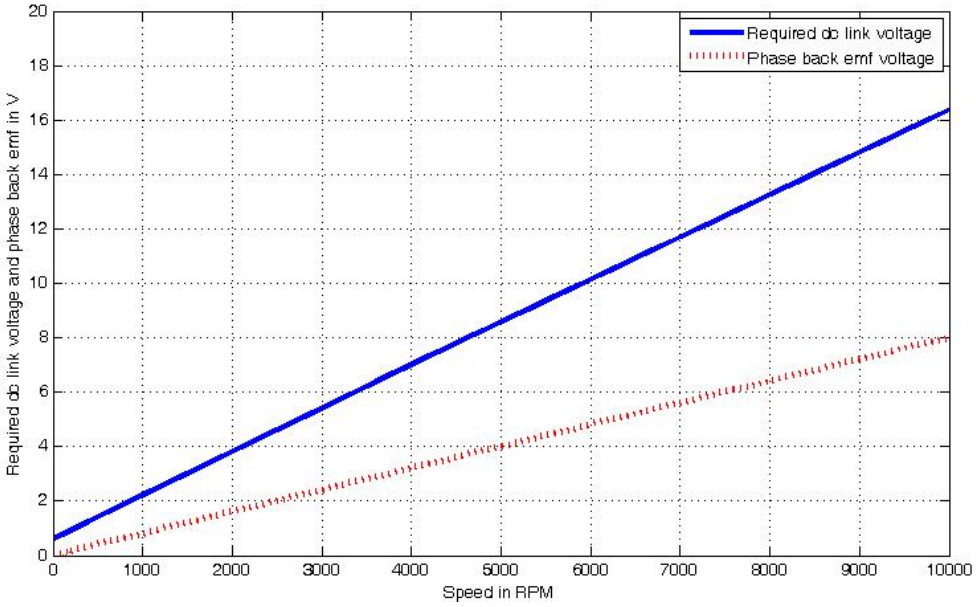

Figure 4-42: Required dc link voltage and back emf voltage for RF 6 pole square wave excitation

4.6.6 Losses over speed range

Core losses and resistive losses can be calculated using the same equations in 0. Obtained results are shown in Figure 4-43.

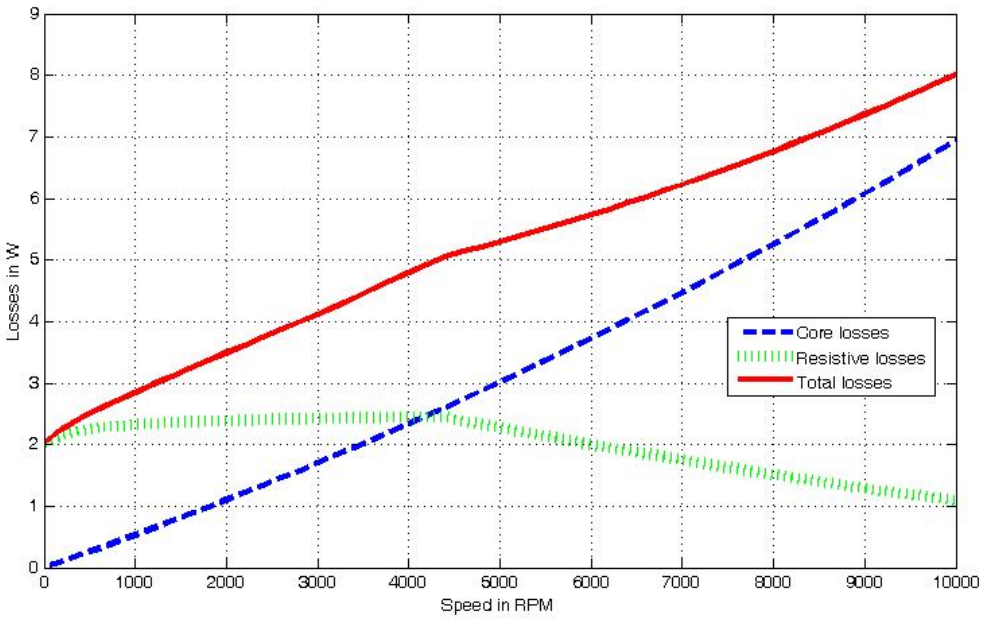

Figure 4-43 Losses in RF 6 pole motor (square wave excitation)

4.6.7 Efficiency

Efficiency is defined as output power over total input power, and it is calculated based on Eq. (4.42). Figure 4-44 shows the efficiency over whole speed range.

$$\eta = \frac{P_{out}}{P_{in}} = \frac{T_{out} \times \omega_r}{T_{out} \times \omega_r + P_{co} + P_{core}} \tag{4.42}$$

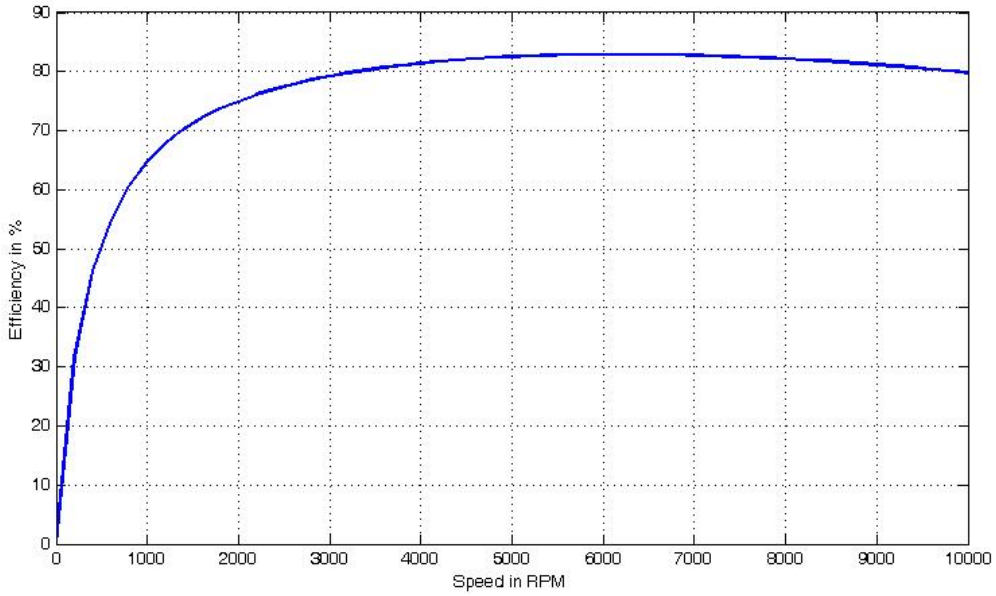

Figure 4-44: Efficiency in RF 6 pole motor (square wave excitation)

4.6.8 Evaluation of RF 6 pole motor under square wave excitation

- Motor electrical loading characteristic is similar in 2 pole case and design is on safe side.
- Maximum current density at stator coils is selected as 7A/mm^2. Peak current on stator coil is calculated as 2.67A (Figure 4-33) during acceleration period. Necessary conductor area is calculated using these two values and it is 0.38 mm^2. It should be checked whether conductors can be inserted into slots. Using 0.4 fill factor and 12 conductors per slot, 11.44 mm^2 slot area is required. Designed slot dimensions are summarized in Table 4-19 and slot area is calculated as 11.6 mm^2 using calculated dimensions, so conductors can be inserted into designed slots.
- Figure 4-43 shows required dc link voltage and phase back emf rms voltage over speed range. Required dc link voltage is maximum at 10000 RPM and its value is 16.37V. This value is less than minimum available

dc link voltage (18V) if we add the transistor voltage drop of 1.4V, so design is on safe side.

4.7 Comparison of Calculated Results for RF 2 pole and 6 pole motors

Table 4-20 summarizes the calculated parameters of RF 2 pole motor and 6 pole motor under square wave excitation.

Table 4-20: Summary of Calculated Parameters for Square Wave Excitation

Parameter	RF 2 pole	RF 6 pole
Core losses at 10000RPM (W)	4.11	6.9
Resistive losses (W) at 10000RPM	1.15	1.1
Total losses (W)	5.26	8
Efficiency at 10000RPM %	%85.7	%79
Mass (g)	272.6	146.3
Volume (m^3)	4.18×10^{-5}	2.45×10^{-5}
Torque/mass Nm/kg	0.183	0.341
Torque/ volume (Nm/m^3)	1196	2040
Inertia (kgm^2)	2.26×10^{-6}	5.23×10^{-6}
Inertia contribution of rotor to total required inertia	% 0.46	%1

- In 6 pole design inner radius to axial length ratio is reestablished and inner radius of the motor becomes larger than 2 pole case. This ratio is selected from design data [22] which is constructed from previous experience motor designs. Main reason is due to have enough number of slots for each pole. Axial length however decreased since torque equation is ideally independent of pole number and in order to compensate the increase in inner diameter axial length becomes shorter. This is an advantage for CMG application because shorter axial length means shorter system on the X axis of CMG (Figure 3-1).

- Since dimensions are changed in 6 pole case, magnetic circuit is solved again, and achievable value of Bg is calculated as 0.53T. Main reason for this is that air gap and magnet areas become smaller in 6 pole case so reluctances in magnetic circuit increased and lower value of Bg can be achievable.
- Outer diameter is nearly the same as 2 pole case. But main difference can be seen on Do/Di ratio. Since flux per pole is less in 6 pole case required back core thickness and volume is less. Another saying for the same inner diameter outer diameter of 6 pole motor is much less than 2 pole motor.
- Main problem in 6 pole design is increase in the core losses due to the increased electrical frequency at rated speed (10000RPM). Core losses are dependent on mass and electrical frequency. Although the mass of 6 pole motor is decreased as compared to 2 pole motor, electrical frequency is 3 times the 2 pole case so core losses are increased in 6 pole configuration. Resistive losses are similar in both case but since core losses are increased in 6 pole design total losses are high in 6 pole design. Efficiency is also less in 6 pole case but by only 6 %.
- On the other hand torque/ mass and torque/volume performance is higher in 6 pole configuration.
- Axial length of the motor and mass of the motor are smaller in 6 pole configuration and this is an advantage of reducing the total volume of the CMG (details will be discussed in Chapter 5).
- Inertia contribution of both case are so small that, there will be no reduction on coupled inertia wheel mass or volume.

4.8 Mechanical Considerations of RF Motor Design

In high speed applications magnets have large amount of force acting on them and mechanical problems can be encountered in keeping the magnets on the surface of the rotor. Usually buried or interior magnet rotor topologies are used in high speed applications. But in small motors mechanical production is difficult for

these kinds of rotor topologies. Surface mounted type rotors are studied in this thesis since manufacturing is easier.

Different methods can be used for keeping magnet mechanically stable at rotor surface, gluing and banding can be used for mechanical enhancement (with materials such as epoxy resin, fiberglass, kevlar, or inconel) but gluing methods are complicated in terms of surface treatment.

A more simple and reliable method is used in this thesis which is heat shrinkable insulation band (or stress control band). Tyco and Woer are manufacturers of these types of bands for aerospace applications. These bands can survive -50-105 ^{0}C and can resist stress levels of 10-12Mpa. In order to verify the selected material can keep the magnets on the rotor surface, force acting on the magnet and pressure on the band should be calculated (Figure 4-45)[24]. Using Eq. (4.47) tangential force and the pressure on magnet contact points are calculated.(Note that Since excitation is selected as square wave excitation, mechanical design considerations will be considered for 2 pole and 6 pole motor under square wave excitation).

$$
\begin{aligned}
R_m &= R_i - l_m/2 - g \\
F &= M_{magnet} w_m{}^2 R_m \\
\sigma_{inner} &= \frac{F}{A_{\min ner}} \\
\sigma_{outer} &= \frac{F}{A_{mouter}} \\
A_{\min nerr} &= \frac{2}{3}\left[2\pi(R_i - l_m - g)/p\right]L \\
A_{mouter} &= \frac{2}{3}\left[2\pi(R_i - g)/p\right]L
\end{aligned}
\tag{4.47}
$$

$A_{\min nerr}$ and A_{mouter} are the inner and outer surfaces of the magnet respectively(Figure 4-45), w_m is mechanical speed, R_m is average radius of magnet (Figure 4-45) and M_{magnet} is weight of magnet and can be calculated using Eq. (4.38).

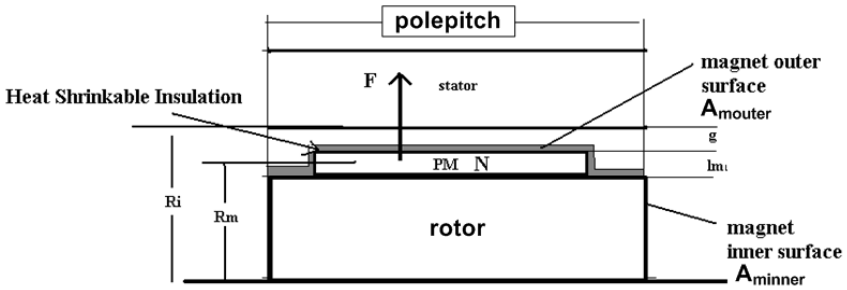

Figure 4-45: Force on magnet

Calculated values of the force on the magnet and stress on the inner and outer surface of the magnet are shown in Figure 4-46 - Figure 4-49.

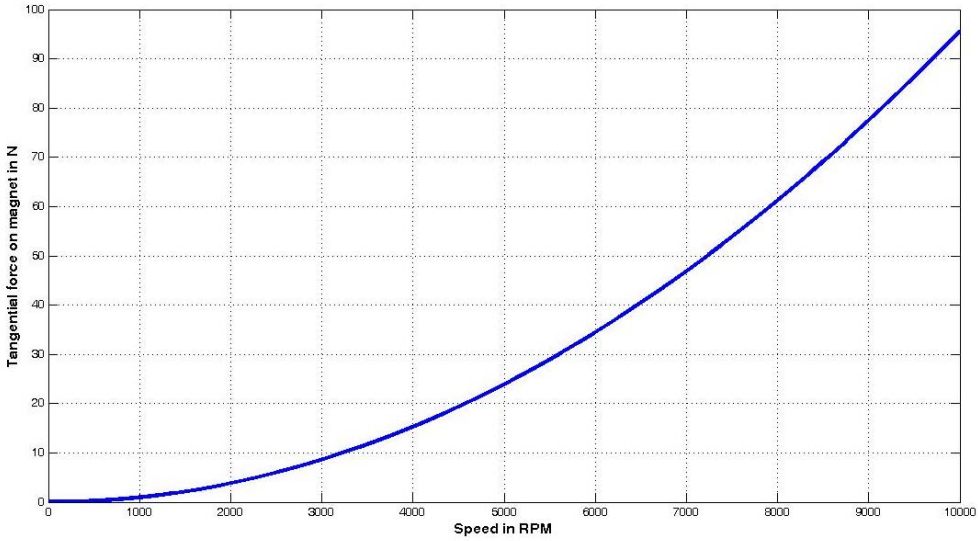

Figure 4-46: Force on magnet (2-pole square wave)

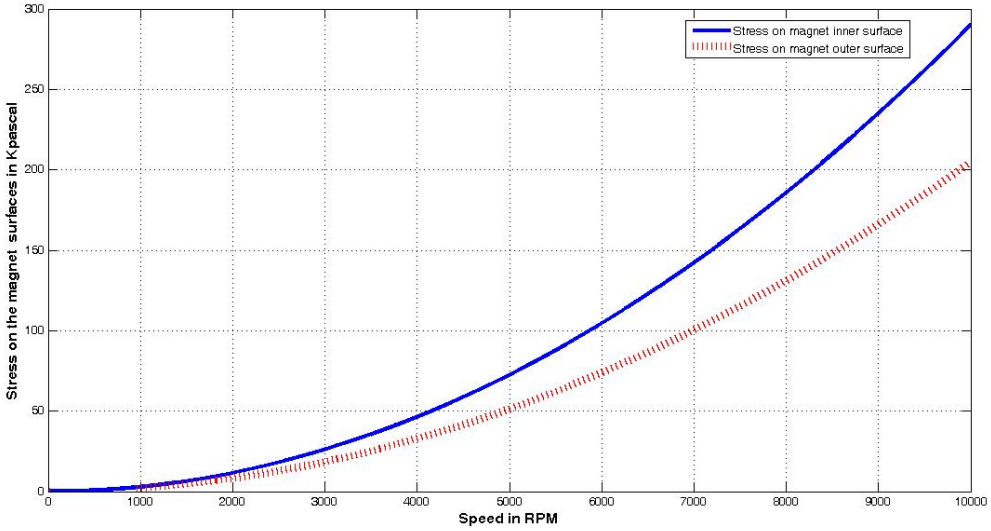

Figure 4-47: Stress on magnet surfaces (2-pole square wave)

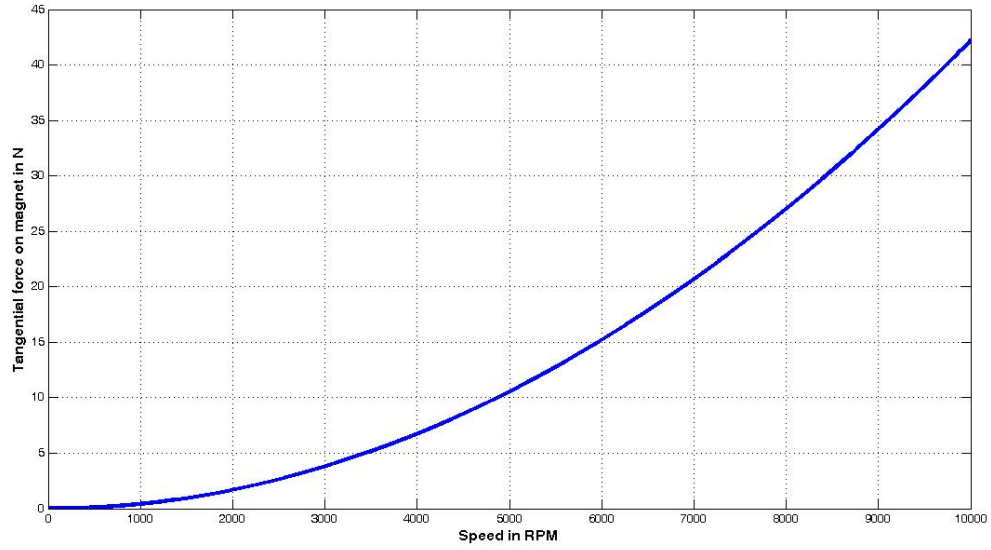

Figure 4-48: Force on magnet (6 pole-square wave)

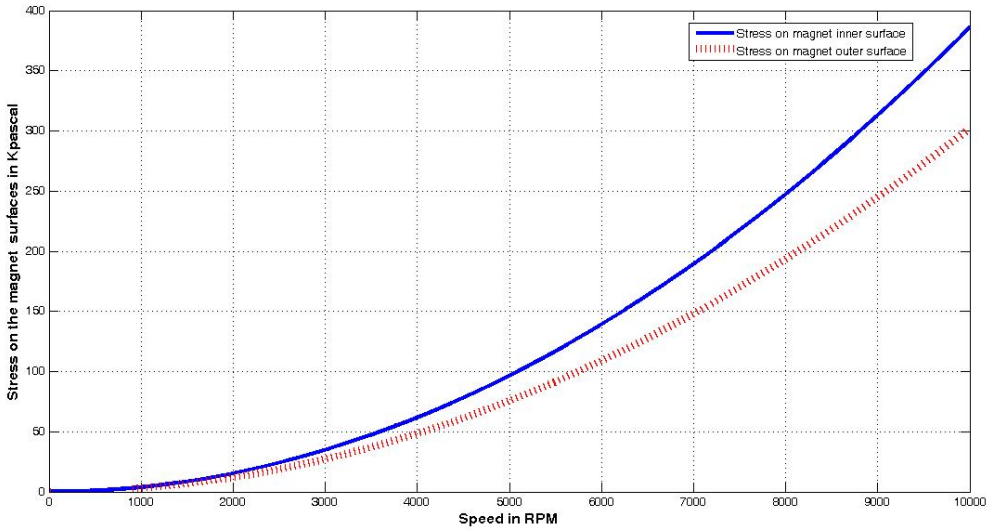

Figure 4-49: Stress on magnet surfaces (6-pole square wave)

Figure 4-49 shows the stress on inner and outer surface of the magnet due to radial force acting on magnet. Inner surface has more pressure since area is small in that part. If adhesive an adhesive is used more stress tolerant adhesive is needed. Since band is at outer surface of the magnet lower pressure is observed on band. Needed pressure resistance is around 110KPa on the band and selected bands can survive up to 10-12MPa so magnets can be mechanically keep on the rotor surface using a sleeve (stress control band). Also Vacomax225 SaCo magnet has a compressive strength of 650Mpa and design and it can easily withstand the forces on it.

4.9 Magnetic circuit of AF motor

Up to this part design calculations of RF motors are done. In the remaining part of this chapter AF motors will be studied. Since square wave and sinusoidal excitations are compared and square wave excitation is selected for design process, AF motors will be designed for square wave excitation. In order to see the effect of pole number 2 pole and 6 pole AF motor designs is considered. Before starting to design process, first magnetic circuit of and magnetic circuit

parameters of AF motor are stated in this part. Flux path and radial cross-section of the axial flux motor is shown in Figure 4-50.

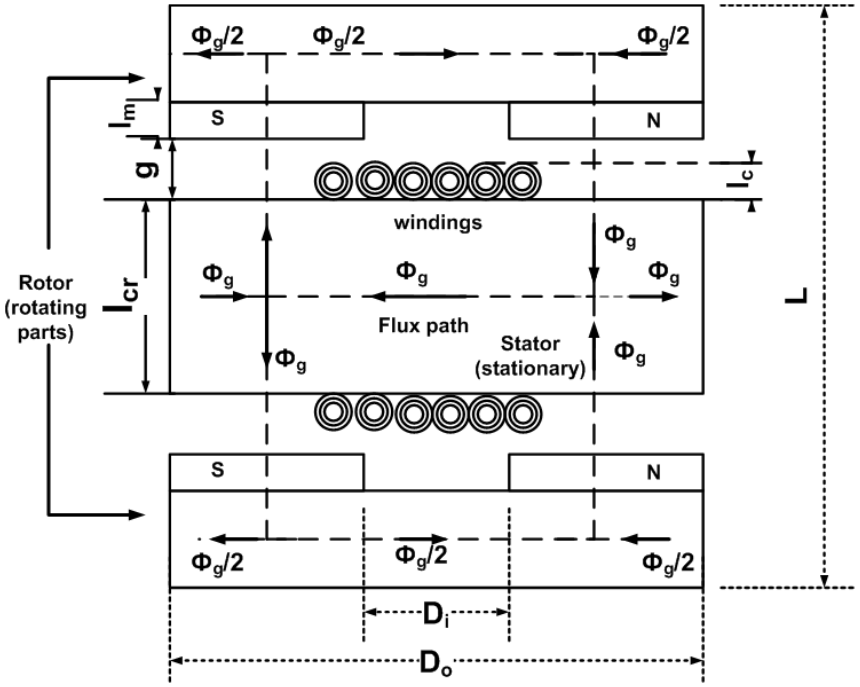

Figure 4-50: Cross section of AF motor

Although this motor has two air gaps we can think that motor composed of two halves. And in each halves flux passes through two air gaps. In each halves of AF motor assuming infinitely permeable core, magnetic circuit is same as in the RF case (Figure 4-51. But of course area of pole and magnets are different due topology.

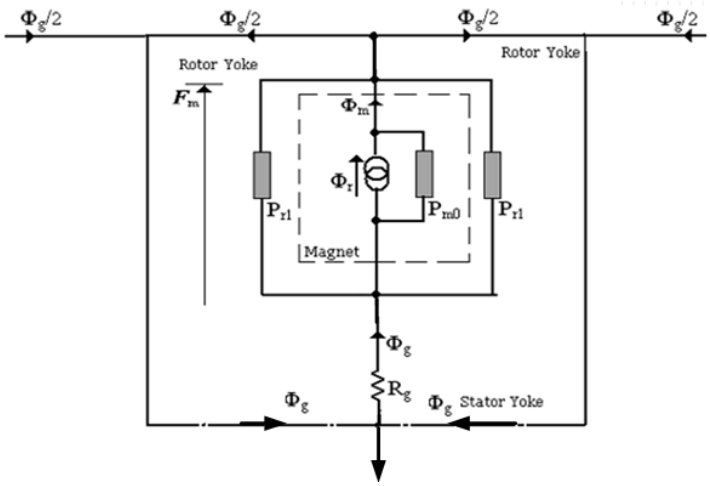

Figure 4-51 Magnetic circuit of AF motor

All the assumptions are same only different parts are area of the magnet and area of the air gap since pole geometry is different from the radial motor. 120^0 magnet span (in order to have zero 3rd harmonic) area of the magnet can be calculated with Eq. (4.48) (Figure 4-52).

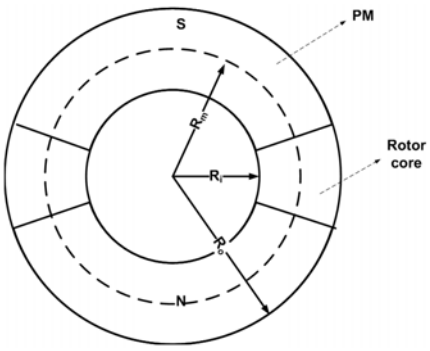

Figure 4-52 AF rotor top view

$$A_m = \frac{\frac{2}{3}\pi\left(R_o{}^2 - R_i{}^2\right)}{p} \tag{4.48}$$

Where p is number of pole and 2/3 is due to 120^0C magnet angle.

In order to determine the air gap area we have added the *g* distance to the edges of PM, in order to have a better approximation for fringing flux.

$$A_g = \frac{\frac{2}{3}\pi\left((R_o+g)^2-(R_i+g)^2\right)}{p} + \left(2g(2g+Ro-Ri)\right) \tag{4.49}$$

Last different point is the air gap reluctance value since we did not use slotted structure air gap is calculated with the real air gap value.

$$R_g = \frac{g}{\mu_0 A_g} \tag{4.50}$$

Remaining equations are same as in the RF motor case.

4.10 Design of AF motor under square wave excitation

In AF motor design process same procedure will be studied as in RF design case. After definition of design inputs to Eq.(4.51)(which is derived in 3.6.2.1) , main dimensions are determined. Electrical parameters like inductance and required motor currents, losses and efficiency is calculated and results are compared. After finishing the performance comparisons, mechanical problems of attaching the magnet on the rotor surface is studied at the end of this part.

$$T_p = \frac{2\sqrt{2}}{\sqrt{3}}\pi B_g q_i R_o^{\,3} K_r (1-K_r^{\,2}) \tag{4.51}$$

In Eq. (4.51), T_p is the peak torque coming from the motor performance requirements and it is 50mNm Figure 3-14.

K_r is the ratio of inner diameter to outer diameter of AF motor. Defining an optimum K_r value is important in AF design. In [23], K_r value optimization is studied for same torque equation under fixed electrical (2800Aturns/m) and magnetic loading (0.23T) on 5600RPM speed. Obtained results in [23] are shown in Figure 4-53. In this thesis and [23] motor design criteria is based on both efficiency and torque density. K_r value is optimum at 0.65 [23] and this value will be used in the thesis.

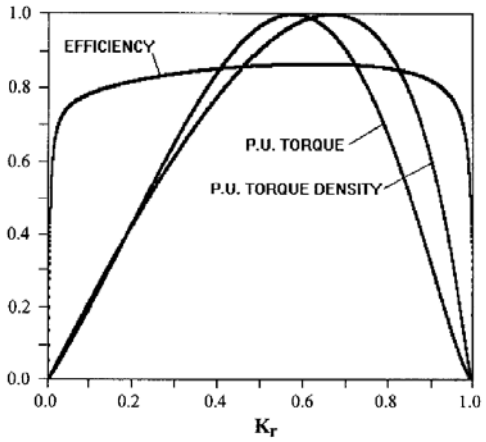

Figure 4-53: Optimum K_r selection

In order to define a proper air gap in AF machine we have to adjust the required air gap to house the winding (l_c in Figure 4-51). Required conductor area at inner surface (A_{tcon}) of the AF motor stator is defined in Eq. (4.52).

$$A_{con} = \frac{3N_{ph}I_{RMS}}{J}$$
$$A_{tcon} = \frac{3N_{ph}I_{RMS}}{JK_{cu}} \tag{4.52}$$

J is current density and K_{cu} is fill factor. Available space area at inner diameter of AF motor is expressed in physical dimensions in Eq. (4.53).

$$A_{tcon} = l_c(2\pi R_i) \tag{4.53}$$

$$q_i = \frac{3N_{ph}I_{RMS}}{\pi D_i}$$
$$N_{ph}I_{RMS} = \frac{q_i \pi D_i}{3} \tag{3.28}$$

Required housing thickness (l_c in Figure 4-51) can be calculated by the following way. Eq. (3.28) is substituted into Eq. (4.42) and Eq. (4.42) and Eq.(4.53) is used for calculation of l_c and required air gap distance for wiring is expressed in Eq. (4.54).

$$l_c = \frac{q_i}{3JK_{cu}} \tag{4.54}$$

Current density is selected as 7A/mm^2 and note that only in acceleration period this current density exists. Cupper fill factor is selected as 0.6 (since wires are linear distributed.). Electrical loading also have an important role in defining the air gap. If same electrical loading value is used in RF case required air gap for wiring becomes 1.4mm. Larger air gap requires thicker magnet and consequently motor weight is increasing. Also cooling of slotless motors are poorer than slotted ones so in order to have some margin %80 of the loading value at radial flux case (4800Aturns/m) is used. Note that selected electrical loading value is at the inner peripheral of the motor since conductors are denser at inner peripheral. Then required air gap for wiring is calculated as 1.15 mm. 0.5 mm is added for mechanical clearance between magnets and total air gap is defined as 1.65mm.

Up to know all the parameters in Eq. (4.51) are defined apart form magnetic flux density in the air gap. Proper value of B_g (flat top value of air gap magnetic flux density in Figure 4-60) should be chosen and in next part a graphical study is done for a proper air gap flux density determination.
There are two main concerns for determination of air gap magnetic flux density. First concern is the same as in the RF motor design which is up to what levels that air gap magnetic flux density can be increased by increasing the magnet thickness under defined design constrains (air gap, current loading, Kr etc).

Second concern which is different from radial flux design is to increase the inertia of rotor in AF motor without increasing the mass much. Since value of B_g is defining the dimensions of the motor, in order to maximize the inertia, a graphical study is done.

In order to study fist concern to check an achievable interval for B_g design value, similar process is done as in RF case. Figure 4-7 shows the process flow for determination of achievable B_g design values for different magnet lengths.

Bg design value is selected between the interval 0.1T to 1T and magnet thickness interval is selected to 0.1mm to 10mm. calculation sequence is summarized in Figure 4-7. Summary of design constrains are shown in Table 4-21.

Table 4-21: Design Constrains of AF Motor

Design parameter	Value
Peak torque requirement *Tp* (mNm)	50
Electrical loading *q* (Aturn/m)	4800
inner radius /outer radius (K_r)	0.65
Air gap *g* (mm)	1.65
B_g design value (T)	0.1-0.9
Magnet thickness l_m (mm)	0.1-10 mm

Calculated results are shown in Figure 4-54.

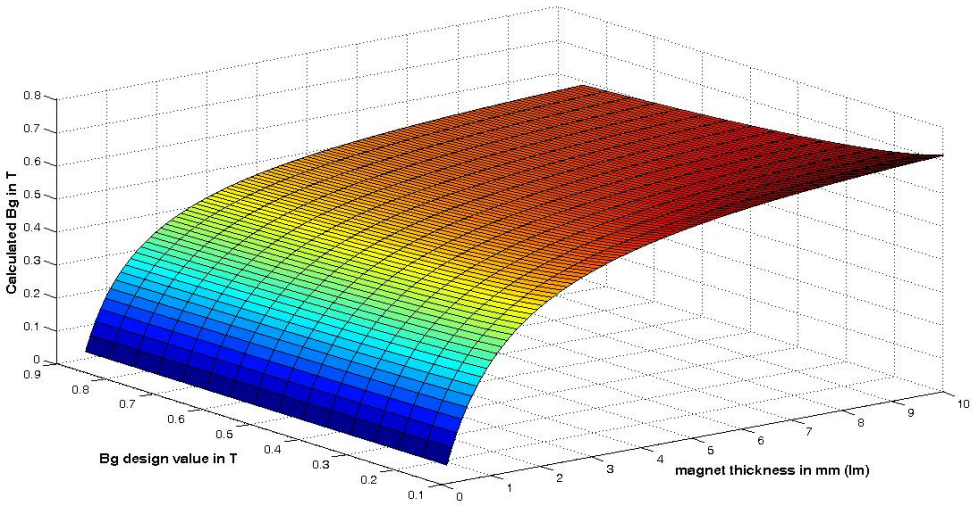

Figure 4-54: Calculated B_g values for different B_g design values and different magnet thickness (AF motor)

For defined design constrains in Table 4-21, it can be seen from Figure 4-54 that the air gap magnetic flux density can not be larger than 0.7T. In order to keep motor smaller B_g value can be selected as this value. But this requires nearly 10mm magnet thickness in a smaller radius.

Second concern in defining B_g is the main reason of selection of AF topology (increasing the inertia of rotor so that required external inertia can be smaller) .In order to maximize the inertia inner and outer radius of the motor should be larger. In order to maximize the inertia without increasing the mass much, B_g design value should be studied in terms of contributing inertia. In order to calculate the rotating inertia first definitions of motor dimension should be done. By defining a B_g value, R_o and R_i of motor can be calculated.

Magnetic circuit is only dependent on Ri, Ro, Bg and lm and constants related to magnet properties. Since all other parameters are defined magnet thickness (l_m) can be calculated using reverse calculation of magnetic circuit equations. Once l_m is calculated mass and inertia of the magnet can be calculated using Eq. (4.55).

$$M_{magnet} = \left[\frac{2\pi(R_o^{\ 2} - R_i^{\ 2})}{3p} \times 2 \times l_m x d_{magnet} \right] \times p$$
$$I_{magnet} = \frac{M_{magnet}(R_o^{\ 2} + R_i^{\ 2})}{2} \tag{4.55}$$

Note that inertia and mass of the magnet is independent of the number of poles of the motor. As number of poles increased only magnet is divided in to sections and total mass and inertia do no change. While calculating the mass of the magnet each magnet weight is multiplied by 2 due to two rotor of motor.

Another inertia contribution is coming from the two rotor of the AF motor. In order to calculate mass and inertia of rotor first thickness of the rotor should be defined.

Flux circulation on the motor is shown in Figure 4-50 . Note that rotor is rotoaing with synchronous speed and flux is stationary at rotor (which means constant flux density). Flux in the rotor core (Φ_r) is half of the pole flux in the air gap (Φ_g) and using flux equality and known parameters rotor back core thickness (l_r) (see Figure 4-50) can be calculated using Eq. (4.56).

$$\begin{aligned} \Phi_g &= B_g A_g \\ A_g &= \frac{\frac{2}{3}\pi(R_o{}^2 - R_i{}^2)}{p} \\ \Phi_r &= \frac{\Phi_g}{2} = \frac{B_{br} A_r}{2} \\ l_r &= \frac{A_r}{R_o - R_i)} \end{aligned} \tag{4.56}$$

Only unknown in Eq. (4.53) is B_{br} (rotor back core flux density). This value is dependent on core material which is selected in chapter 2. Rotor is rotating with synchronous speed flux is stationary on the rotor. Selected ferro magnet has a 1.2 T saturation flux density. This value can be selected as rotor back core flux density but rotor thickness and mass will be smaller and inertia contribution will be lower. 0.9T is selected as flux density in the rotor back core to increase inertia contribution. Once l_r is determined mass and inertia contribution of the two rotors can be calculated using Eq. (4.57).

$$\begin{aligned} M_{rotor} &= 2\pi(R_o{}^2 - R_i{}^2) l_r d_{steel} \\ I_{rotor} &= \frac{M_{rotor}(R_o{}^2 + R_i{}^2)}{2} \end{aligned} \tag{4.57}$$

Last parameter which is affecting the total motor mass is stator core. Note that stator core is not contributing the inertia but it affects the total system mass and its mass dependent on selection of B_g value. Stator core thickness can be calculated using flux relation between air gap and stator core. Flux in the stator is same as the flux per pole.

$$
\begin{aligned}
&\Phi_s = \Phi_p \\
&\Phi_s = B_{bs} A_s \\
&\Phi_p = B_{gav} A_{pole} \\
&B_{gav} = 0.7 B_g \\
&A_{pole} = \frac{\pi(R_o^{\,2} - R_i^{\,2})}{p} \\
&l_{cr} = \frac{A_s}{(R_o - R_i)}
\end{aligned}
\qquad (4.58)
$$

All parameters are defined for a fixed B_g value in Eq. (4.58) except average stator back core flux density (B_{bs}). This value is again determined by selected core material. Selected material is same material used in RF motor design. As shown in Figure 4-13 it is assumed to begins saturation at 1.2T. And flux in the stator is time varying. Assuming a sinusoidal flux variation average flux density in the stator is 2/pi times the peak value of flux density in the stator. Although selected material has 1.2T saturation flux density peaks are permissible up to 1.4T and using this fact stator back core average density can be assumed as 0.9T, in order to reduce the total weight of stator by letting some MMF drop in the magnetic circuit at peak instants of flux. Required stator thickness (l_{cr} see Figure 4-50) can be calculated using (4.58). Since all parameters are defined mass of the stator can be calculated using Eq. (4.59).

$$M_{stator} = \pi(R_o^{\,2} - R_i^{\,2}) l_{cr} d_{steel} \qquad (4.59)$$

Total mass of the motor and total rooting inertia can be calculated using Eq. (4.60)

$$
\begin{aligned}
&M_{motor} = M_{stator} + M_{rotor} + M_{magnet} \\
&I_{motor} = I_{rotor} + I_{magnet}
\end{aligned}
\qquad (4.60)
$$

Achievable Bg values for different magnet thickness are already studied and results are shown in Figure 4-54.

As stated before effect of selected Bg on motor inertia and mass should be considered. Mass and inertia calculations are shown in Eq. (4.55) – (4.60). In

order to see the effect of selected Bg on inertia and mass calculation flow in Figure 4-55 is done in Matlab software.

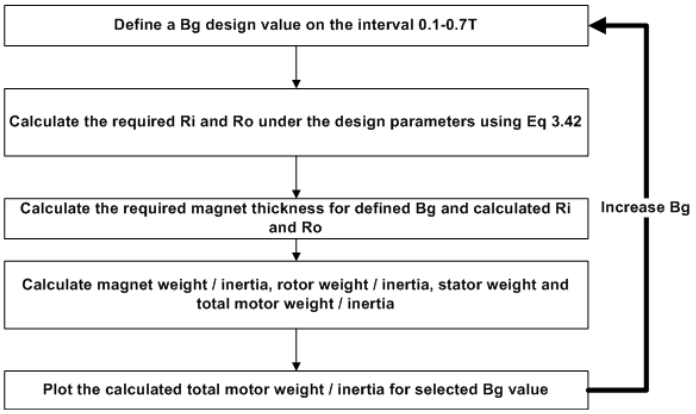

Figure 4-55: Effect of B_g value on motor mass and inertia calculation flow

Results of calculation are shown in Figure 4-56 to Figure 4-58.

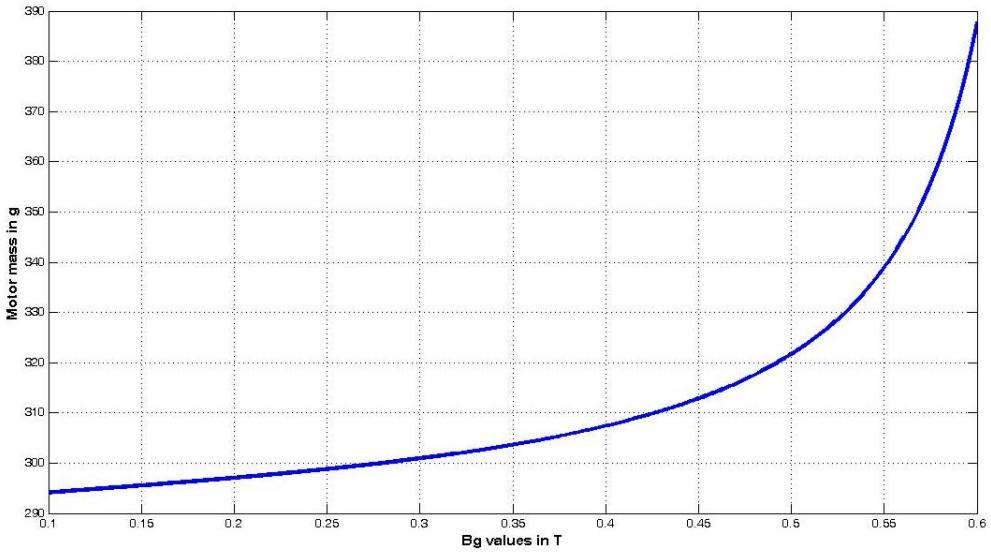

Figure 4-56: Motor mass for different B_g values

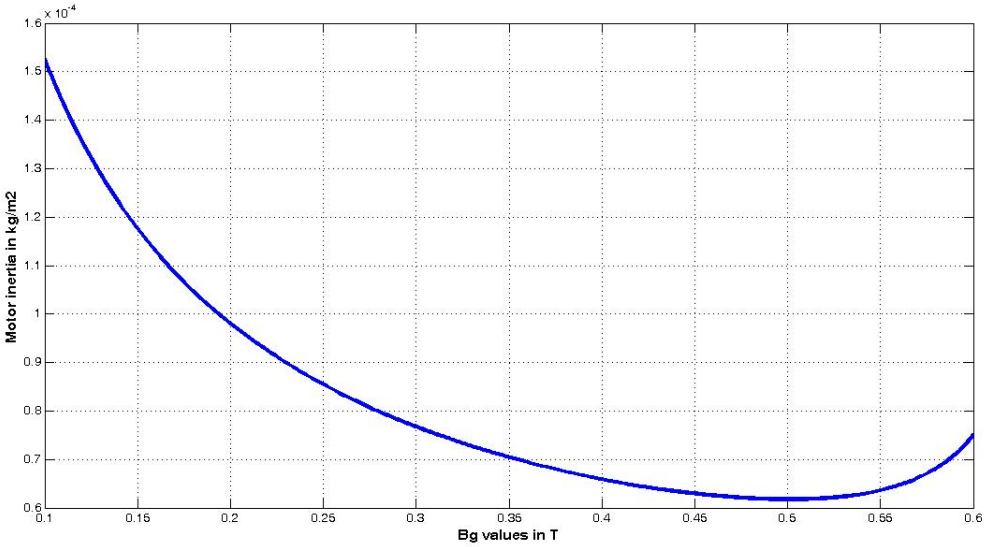

Figure 4-57: Motor inertia for different B_g values

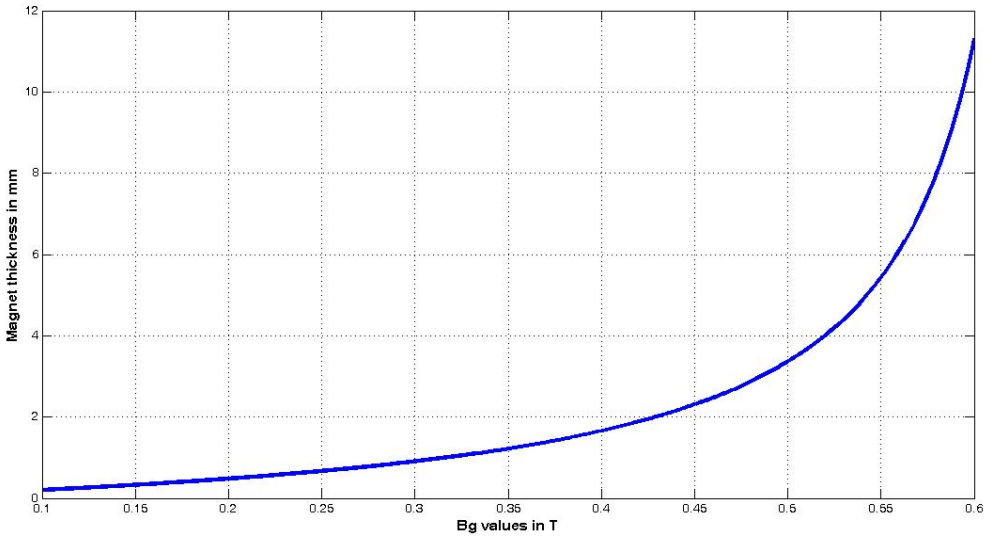

Figure 4-58: Required magnet thickness for different B_g values

If lower values of B_g selected motor inner and outer radius are increased and required magnet, rotor and stator thicknesses are reduced and as a result of that motor weight is decreased. As radius values are increased inertia of motor also increases due to dependency of inertia to radius. Selecting low B_g values has two

main drawback. One is motor volume is increasing due to larger inner and outer radius. In CMG application this is not a disadvantage, since there is a need to larger inertia and larger radius means larger inertia. Second drawback is the magnet thickness. Usually thickness values less than 1mm are not used since magnets can be broken. Under the calculation results B_g value is selected as 0.32T which is corresponding to 1mm magnet thickness.

Main dimensions of AF motor are magnet thickness lm, inner radius R_i, outer radius R_o, motor axial length L, rotor back core thickness l_r, stator back core thickness l_{cr} .

Design parameters have already been defined and summary of defined parameters are shown in Table 4-22.

Table 4-22: Design Parameters of AF Motor

Design parameter	Value
Peak torque requirement T_p (mNm)	50
Electrical loading q (Aturn/m)	4800
inner radius /outer radius (K_r)	0.65
Air gap g (mm)	1.65
B_g design value (T)	0.32

Under the stated design parameters in Table 4-22, inner radius and outer radius of AF motor for 2 pole and 6 pole can be calculated using Eq. (4.51). After calculation of R_i and R_o and using B_g and magnetic circuit equations required magnet thickness can be calculated. Figure 4-59 shows the calculated value of B_g for different magnet thicknesses and 1mm magnet thickness is required to have 0.32T B_g value.

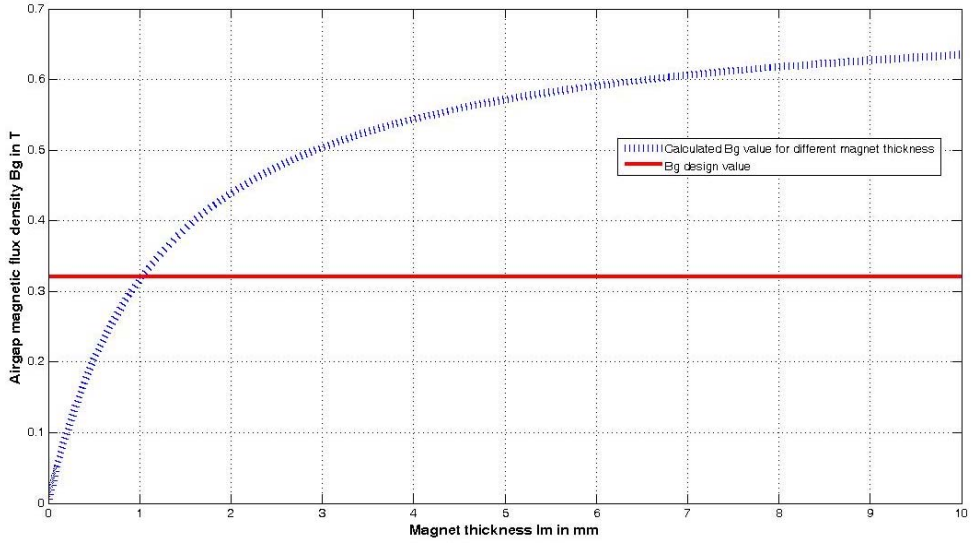

Figure 4-59: Resulting B_g values for different magnet thicknesses and required B_g

Note that B_g is independent of number of poles, as number of pole increases only magnet area per pole is decreasing total mass of the magnet and magnet thickness is not affected from the change of number of poles in AF motor. Secondly since magnet area is independent of magnet thickness magnetic flux density can be increased with magnet thickness (which is nit the case in RF motor.)

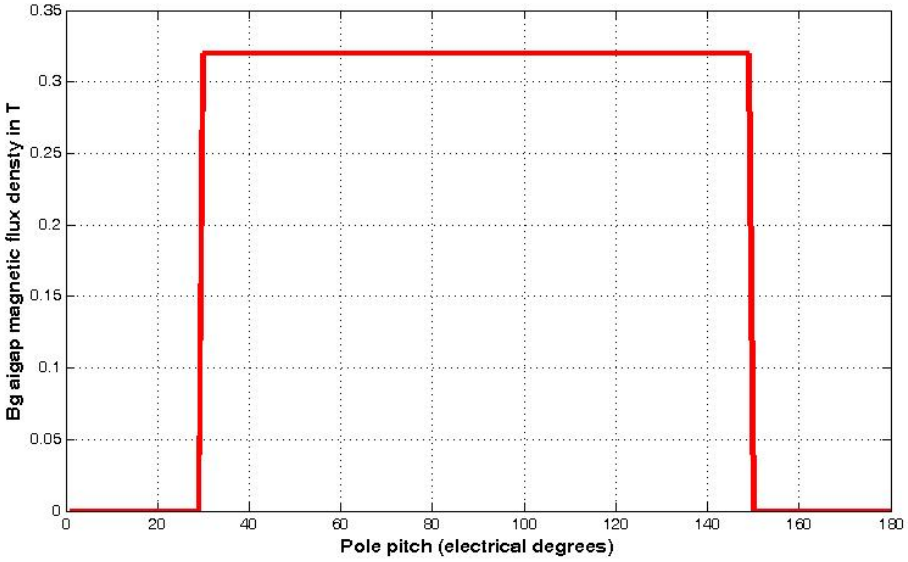

Figure 4-60: Magnetic flux density of AF motor over pole pitch

Figure 4-60 shows magnetic flux density distribution over a pole pitch. Rotor and stator core back core thickness values l_c and l_{cr} is calculated using Eq. (4.56) and Eq. (4.58). Note that since flux per pole is different for different number of poles required rotor and stator back core thickness values are different for different number of pole configurations. Motor axial length (L) can be calculated using Eq. (4.61).

$$L = l_{cr} + 2l_r + 2g + 2l_m \tag{4.61}$$

Summary of all calculated dimensions are shown in Table 4-23.

Table 4-23: Dimension of AF 2-pole and 6-pole Motors

Parameter	2pole	6pole
Inner radius of motor R_i (mm)	16.7	16.7
Outer radius of motor R_o (mm)	25.7	25.7
Magnet thickness l_m (mm)	1	1
Rotor thickness l_r (mm)	7.8	2.6
Stator core thickness l_{cr} (mm)	15.7	5.2
Motor axial length L (mm)	36.8	15.8

4.10.1 Winding design

Number of turns per phase is calculated using Eq. (4.62) in AF motor. Note that E_{ph} is the flat top value of phase back emf voltage.

$$N_{ph} = \frac{E_{ph}}{B_g R_o^{\ 2}(1-K_r^{\ 2})\omega_m} \tag{4.62}$$

Since available minimum dc link voltage is 18 V and 2 V is a margin for resistive voltage drop at 10000 RPM, peak value of back emf voltage should be less than 8V. Calculated value of number of turns per phase is summarized in Table 4-24.

Table 4-24: Number of turns per phase of AF Motors

Parametrer	AF 2 pole	AF 6 pole
N_{ph} calculated value	62.76	62.76
N_{ph} assumed value	60	60

Winding configuration of 2-pole and 6-pole AF motor on the stator is shown in Figure 4-61 and Figure 4-62.

winding section	1	2	3	4	5	6
phase winding	A1	-C1	B1	-A1	C1	-B1
number of turns per winding section	30	30	30	30	30	30
poles	1			2		

Figure 4-61: Winding distribution of 2 pole AF motor

winding section	1	2	3	4	5	6	7	8	9	10	11	12	13	14	15	16	17	18
phase winding	A	-C	B	-A	C	-B	A	-C	B	-A	C	-B	A	-C	B	-A	C	-B
number of turns per winding section	10	10	10	10	10	10	10	10	10	10	10	10	10	10	10	10	10	10
poles	pole1			pole2			pole3			pole4			pole5			pole6		

Figure 4-62: Winding distribution of 6 pole AF motor

Note that in each phase winding is divided into to sections and each section has half of the number of turns per phase per pole. Conductors are distributed at one or two layer. And these sections are symmetrically placed on the stator in order to reduce possible flux circulations on the stator core (Figure 4-63).

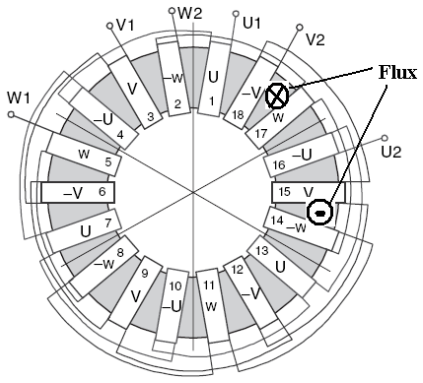

Figure 4-63: Winding distribution of 6 pole AF motor 2

4.10.2 Equivalent circuit parameters

4.10.2.1 Determination of phase resistance

Phase resistance calculation is done using motor dimensions shown in Figure 4-64 and Eq. (4.63).

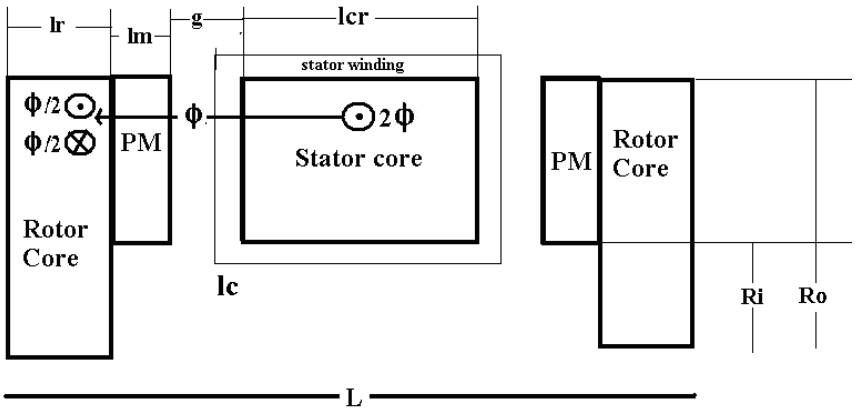

Figure 4-64: Radial Cross Section of AF Motor

$$
\begin{aligned}
R_{ph} &= \frac{\sigma L}{A_{cu}} = \sigma \frac{LMC \times N_{ph}}{A_{cu}} \\
Acu &= \frac{I_{rms}}{J} \\
q_i &= \frac{3N_{ph} I_{rms}}{2\pi R_i} \\
Acu &= \frac{2q_i \pi R_i}{3JN_{ph}} \\
LMC &= 2(R_o - R_i + 2l_c) + 2(l_{cr} + 2l_c) + (4 \times 0.003)
\end{aligned}
\tag{4.63}
$$

In order to keep the effect of end winding wire bending at 4 edges, 3mm is added to have margin. The phase resistances are calculated as 146.5 and 87 mΩ for 2-pole and 6-pole cases, respectively. Note that 6-pole motor resistance is lower since stator core length is smaller in 6 pole configuration.

4.10.2.2 Determination of phase inductance

Phase inductance (L_{ph}) of AF motor composed of 2 inductances. One is air gap inductance L_g, and second is coil leakage inductance. Note that selected AF motor is slotless type and there is not slot leakage inductance. Also since there is no slots coil self inductance will be much smaller than the air gap inductance and it will be ignored in the calculations. And phase inductance is assumed to be equal to irgap inductance. In AF motor stator flux passes through 2 air gap in each pole. Air gap inductance is calculated using Eq. (4.64).

$$\begin{aligned} \lambda s &= N\Phi_{sbc} \\ \lambda s &= \frac{L}{I} \\ \Phi_{sbc} &= \frac{NI}{2Rg + 2Rm} \\ Rm &= \frac{1}{Pm} \\ L &= \frac{N^2}{2Rg + 2\frac{1}{Pm}} \\ L_g &= \frac{p}{2}L \end{aligned} \tag{4.64}$$

λs is flux linkage inside the stator

N is number of turns per phase per pole (30 for 2 pole, 10 for 6 pole)

R_g, is reluctance of air gap

P_m is permeance of magnet

I is current in the stator coils

L is inductance for each pole pair.

Permeance of the magnet and reluctance of air gap is calculated using magnetic circuit equations.

Calculated results of phase inductances are summarized in Table 4-25.

Table 4-25: Inductances of AF Motors

Parameter	AF 2 pole	AF 6 pole
Phase inductance L_{ph} (μ H)	122.3	14.5

4.10.3 Calculation of losses

Calculation of core losses can be done using Eq. (4.32) and Eq.(4.34). Note that since AF motor is slotless only losses at stator core should be calculated and peak value of flux density is selected as 1.4T at stator core (see section 4.10). In order to calculate stator mass of AF motors Eq. (4.59) should be used in Eq.(4.34). Calculation of resistive losses can be done using Eq. (4.45).

4.10.4 Calculation of motor volume and mass

Volume of the RF motor can be calculated using Eq. (4.65).

$$V_{motor} = \pi R_o^{\ 2} L \tag{4.65}$$

Mass and inertia of the AF motor can be calculated using Eq. (4.55), Eq. (4.57), Eq. (4.59) and Eq. (4.60). Calculated results are summarized in Table 4-26.

Table 4-26: Mass and volume of AF motors

Parameter	AF 2 pole	AF 6 pole
Inertia of total rotor (magnets + rotors) (kgm^2)	7.39×10^{-5}	2.87×10^{-5}
Volume of motor (m^3)	4.40×10^{-5}	1.89×10^{-5}
Mass of motor (kg)	301.6	109.6

4.10.5 Performance of AF motor under square wave excitation

4.10.5.1 Required motor current and electrical loading over speed range

Air gap magnetic flux density is assumed to be constant over speed range. Current loading at inner surface and required current over speed range is calculated using Eq. (4.66). In calculations Tm is required motor torque in Figure 3-14.

$$q = \frac{\sqrt{3}}{2\sqrt{2}} \frac{T_m}{B_g \pi R_o^{\ 3} K_r (1 - K_r^{\ 2})}$$
$$I_{rms} = \frac{q_i \pi D_i}{3 N_{ph}} \tag{4.66}$$

Note that required rms phase current and electrical loading are independent of number of poles. Results of calculation are shown in Figure 4-65.

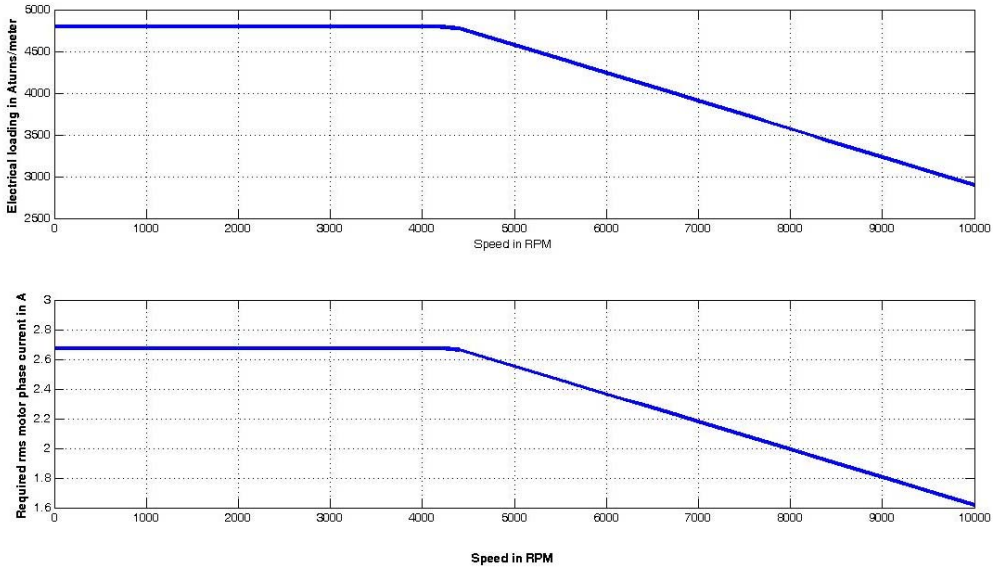

Figure 4-65: Electrical loading and required motor rms phase current of AF motor

4.10.5.2 Required line to line voltage and back emf voltage over speed range

Flat top value of back emf voltage and required applied dc link voltage is calculated using Eq. (4.45). Calculated results are shown in Figure 4-66and Figure 4-67.

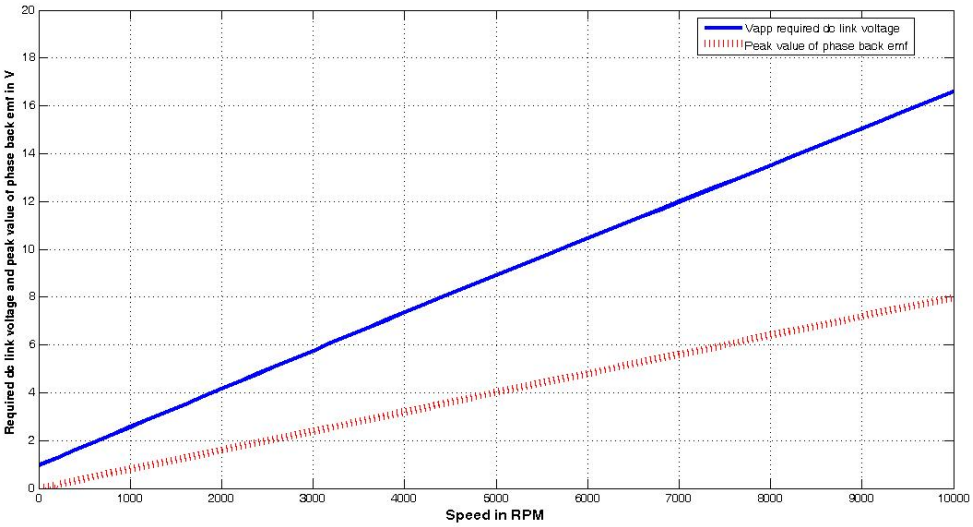

Figure 4-66: Required dc link voltage and peak value of phase back emf (AF 2pole)

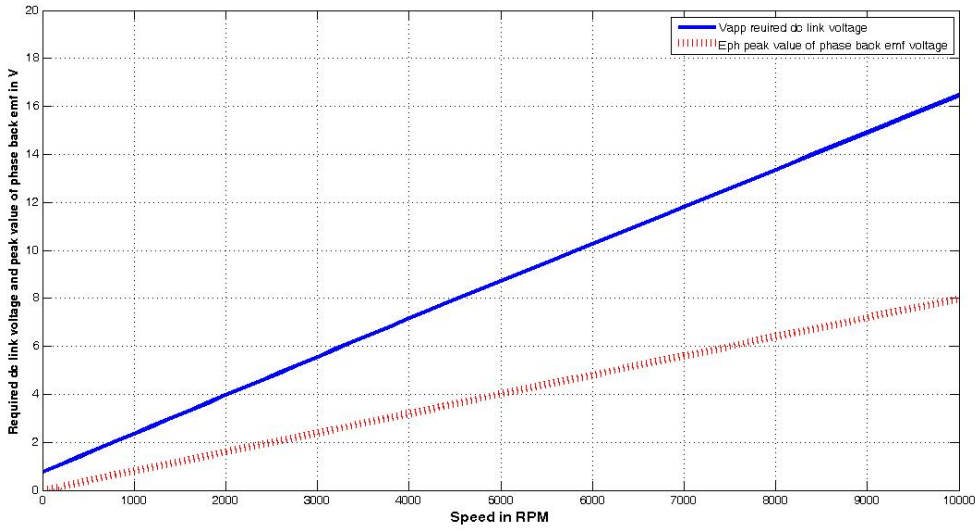

Figure 4-67: Required dc link voltage and peak value of phase back emf (AF 6 pole)

Note that since 2 pole motor phase resistance is larger more voltage (16.5 V(2pole)-16.3V(6pole)) is needed at dc link.

4.10.6 Losses over speed range

Calculation of core losses can be done using Eq. (4.32) and Eq.(4.34). Note that since AF motor is slotless only losses at stator core should be calculated. In order to calculate stator mass of AF motors Eq. (4.59) should be used in Eq.(4.34). Obtained results are shown in Figure 4-68 - Figure 4-70.

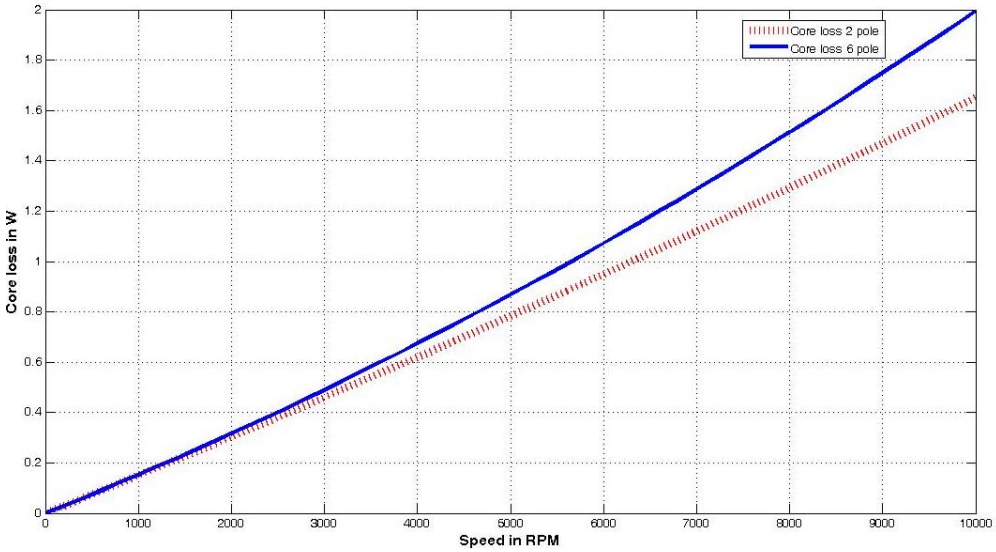

Figure 4-68: Core loss in AF motor

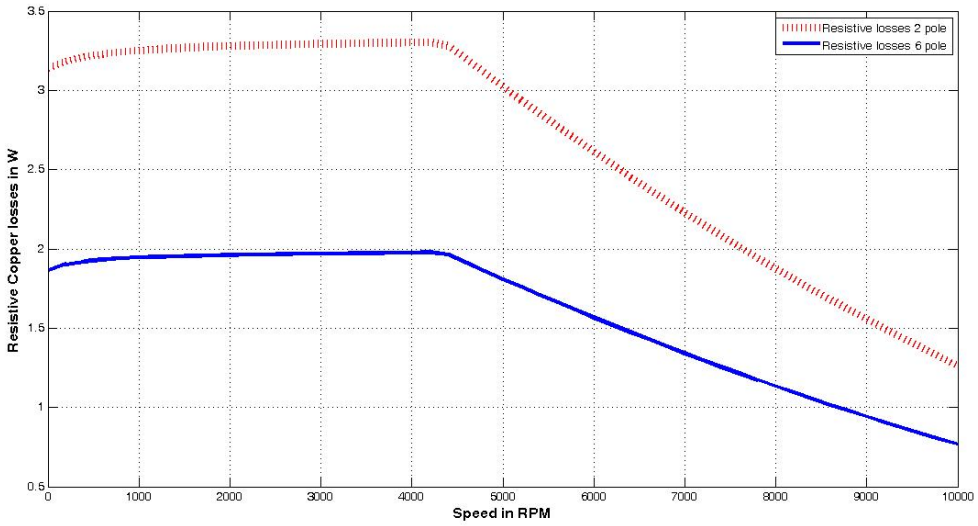

Figure 4-69: Resistive losses in AF motor

Since stator thickness is large in 2-pole case wire length becomes larger and phase resistance increases. Large resistance results in high resistive losses in 2 pole case.

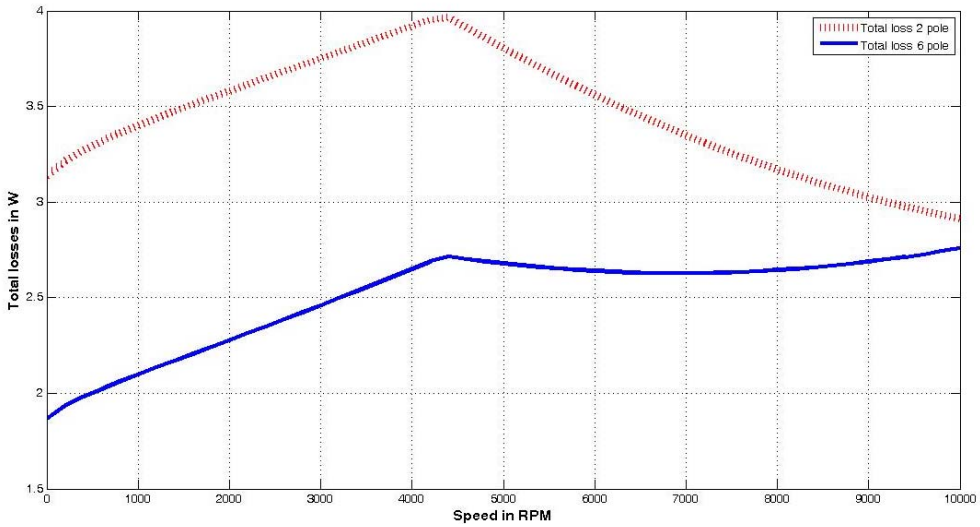

Figure 4-70: Total losses in AF motor

Figure 4-70 shows the total losses. Since resistive losses are dominant, in 2-pole case total losses are high.

4.10.7 Efficiency

Efficiency is defined as output power over total input power, and it is calculated based on Eq. (4.42). Figure 4-71 shows the efficiency over whole speed range.

$$\eta = \frac{P_{out}}{P_{in}} = \frac{T_{out} \times \omega_r}{T_{out} \times \omega_r + P_{co} + P_{core}} \tag{4.42}$$

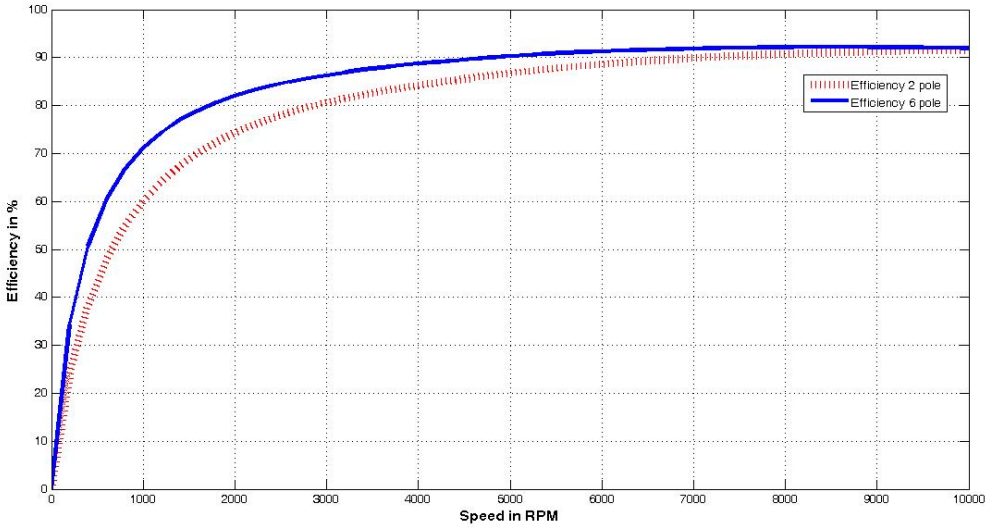

Figure 4-71: Efficiency in AF motor

4.10.8 Evaluation of AF motor under square wave excitation

- Motor peak electrical loading value vas determined as 4800Aturn/m, calculated value of electrical loading is shown in Figure 4-24, and during acceleration period electrical loading value is not more than the limit value. During steady state at 10000RPM electrical loading value is around 2900Aturn/m, but note that core losses are not added to calculation of electrical loading. In RF case it is shown that electrical loading is increasing 10 % when core losses are added (Figure 4-28). Core losses in AF motor is less than the RF motor case so core loss currents are expected to be less than RF motor case, another words electrical loading will not be higher than 10% of calculated values in Figure 4-24 so design is on safe side.
- Maximum current density at stator coils is selected as 7A/mm^2. Peak current on stator coil is calculated as 2.65A (Figure 4-65) during acceleration period. Necessary conductor area is calculated using these two values and it is 0.37 mm^2. It should be checked whether conductors

can be inserted into inner peripheral of stator. Using 0.6 fill factor and 60x3 (number of turns per phase x number of phase) stator conductors at inner peripheral of stator, 68 mm^2 total conductor area is required. Total available conductor area at inner peripheral of the stator is calculated as 120mm^2 using designed dimensions are summarized in Table 4-23 and total conductor area is calculated using dimension values and Eq.(4.53) ($A_{tcon} = l_c(2\pi R_i)$) . So conductor can be placed on the inner peripheral of stator.

- Figure 4-66 and Figure 4-67 required dc link voltage and phase back emf rms voltage over speed range. Required dc link voltage is maximum at 10000 RPM and its value is (16.5 V(2pole)-16.3V(6pole)). This value is less than minimum available dc link voltage (18V) if we add the switch voltage drop of 1.4V, so design is on safe side.

4.10.9 Comparison of calculated results for AF 2 pole and 6 pole motors

Table 4-27 summarizes the calculated parameters of RF 2 pole motor and 6 pole motor under square wave excitation.

- Rotor and stator thickness values are high in 2 pole configuration since flux per pole is larger in 2 pole case.
- Motor axial length is dependent on stator and rotor thickness, as a result of that motor axial length is larger in 2 pole configuration
- Phase resistance and inductance values are higher in 2 pole configuration because stator thickness is larger in 2 pole configuration
- Core losses are larger in 6 pole configuration since electrical frequency is 3 times of 2 pole case
- Resistive losses are high in 2 pole case due to larger resistance and since resistive losses are dominant at acceleration period total losses are higher in 2 pole case, but at steady state core losses and resistive losses are closer and total losses are closer. Efficiency is closer at rated speed because

although resistive losses are smaller in 6 pole case core losses becomes higher in 6 pole at 10000 RPM

- Mass and volume are larger in 2 pole configuration since stator and rotor thicknesses are high, torque/mass and torque/volume are higher in 6 pole configuration as a result of lower mass and volume.
- Inertia contribution of both motor is sufficiently large to reduce the externally added wheel mass and volume. Details of this issue will be studied in next chapter.

Table 4-27: Summary of Calculated Performance Parameters of AF Motors

Parameter	AF 2-pole	AF 6-pole
Inner radius of motor R_i (mm)	16.7	16.7
Outer radius of motor R_o (mm)	25.7	25.7
Rotor thickness l_r (mm)	7.8	2.6
Stator core thickness l_{cr} (mm)	15.7	5.2
Motor axial length L (mm)	36.8	15.8
Phase Resistance R_{ph} (mΩ)	146.5	87
Phase inductance L_{ph} (μ H)	122.5	14.6
Core losses at 10000RPM (W)	1.65	2
Resistive losses (W) at 10000RPM	1.26	0.76
Total losses (W)	2.9	2.75
Efficiency at 10000RPM %	%91.5	%92
Mass (g)	301.6	109.6
Volume (m^3)	4.401×10^{-5}	1.889×10^{-5}
Torque/mass Nm/kg	0.166	0.458
Torque/ volume (Nm/m^3)	1136	2645
Inertia kgm^2	7.379×10^{-5}	2.877×10^{-5}
Inertia contribution to total required inertia	% 15.2	%5.9

4.11 Mechanical Considerations of AF Motor Design

Magnet attachment on rotor surface for AF motor is studied in this part. Heat shrinkable insulation band is used in radial flux motor and this method was a solution for radial flux motor. In axial flux however force can be handled by adding an external ring to the rotor (Figure 4-72).

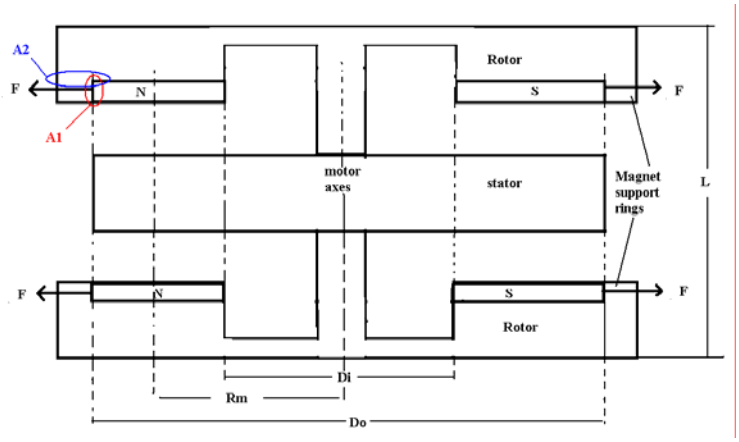

Figure 4-72: Ring support on rotor surface 1

In conventional applications such solutions are avoided because this solution increases the inertia and mass. But in this application inertia is strongly needed and support rings increase the rotor inertia since they are far from rotation axis. Necessary thickness and stress values at area A1 and area A2 should be calculated.

Force on the A1 (see Figure 4-72) can be calculated using the Equations (4.67).

$$R_m = \frac{R_o - R_i}{2}$$
$$F = M_{magnet} w_m{}^2 R_m \qquad (4.67)$$

R_m is averge magnet radius, w_m is mechanical speed of motor, M_{magnet} is mass of one magnet, F is radial force due to rotation. Ring inner surface (A1) area which is facing with magnet is calculated using Eq. (4.68).

$$A1 = \frac{\frac{2}{3}(2\pi R_o) l_m}{p} \tag{4.68}$$

By definition of the stress is force per unit area, there fore stress on surface A1 is calculated using Eq. (4.69) [24].

$$\sigma_{A1} = \frac{F}{A_{A1}} \tag{4.69}$$

Calculated values of radial force on one of the magnets is shown in Figure 4-73 and stress on A1 surface of the magnet and steel ring are shown in Figure 4-74.

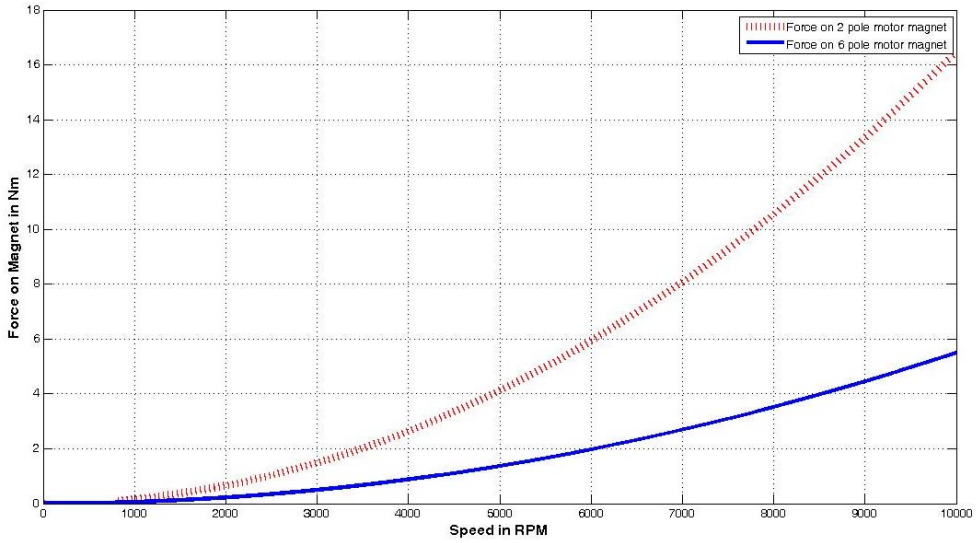

Figure 4-73: Force on magnet in AF motor

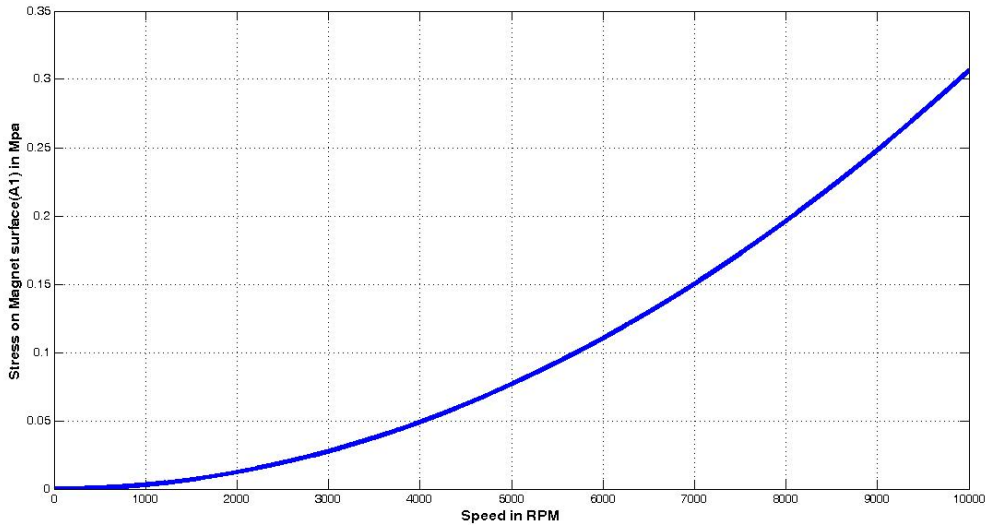

Figure 4-74: Stress on surface A1

Note that force/area is same in 2-pole and 6-pole configuration. Selected ferromagnetic Cogent power no 12 has a tensile strength (maximum value at which a material breaks or permanently deforms) of 505MPa and a yield strength (at which a material begins to deform plastically) of 400MPa. nd selected Vacomax225 SaCo magnet has a compressive strength of 650Mpa (Bending strength 90-151Mpa) and design is at safe side.

Second important point for magnet stability is whether the stress at A2 is in the achievable scale of ferro magnet.

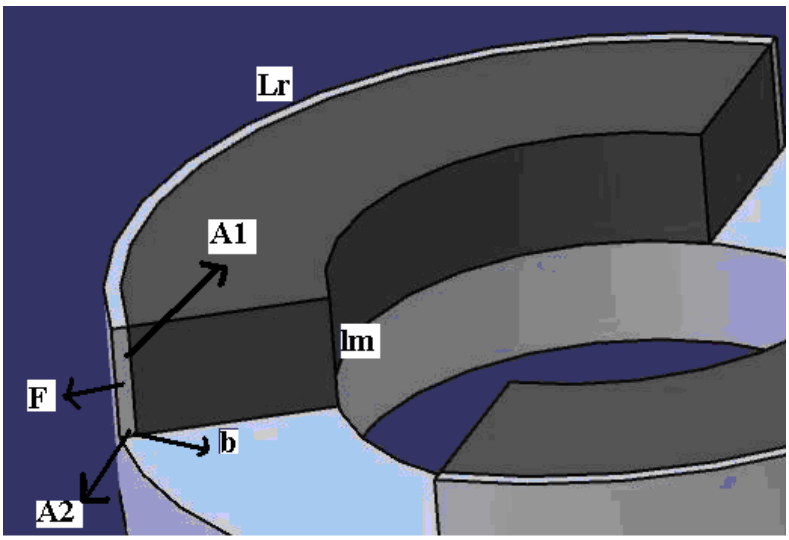

Figure 4-75: Ring support on rotor surface 2

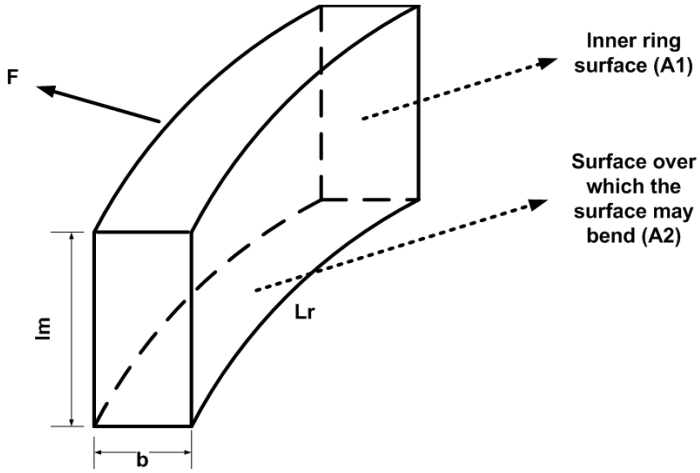

Figure 4-76 Ring support on rotor surface 3

In order to check the steel stability not to deform or break down, bending stress is calculated at area A2 (Figure 4-75 and Figure 4-76). Support ring is circular and circular bending stress calculations are a little complex. Ring is assumed as a rectangular shape (Lr x b) and height is assumed as l_m. Bending stress will be calculated on rectangular shape and circular shapes are more resistive on stress or

another words stress on circular shape will be less than rectangular shape so design will be safe side.

Bending stress on surface A2 can be calculated using Equation (4.68)[24].

$$\sigma_b = \frac{F \times (\frac{l_m}{2})}{I}$$
$$I = \frac{Lr \times b^2}{6} \tag{4.68}$$
$$Lr = \frac{2\pi(Ro + \frac{b}{2})\frac{2}{3}}{p}$$

Calculated bending stress values for 1mm ring thickness (b) speed range is shown in Figure 4-77.

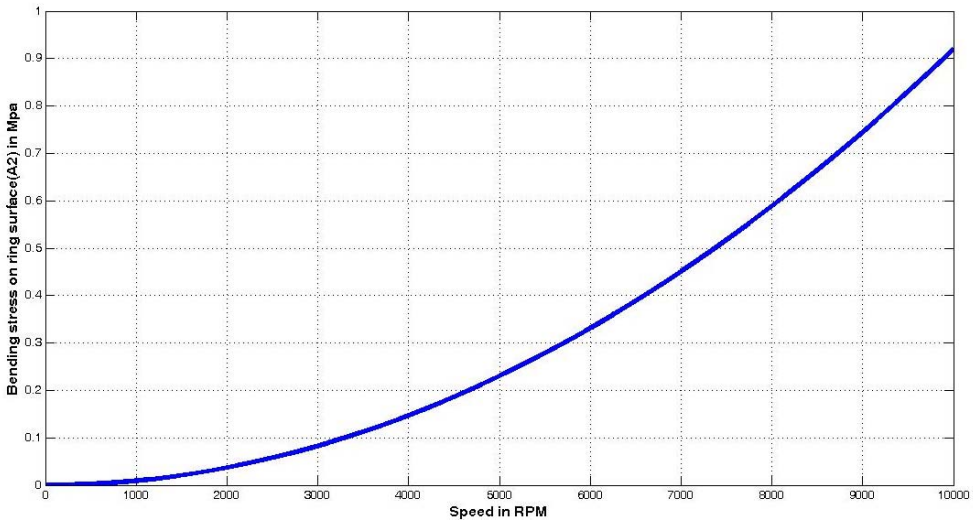

Figure 4-77: Bending stress at surface A2

Ring should withstand a stress value of 1 MPa. Selected steel core Cogent power no 12 has a tensile strength (maximum value at which a material breaks or permanently deforms) of 505MPa and a yield strength (at which a material begins

to deform plastically) of 400MPa so design is on the safe side. (Note that this ring can be made of a different material (wheel material i.e.) which has a larger strength value of 1 MPa and this will be discussed in chapter 5)

CHAPTER 5

NUMERICAL RESULTS AND DISCUSSIONS

In this part of the thesis firstly calculated results in Chapter 4 will be summarized. Calculated values of mass, torque/mass, torque/volume, efficiency and inertia contribution of RF and AF motors are compared. Secondly performance of motors will be studied at CMG level. Integration of motors to CMG system will be discussed by comparing each other and the existing system. Finally all the results are discussed and possible future work is discussed.

5.1 Discussion of Numerical Results

5.1.1 Comparison of AF and RF Motors

Comparison criterias for AF and RF motors was determined as efficiency, torque/mass and torque/volume in Chapter 3. These values are already calculated in Chapter 4 for RF and AF motors. But note that bearing and mechanical fixture weights are ignored while calculating mass and volume of motors. These additional masses are assumed to be having same effect on both motors and only bare motor mass and volumes (which are calculated in chapter 4) are compared in this part. Effect of mechanical fixtures will be discussed in next part while integration to CMG case is considered. Figure 5-1 to Figure 5-6 shows the calculation results in Chapter 4 in graphical representation.

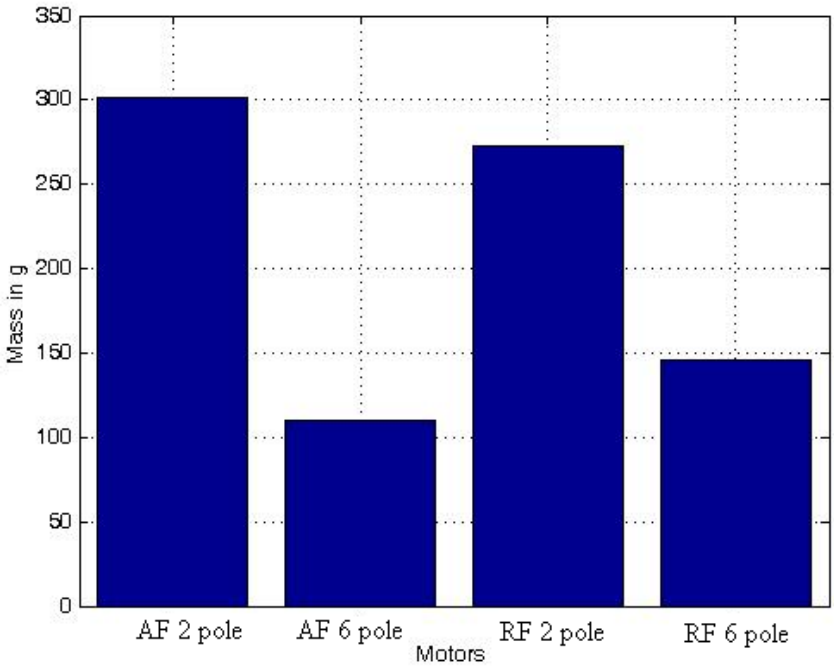

Figure 5-1: Calculated mass of motors

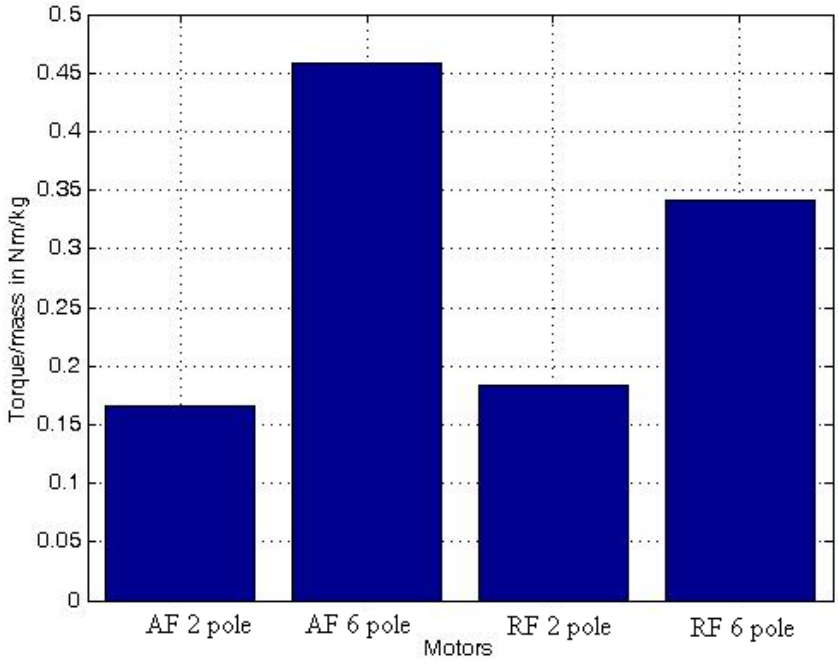

Figure 5-2: Calculated torque/mass of motors

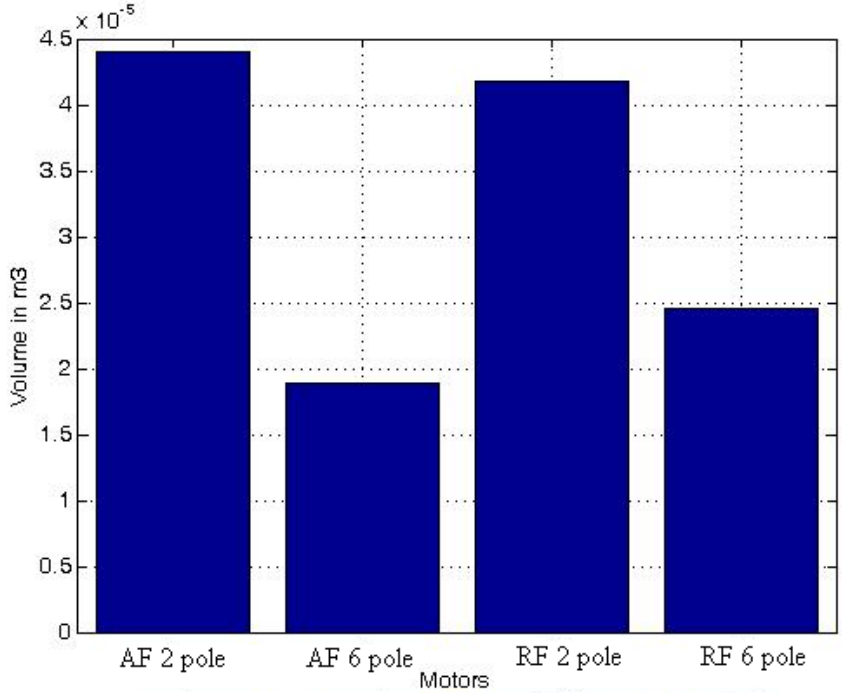

Figure 5-3: Calculated volume of motors

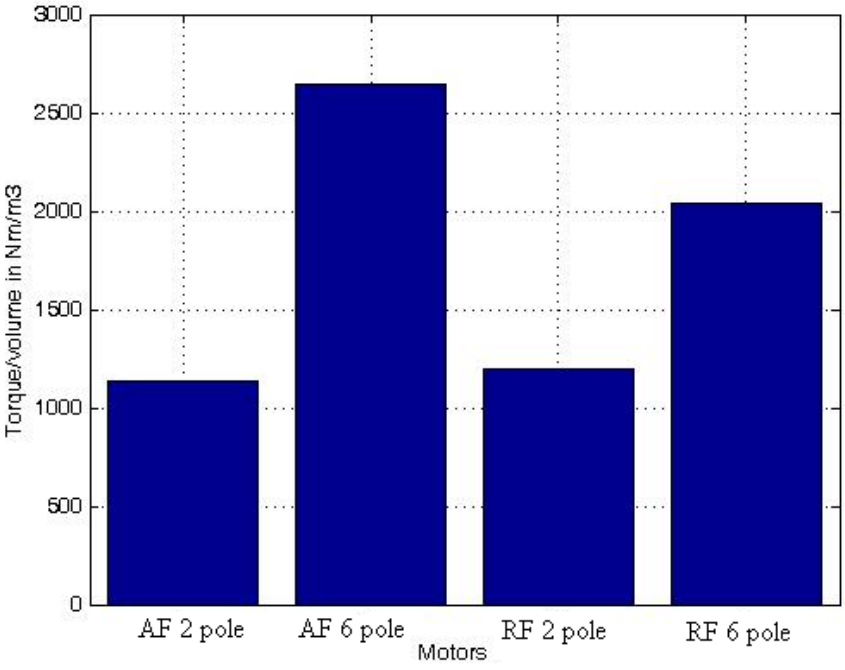

Figure 5-4: Calculated torque/volume of motors

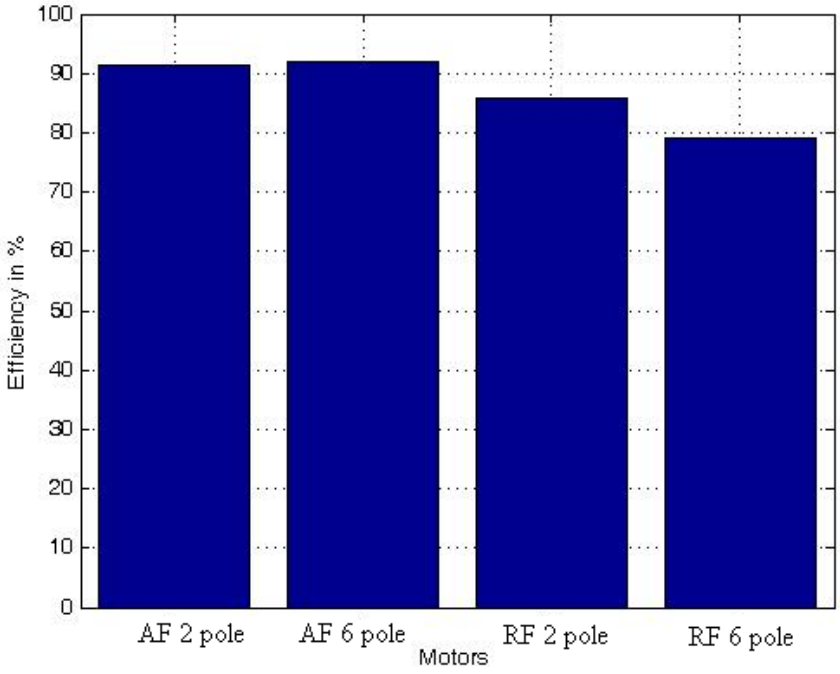

Figure 5-5: Calculated efficiency of motors at 10000RPM

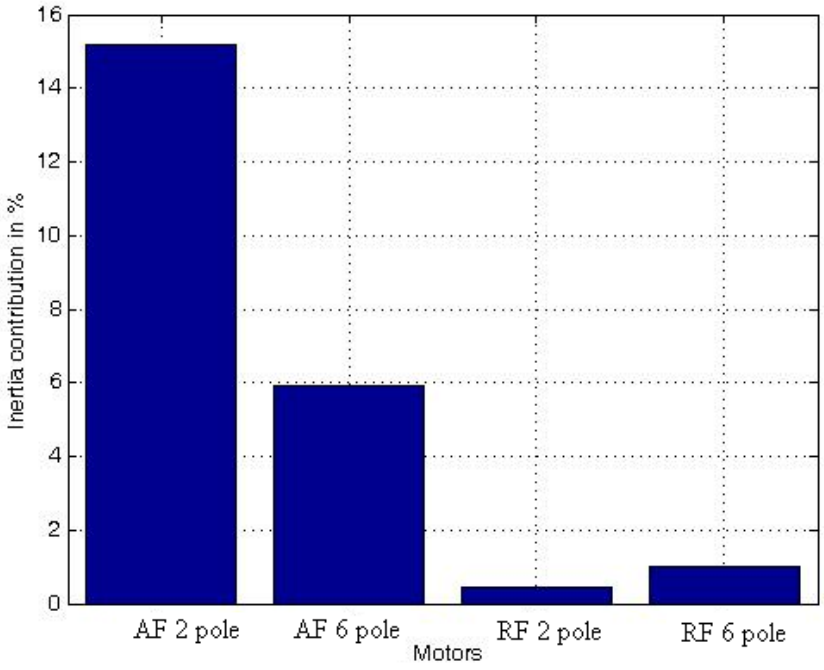

Figure 5-6: Calculated inertia contribution of motors

- When mass of the motors are compared, as number of pole increases both AF and RF motors have lower weight due to smaller stator weight. Decrease in stator weight is due to smaller flux per pole is flowing through the stator back core, so required stator back core thickness is less in 6 pole configurations. In 6 pole configurations AF motor mass is the smallest one.
- Expected starting torque (50mNm) and steady state friction torque (32mNm) from all motors are same. As a result of this, torque/mass performance is in parallel to motor mass requirements. Smallest mass results in largest torque/mass ratio, which is in AF 6 pole case.
- Volumes of the motors are shown in Figure 5-3 and since expected torque is same for all motors, torque/volume performance is dependent on volume of the motor. Smallest volume and highest torque/volume performance belongs to AF 6 pole configuration.
- Efficiency is dependent on total losses at steady state. In RF configurations core losses are dominant on total losses (Table 4-20). Core losses are dependent on mass of the stator and square of electrical frequency (for same peak flux density at stator back core). Although mass of stator is less in 6 pole case, electrical frequency is 3 times more and consequently core losses are larger at high number of pole. Since core losses are larger in RF 6 pole motor, efficiency of 6 pole motor is less than two pole case. When total losses in AF motor are considered at steady state (Table 4-27), total losses are closer at both number of poles and efficiency value is also closer. When both topologies are compared in terms of efficiency AF motor efficiency values are larger (Figure 5-5).
- Inertia contribution is defined as inertia of motor/ total required inertia (4.83×10^{-7} kgm^2, note that this value is the inertia of already designed and wheel see Figure 3-4 and Table 3-1). Due to geometry of AF motors, inertia contribution is larger.

When we compare the RF topologies between each other 6 pole configuration has better performance in terms of torque/ mass and torque/volume. But efficiency is slightly less (6.7%) than 2 pole case. Also axial length of 6 pole RF motor is 14.5 mm whereas 2 pole motor has 21.9 mm axial length which means larger dimensions in Y axis of CMG (Figure 3-1) and this is not preferred situation since inertial at y axis increase and this results in higher power consumption in CMG gimbal motor (see section 3.3). Weight of the motor in existing CMG is 263g (Maxon EC 32) and RF 2 pole motor has 272.6 g weight and this weight do not include the mechanical fixtures so 2 pole RF motor is eliminated. RF 6 pole motor (146.3g) will be used in order to compare with AF motor integrated CMG system and existing CMG solution.

When AF motor topologies are compared between each other, 6 pole motor has better performance apart from the inertia contribution. Although 2 pole case has larger inertia contribution mass of 2 pole AF motor (301.6g) is much larger than 6 pole AF motor (109.6g) and the motor in existing CMG is (Maxon EC 32 (263g)), so AF 2 pole configuration is eliminated. . AF 6 pole motor will be used in order to compare with RF 6 pole motor integrated CMG system and existing CMG solution.

Note that efficiency value of the motor in existing CMG is %78 (Maxon EC 32) and both AF (92%) and RF (79 %) 6 pole motors have comparable efficiency values with existing motor (Maxon EC 32).

5.1.2 Comparison of AF and RF Motors on the CMG System

In order to make a complete comparison between AF and RF motors for CMG wheel application, mass and volume should be calculated considering the CMG system. Total mass and volume of the CMG system is designed by considering the structural requirements of wheel and motor volumes. Another saying if new motor or wheel is used structure of total CMG should be designed again. But if mass and volume of the wheel and motor is less total mass and volume of the

system will definitely be smaller. Since total structural design of CMG is not in the scope of this thesis, main concentration will be on the mass and volume of wheel and motor which is called wheel system.

Figure 5.7 shows the RF 6 pole motor integrated CMG system. Two bearings are added to the system. It is assumed that since motor is not commercial of the shelf, load on the bearings can be calculated and a proper bearing can be inserted into motor to carry the loads due to wheel (Note that in existing system Maxon EC 32 bearings are not used for carrying the wheel an external bearing is used see Figure 3-1.). Selection of bearing is not in the scope of this thesis and a sample bearing is selected in order to have the mass of the bearing in the calculations (SKF 7200 BECBP whose weight is 30g).

Second issue to be considered is housing in RF 6 pole motor. A housing thickness 3 mm is selected and included into mass calculations (note that 7mm should be added for end windings to the both axial end of the motors). Material for housing is selected as Aluminum 2014(Its density is 2800 kg/m^3). Last issue is the weight of wiring and it is assumed to be 20g in mass calculations.

Since inertia contribution in RF case is less than %1 and the wheel that is used in the existing system is considered for calculating the wheel system mass and volume. (In AF case however there is significant contribution to rotating inertia.)

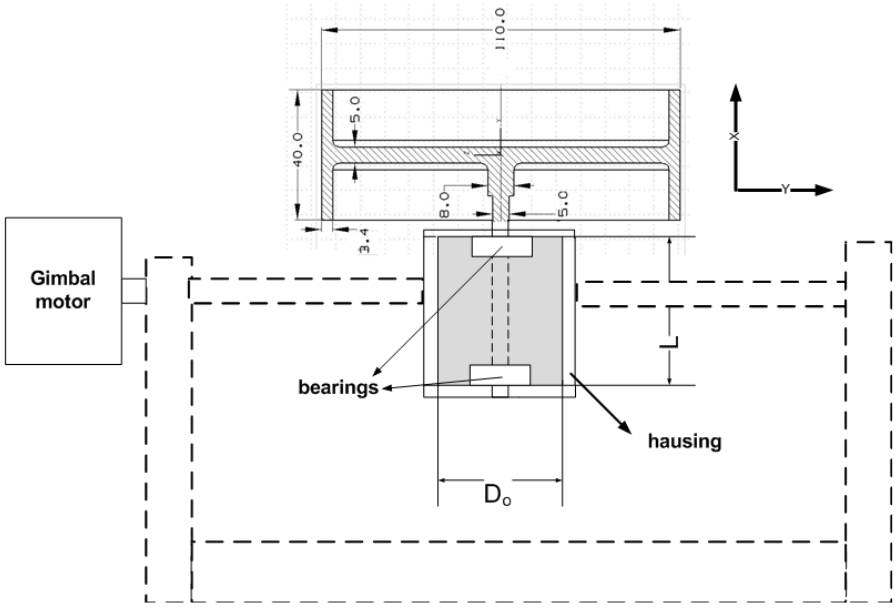

Figure 5-7: RF 6 pole motor integrated wheel CMG system

Figure 5-7 shows the wheel system integrated to the designed RF 6 motor. Summary of mass and volume of the wheel system is given in Table 5-1. While calculating volume of the wheel largest dimensions are used (diameter 110mm and height 40mm). While calculating the volume of motor effect of housing is considered and since bearings and windings are inside the motor they are not included in to volume calculations. Figure 5-8 shows assumed total volume the designed RF 6 pole integrated wheel system.

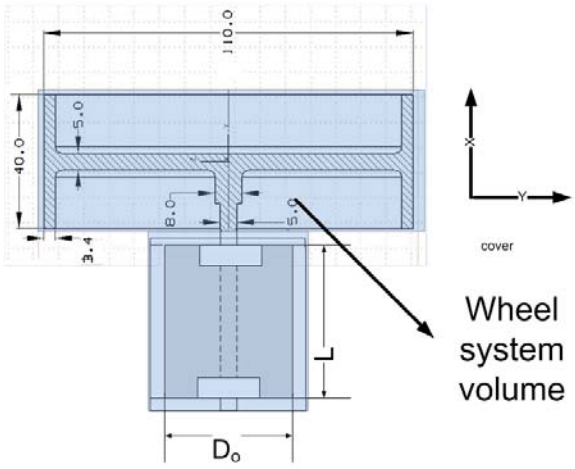

Figure 5-8: Volume of RF 6 pole motor integrated wheel system

Table 5-1: Calculated parameters of RF motor integrated wheel system

Parameters	RF 6 pole
Mass of motor (bare motor) (g)	146.3
Mass of the hausing (g)	26
Mass of bearings (g)	60
Mass of windings (g)	20
Mass of wheel (g)- existing wheel is used	240
Volume of motor (m^3) (including the housing)	3.75×10^{-5}
Volume of wheel (m^3)	7.598×10^{-4}
Inertia of wheel (kgm^2)- existing wheel is used	4.83×10^{-4}
Inertia of motor	Less than%1 ignored
Volume of wheel system	7.96×10^{-4}
Total mass of wheel system (g)	492.3
Total volume of wheel system (m^3)	7.97×10^{-4}

In order to calculate performance of AF integrated wheel system, a new wheel is defined for remaining part of rotating inertia (since AF motor rotor is contributing to total rotating inertia (5.9 %)). In order to keep symmetry on gimbal axis (Y axis

in Figure 3-1), two symmetrical additional ring shapes is used. Also in order to keep magnets on the rotor surface, required ring thickness (d4=1mm) was calculated in previous chapter. This ring is also assumed to be a part of wheel. Outer diameter (d5=110mm) of the new wheel is limited and assumed be same as existing wheel.

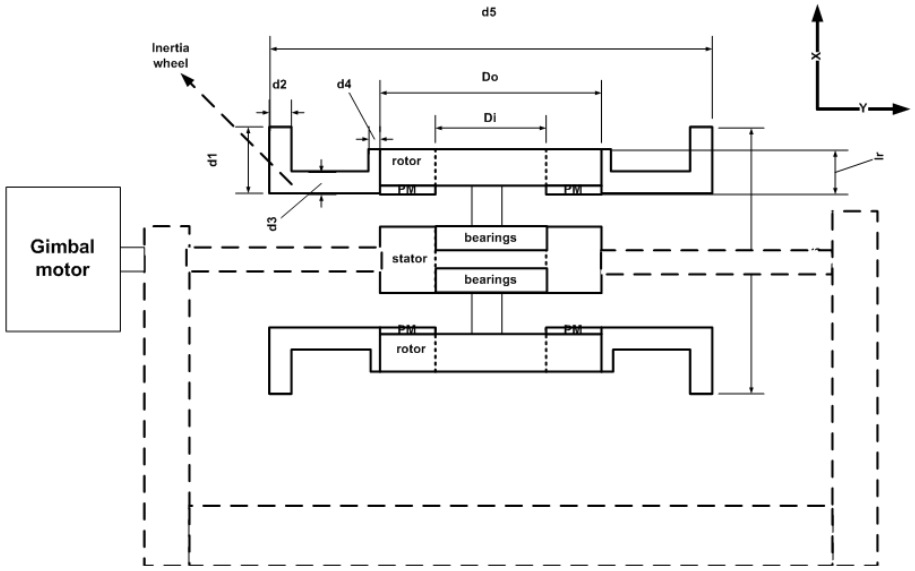

Figure 5-9: AF 6 pole motor integrated CMG system

Figure 5-9 shows the AF motor integrated wheel system. In designing wheel same material is used in RF case which is Aluminum 2014. Its density is 2800 kg/m^3. Required stress value for magnet keep on rotor surface was 1Mpa and Al 2014 has yield strength of 97Mpa so design is still on safe side for the stress values calculated in section 4.11.

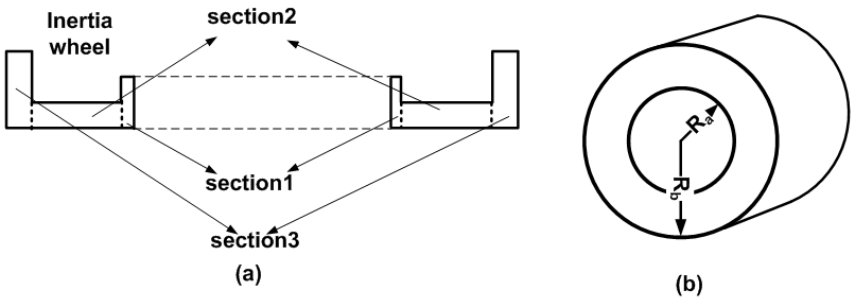

Figure 5-10: Inertia calculation approach for new wheel

While calculating the inertia of the wheel, wheel is divided into 3 sections (Figure 5-10-(a)) as individual hallow discs. Inertia of a hallow disc ((Figure 5-10-(b))) on its rotating axis is defined in Eq. (5.1).

$$I = \frac{1}{2} M (R_a{}^2 + R_b{}^2) \tag{5.1}$$

I is inertia of disc, M is mass of disc, R_a is inner radius of disc and R_b is outer radius of disc. Inertia of each section is calculated using Eq. (5.1) and total inertia of new wheel is summation of each section inertia. Density of wheel material is 2800 kg/m^3 and necessary dimensions for calculating mass and inertia of the wheel is shown in Figure 5-9 and Table 5-2.Table 5-2 shows the dimensions and inertia of re-defined wheels for AF motors.

Table 5-2: Dimension and inertia values for AF integrated wheel

Parameters	AF 6 pole
d1 (mm)	16.5
d2 (mm)	3.4
d3(mm)	2.6
d4(mm)	1
d5(mm)	110
Inertia of wheel (2 wheels kgm^2)	4.51x10^{-4}
Mass of wheel (2 wheels g)	197

It is assumed that in AF motor the same bearings are used in RF configuration (SKF 7200 BECBP whose weight is 30g). Winding weight is also assumed to be same as in RF 6 pole motor case (20g). Bearing and windings are not included in the volume calculations since they are inserted into motor. Housing is ignored in AF motor calculations since motor windings are on the outer surface of stator and generally housing is not used for AF motors. Rotors of AF motor are inside the wheel so that volume of the rotors are already included in the wheel volume calculations since largest dimensions of wheel (d1 and d5) are used in calculation of wheel volume (Figure 5-11). Only air gap and stator volume are considered in total volume calculations. Designed AF 6 pole motor integrated wheel system proprieties are summarized in Table 5-3

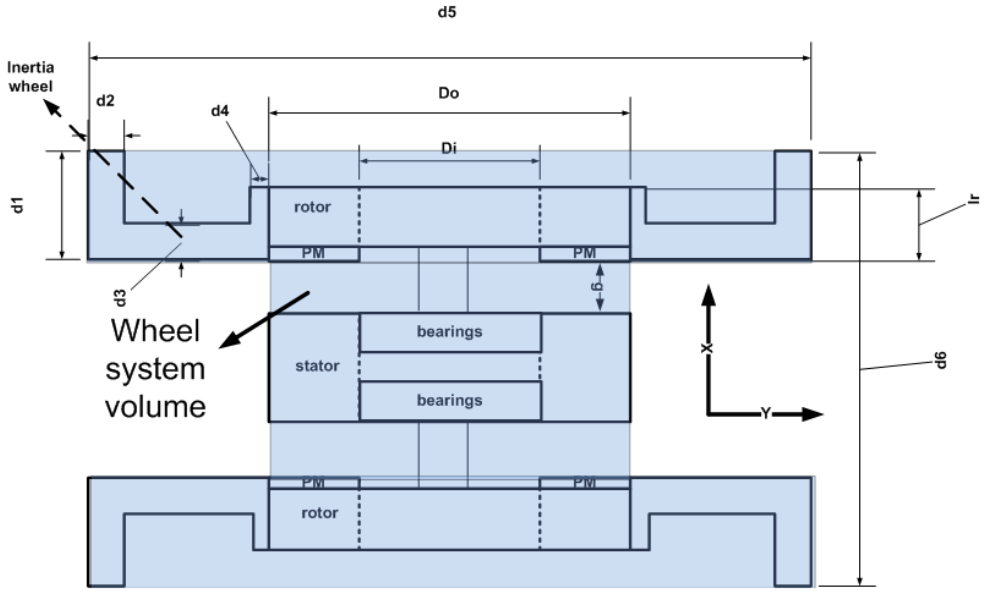

Figure 5-11: Volume of AF motor integrated wheel system

Table 5-3: Calculated parameters of AF motor integrated wheel system

Parameters	RF 6 pole
Mass of motor (bare motor) (g)	109.6
Mass of bearings (g)	60
Mass of windings (g)	20
Mass of wheel (g)	197
Volume of motor stator and air gap only (m^3)	3.62×10^{-5}
Volume of wheel (m^3)	3.13×10^{-4}
Inertia of wheel (kgm^2)	4.55×10^{-4}
Inertia of motor (kgm^2)	0.28×10^{-4}
Inertia of wheel system(kgm^2)	4.83×10^{-4}
Total mass of wheel system	386.6
Total volume of wheel system (m^3)	3.492×10^{-4}

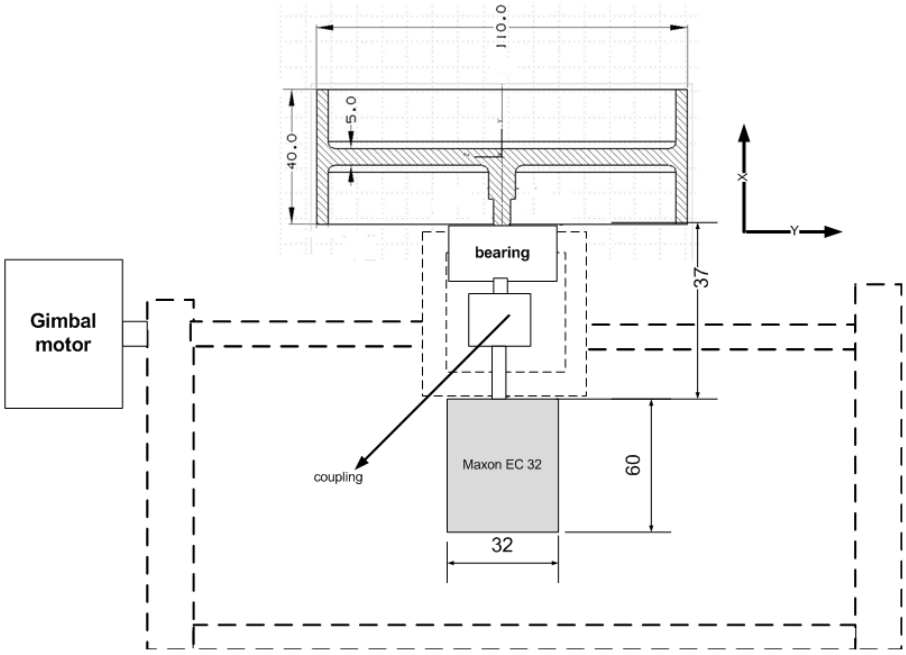

Figure 5-12: Existing CMG system dimensions

In order to make comparison between new designed AF and RF 6 pole integrated CMG wheel system and existing system, dimensions weight and volume of the

existing CMG wheel system should be defined. Figure 5-12 shows the dimensions in existing system. Note that one additional bearing is used to carry the wheel.

While calculating the mass of the wheel system mass of Maxon Ec 32 motor and mass of the existing wheel is used (263 g). Only additional mass is additional bearing unit and assumed to have 30g mass. Coupling weight is ignored since weight is small.

Volume of the existing wheel system include wheel volume, motor volume and required interface volume (Figure 5-13).

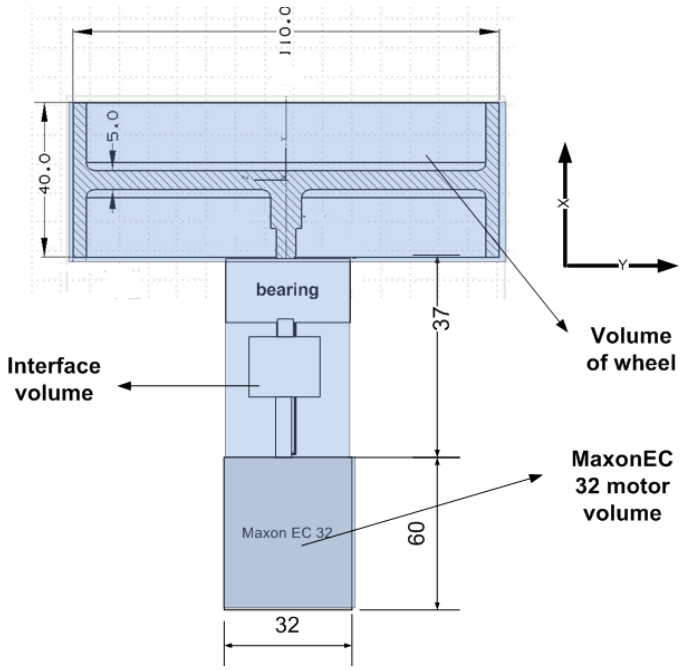

Figure 5-13 Volume of wheel system in existing CMG prototype

Summary of mass and volume of the existing system is summarized in Table 5-4.

Table 5-4: Mass and volume of existing wheel system

Parameters	RF 6 pole
Mass of motor (g)	263
Mass of external bearing (g)	30
Mass of wheel (g)- existing wheel is used	240
Volume of motor (m^3)	4.82×10^{-5}
Interface volume	2.97×10^{-5}
Volume of wheel (m^3)	7.598×10^{-4}
Inertial of wheel (kgm^2)- existing wheel is used	4.83×10^{-4}
Inertia of wheel system	4.83×10^{-7}
Total mass of wheel system (g)	533
Total volume of wheel system (m^3)	8.36×10^{-4}

Main aim of this thesis study was reducing the mass and volume of total CMG system. If the mass of the wheel system is reduced mass of the total CMG will reduce with same amount, and if volume of the wheel system is reduced total volume of the CMG will decrease depending on the new structural design of CMG. Also efficiency was another constrain and note that designed AF 6 pole and RF 6 pole motors have comparable efficiency value with existing motor (Maxon EC 32). Table 5-5 shows the calculated results for AF 6 pole motor integrated, RF 6 pole motor integrated and existing CMG wheel system parameters.

It can be seen from Table 5-5 mass of the CMG wheel system is reduced by 7.6% if designed RF 6 pole motor is used. This corresponds to 40.7g reduction in total CMG mass. If AF 6 pole motor is used in the CMG wheel system, of the CMG wheel system is reduced 27.4% and total mass of the CMG system will decrease 146.4g.

Table 5-5: Comparison of wheel systems

Parameters	RF 6 pole integrated wheel system	AF 6 pole integrated wheel system	Existing wheel systems
Total mass of wheel system (g)	492.3	386.6	533
Total volume of wheel system (m^3)	7.96×10^{-4}	3.492×10^{-4}	8.36×10^{-4}
Efficiency of motors	%79	%92	%78

Similarly when we compare the volume values of wheel system, if designed RF 6 pole motor is used, volume of wheel system will reduce 4.7%. This is mainly due to elimination of external coupling and bearing unit since motor is directly coupled to wheel (Figure 5-7).

If designed AF motor is used, volume of wheel system will reduce 58%. Reduction at the volume is quite large and this is mainly due to the fact that rotors of AF 6 pole motor is inserted in to existing wheel so there is no need to have separate space for AF motor rotors Figure 5-9.

The results mentioned above shows that selected AF 6 pole topology (Figure 3-25-(a)) has superiority over conventional slotted RF topology and exiting CMG prototype motor (Maxon EC 32) in terms of specific performance requirements of CMG wheel applications (efficiency, torque/ volume of wheel system and torque/ mass of wheel system). Note that reduction in mass and volume will be observed on the total mass and volume of the CMG. In addition to wheel drive performance improvement , since AF motor mass distribution is symmetrical along gimbal axis (Y) of CMG (Figure 5-9 and Figure 3-1), inertia at gimbal axis will be smaller than in RF case and this will reduce the power consumption of gimbal motor.

5.2 Future Work

It is observed that AF motors have better performance in terms of efficiency, torque/mass and torque/volume. Mechanical design considerations of wheel integration to AF motor rotor are not included in the RF motor design process. Since there are two air gaps in AF motor, mechanical design should be carefully studied to assure that the air gap size as desired is achievable. Supporting the stator, the ring and mounting the gimbal motor axis are other issues that need investigation. Another important mechanical design issue is selection of bearing since it is strongly determining the friction torque at steady state. Also magnetic circuit and equations for calculating the dimensions of motor are solved analytically with assumptions such as magnet leakage flux etc, these calculations can be done by FE magnetic circuit analysis to reach more realistic motor performances.

Thermal concerns of AF motor are not studied in any detail. Only assumption was taking the electrical loading of motor as %60-80 of suggested values for the same output ranges of motor (Figure 4-5). Since motor is designed to operate in vacuum environment, there will be no heat removal by convection on motor (only conduction and radiation are possible). In order to see motor performance under vacuum environment, detailed thermal analysis should be studied.

It is seen on the design process that main mass and loss increase is due to stator of AF motor. If better analyses are done exact values for core losses can be calculated. AF topologies with coreless stators can be studied in the same manner in order to reduce the core losses in AF motor.

Finally a comparison between AF topologies and outer rotating slotted or slotless RF motor topologies can be studied for CMG wheel system applications.

REFERENCES

[1] Lappas V. J., *A Control Moment Gyro Based Attitude Control System For Agile Satellites*, PhD Thesis, University of Surrey, Guildford, Surrey, United Kingdom, October 2002

[2] Yavuzoglu E., *Steering Laws For Control Moment Gyroscope Systems Used In Spacecrafts Attitude Control*, MSc Thesis, METU, Turkey, Ankara, November 2003

[3] Berne R., *Control Moment Gyro for Small Satellite Applications*, MSc Thesis, University of Stellenbosch, South Africa, April 2005

[4] *Selection Of Electric Motors For Aerospace Applications*, Preferred Reliability Practices, NASA MFS

[5] Novotny D. W., Lipo T. A., *Vector Control and Dynamics of AC Drives*, Oxford University Press, 1996

[6] Öztürk S.B., Modelling, *Simulation and analysis of low-cost direct torque control of PMSM using hall-effect sensors*, MSc Thesis Texas A&M University, December 2005.

[7] Krishnan S., *Electric Motor Drives Modeling, Analysis and Control*, Penticehall,2001

[8] Gieras F. J., Wing M., *Permanent Magnet Motor Technology*, Marcel Dekker Inc. 2002

[9] Gieras F. J., Wang R., Kamper M. J., *Axial Flux Permanent Magnet Brushless Machines*, Spinger, 2008

[10] Chapman C. J., *Electric Machinery Fundamentals*, McGraw-Hill, 1991

[11] Miller T. J. E., *Brushless Permanent-Magnet and Reluctance Motor Drives*, Oxford Press,1989

[12] Şahin F., *Design and Development of a High Speed Axial Flux Permanent Magnet Machine*, PhD Thesis Technische Universiteit Eindhoven, 2001

[13] Fitzgerald A.E., Kingsley C. Jr., Umans S. D., *Electric Machinery*, McGraw-Hill, 1988

[14] Chen Y., Pilllay P., *An Improved Formula for Lamination Core Loss Calculations in Machines Operating with High Frequency and High Flux Density Excitation*, IEEE Industry Applications Conference, vol.2, pp.759-766, 13-18 October 2002

[15] Sitapati K., Krishnan R., *Performance Comparisons of Radial and Axial Field Permanent-Magnet Brushless Machines*, Industry Applications Conference, vol.1, pp.228-234, 8-12 October 2000

[16] Cavagnino A., Lazzari M., Profumo F., Tenconi A., *A Comparison Between the Axial Flux and the Radial Flux Structures for PM Synchronous Motors*, IEEE Transactions on Industry Applications, vol.38 issue.6 pp 1517-1524, 2002

[17] Aydin M., Lipo T., Ronghai, Q., *Performance Comparison of Dual-Rotor Radial-Flux and Axial-Flux Permanent-Magnet BLDC Machines*, Tech IEEE International Conference on Electrical Machines and Drives, 2003.

[18] Şimşir N., Ertan H.B., *A Comparison of Torque Capabilities of Axial Flux and Radial Flux Type of Brushless DC (BLDC) Drives for Wide Speed Range Applications*, PEDS, 1999

[19] Karacan C., *Comparison of Performance of Switched Reluctance Motors, Induction Motors and Permanent Magnet dc Motors*, MSc Thesis, METU, 2004

[20] Hanselman D., *Brushless Permanent Magnet Motor Design*, The Writers Collective, 2003

[21] Luna H. B., Maruyama X. K., Colella N. J., Hobbs J. S., Hornady R. S., Kulke B., Palomar J. V., *Bremsstrahlung Radiation Effects in Rare Earth Permanent Magnets*, 10th International Free-Electron Laser Conference, 1988

[22] Ertan H.B., *EE-564 Machine Design Lecture Notes*, METU

[23] Caricchi F., Crescimbini F., Honorati O., *Low Cost Compact Permanent Magnet Machine for Adjustable Speed Pump Application*, IEEE Transactions on Industrial Applications, Vol. 34, No.1,pp.109-116, 1998

[24] Shigley J.E., *Mechanical Engineering Design*, McGraw-Hill, 2004